NOAA Technical Memorandum NWS SR-135

A QUANTITATIVE ANALYSIS OF QUASI-GEOSTROPHIC FORCING DURING RECENT SEVERE WEATHER OUTBREAKS ACROSS THE SOUTHERN GREAT PLAINS

David Andra
National Weather Service Forecast Office
Norman, Oklahoma

Scientific Services Division
Southern Region
Fort Worth, Texas
May 1991

UNITED STATES
DEPARTMENT OF COMMERCE
Robert A. Mosbacher, Secretary

National Oceanic and Atmospheric Administration
John A. Knauss
Under Secretary and Administrator

National Weather Service
Elbert W. Friday
Assistant Administrator

ACKNOWLEDGEMENTS

The majority of this work was originally performed as an M.S. Thesis at the University of Oklahoma School of Meteorology. I wish to express my gratitude to my thesis committee, Dr. Kenneth Crawford, Dr. Frederick Carr and Donald Burgess for their insight, suggestions, and assistance in the preparation of this manuscript.

I also wish to thank Michael Foster for his assistance with the Upper-Air Diagnostics program and for his stimulating discussions on related topics. Mark Antolik provided assistance in the acquisition of the NSSL upper-air data and Dick Pritchard from NESDIS provided satellite data. Lans Rothfusz at NWS Southern Region SSD assisted in obtaining surface weather data and Joan Kimpel skillfully drafted several figures.

Financial support for initial phases of this research was provided by the National Weather Service through a graduate assistantship during the early portion of my studies at the University of Oklahoma. Financial support also was provided by the University of Oklahoma School of Meteorology and the Oklahoma Climatological Survey.

TABLE OF CONTENTS

ABSTRACT

Numerous authors have proposed and discussed severe thunderstorm forecasting techniques based upon synoptic scale data. Although traditional techniques play an important role in forecasting, they are somehow unsatisfying in the sense that they sometimes do not provide quantitative guidance information, and frequently provide little insight and understanding into the physical processes responsible for the ensuing weather. In contrast, objective analyses of quasi-geostrophic quantities, developed recently for the operational environment, show promise for forecasters on both of these points. It is important to learn more about the applications of these new tools toward severe storms forecasting, especially since major new technologies and training initiatives are scheduled for deployment into the operational forecast environment during the decade of the 1990s.

To meet these goals, an objective analysis of upper air data was performed for 25 recent severe weather events in the southern Great Plains.

Results indicate the analysis routines were useful in the quantitative assessment of certain aspects of the convective environment, particularly moisture and mid tropospheric static stability. Furthermore, the analyses of differential thickness advection, moisture advection, and Q-vector divergence provided insight into large-scale physical mechanisms acting to modify static stability and moisture (and hence buoyant energy). The results suggest "large scale" or quasi-geostrophic motions have their primary role in the creation of an environment favorable for severe convection, rather than its initiation.

Finally, four of the 25 severe events are examined in detail to illustrate the effects of quasi-geostrophic motions in the convective environment.

A Quantitative Analysis of Quasi-geostrophic Forcing During Recent Severe Weather Outbreaks Across the Southern Great Plains

CHAPTER I

INTRODUCTION

Since the Thunderstorm Project (Byers and Braham, 1949) deep moist convection has been a major topic of meteorological research. As a result, considerable insight has been attained into thunderstorm structure and evolution (Doswell, 1985). Development of satellite, radar, and computer technologies have further enhanced our ability to observe and understand convective processes.

Yet, in spite of apparent scientific and technological advances,the forecasting of convection (particularly severe convection) remains one of the greatest challenges to the operational meteorologist. Each year in the United States hundreds of people die and billions of dollars are lost due to thunderstorm-related phenomena (NOAA NWS, 1990).

Numerous authors have proposed and discussed severe thunderstorm forecasting techniques based upon synoptic scale data. In 1954, Fawbush, **et al.** proposed an empirically derived method of tornado forecasting. A statistical approach to severe storms forecasting was proposed by Charba (1977), while Bothwell (1988), developed a decision tree utilizing objectively analyzed meteorological quantities for the same purpose. A decision tree technique also was proposed by Colquhoun (1987) for thunderstorm, severe thunderstorm, and tornado forecasting. But, perhaps the most familiar and enduring method was proposed by Miller (1972). In his study Miller identified several qualitative features or "patterns" from conventional surface and upper air analyses that were indicative of subsequent severe thunderstorm development. The "Miller Technique," and other empirical techniques, comprise the backbone of severe storms forecasting today.

Although traditional techniques play an important role in forecasting, they are somehow unsatisfying in the sense that they sometimes do not provide quantitative guidance information, and frequently provide little insight and

understanding into the physical processes responsible for the ensuing weather. In contrast, recently developed objective analyses of quasi-geostrophic quantities show promise for forecasters on both of these points (Barnes 1985, 1986, 1987). It is important to learn more about the applications of these new tools toward severe storms forecasting, especially since major new technologies and training initiatives are scheduled for deployment into the operational forecast environment during the decade of the 1990s (NOAA NWS, 1989).

With the above considerations in mind, the goals of this research are threefold:

-- Demonstrate how an objective analysis of upper air data may be used to provide quantitative information about the convective environment.

-- Identify the underlying quasi-geostrophic mechanisms present and their role in altering the convective environment.

-- Examine the range of quasi-geostrophic forcing present during significant severe storm events over the southern Great Plains.

To meet these goals, an upper-air objective analysis scheme developed by Barnes (1985, 1986, 1987) and implemented by Foster (1988), was performed on 25 recent severe weather events in the southern Great Plains.

Results indicate the analysis routines were useful in the quantitative assessment of certain aspects of the convective environment, particularly moisture and mid-tropospheric static stability. Furthermore, the analyses of temperature advection, moisture advection, and Q-vector divergence provided insight into large-scale physical mechanisms acting to modify static stability and moisture (and hence buoyant energy). However, the analysis routines lacked the important mesoscale and boundary layer information necessary for the evaluation of convective initiation.

The results also would seem to support the conclusions of Doswell (1985, 1987) where "large scale" or quasi-geostrophic motions have their primary role in the creation of an environment favorable for severe convection, rather than its initiation.

Finally, four cases are examined in detail from the 25 cases selected.

CHAPTER II

DATA

Four types of data covering the period October 1981 through June 1988 were utilized in this study: North American rawinsonde observations from the upper air data base at the National Severe Storms Laboratory (NSSL), infrared satellite imagery from the National Environmental Satellite, Data and Information Service (NESDIS), North American surface weather analyses from the National Meteorological Center (NMC), and severe weather events as recorded in STORM DATA (Dept. of Commerce, 1981-1988).

2.1 Selection of Study Days

For the purpose of this research, study days were selected according to the following criteria:

Geographically, the study area was confined to Oklahoma and North Texas, north of 32 degrees North latitude (Figure 1). This geographical constraint was imposed in an effort to make the data set manageable in terms of size, and to minimize the potential relationships that a non-homogeneous regional climatology might have on severe storm morphology.

The data set was further restricted to those days on which tornadoes occurred with an intensity of F3 or greater (Fujita, 1981) as recorded in STORM DATA. This criterion was selected since tornadic thunderstorms are by definition severe (NOAA NWS, 1986b) and typically are accompanied by other severe thunderstorm phenomena (such as hail $\geq$ 3/4 inch or winds $\geq$ 50 knots).

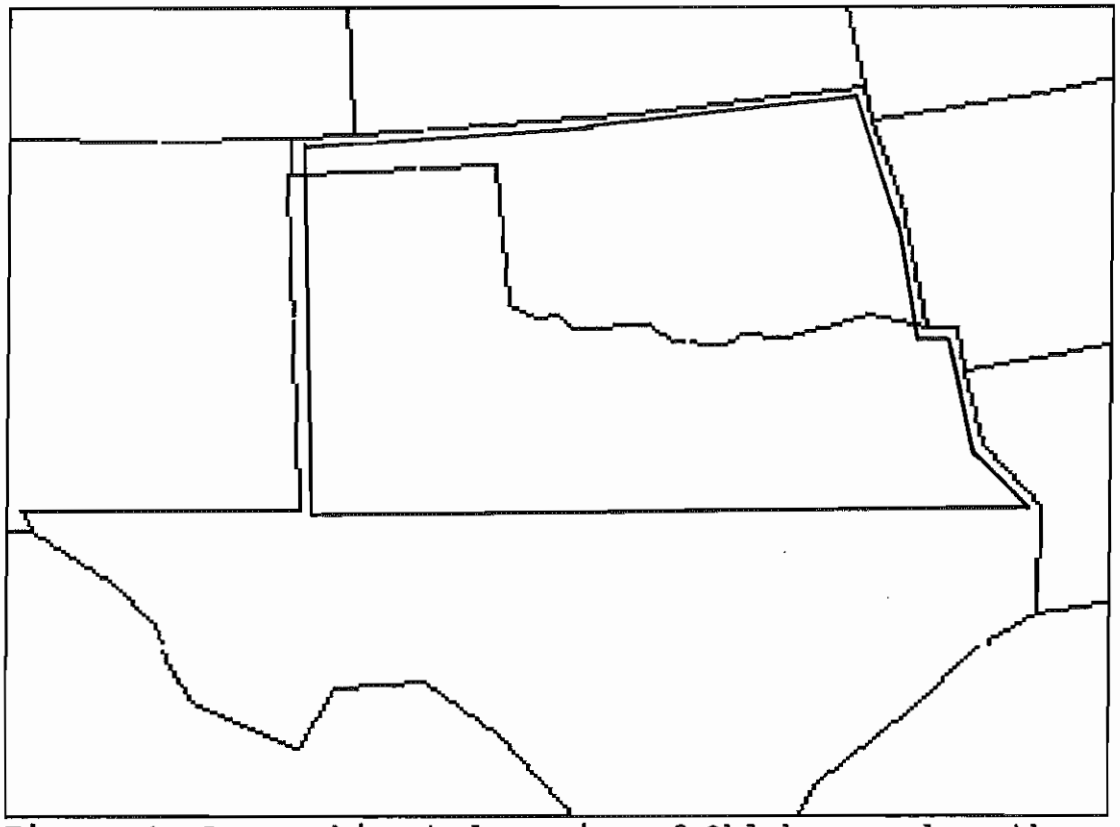

Figure 1. Geographic study region of Oklahoma and northern Texas.

Application of the geographic and event criteria for the period October 1981 through June 1988 yielded 25 days for potential inclusion in the thesis data set; they are listed in Table 1.

Table 1. Selected study days.

EVENT	DATE	TIME(CST)	F	STATE	COUNTY
1	811013	0800	3	N TX	Navarro
2	820314	0140	3	N TX	Runnels
3	820315	1902	3	OK	Washington
	820315	1757	3	OK	Pontotoc
4	820318	2355	4	W TX	Moore, Hansford
	820319	0100	3	OK	Beaver
5	820402	1450	3	OK	Love
	820402	1510	3	OK	Choctaw
	820402	1520	3	N TX	Fannin, Lamar
	820402	1550	5	OK	Choctaw, McCurtain
	820402	1600	4	N TX	Lamar, Red River
	820402	1640	3	N TX	Red River, Bowie
6	820511	1650	3	OK	Jackson
	820511	1702	3	OK	Jackson
	820511	1810	3	W TX	Hall
	820511	1755	3	OK	Kiowa
7	820512	1410	3	N TX	Palo Pinto, Erath
	820512	1805	3	N TX	Comanche
8	820516	1850	3	N TX	Wilbarger
9	820519	1825	3	W TX	Gray
10	830513	1905	3	OK	Kingfisher
11	831122	1600	3	OK	Pushmataha
	831122	1640	3	OK	LeFlore
	831122	1740	3	OK	LeFlore
12	840426	2333	3	OK	Okmulgee
	840426	2205	4	OK	Creek, Pawnee
13	840429	0920	4	OK	Creek, Pawnee, Osage
14	840501	1944	3	N TX	Motley
15	841031	1756	3	OK	Woodward, Major
16	841213	0945	3	N TX	Dallas, Collin
17	850421	1745	3	N TX	Young, Throckmorton

Table 1. (cont.) Selected study days.

EVENT	DATE	TIME(CST)	F	STATE	COUNTY
18	860419	0715	3	W TX	Nolan
19	860507	1635	3	W TX	Hemphill
20	860508	1812	3	OK	Oklahoma
21	860514	1830	3	N TX	Archer, Clay
22	870322	1745	3	W TX	Lipscomb
23	870525	1720	3	W TX	Hansford
	870525	1912	3	W TX	Ochiltree
24	871115	1503	3	N TX	Anderson
	871115	1545	3	N TX	Smith
	871115	1830	3	N TX	Shelby, Panola
	871115	1835	3	N TX	Cass
25	880401	1642	3	N TX	Gregg, Upshur

2.2 Upper-Air Data

Upper-air data were obtained from the upper-air data base for North America that is archived at the National Severe Storms Laboratory. The data base resides on magnetic tape and is composed of thermodynamic and wind information from the operational rawinsonde network of the United States, Canada, and Mexico. Data beginning in the 1940s are available in a standard format with pressure reported to the nearest millibar, geopotential height to the nearest meter up to 500 mb, and temperature and dewpoint to the nearest tenth degree Celsius. Wind direction is recorded to the nearest five degrees and wind speed is recorded to the nearest meter per second. Figure 2 depicts a typical NSSL data entry.

```
3                OKC
9      953       392       197       151       160        70
4     1000     32767     32767     32767     32767     32767
4      850      1369       155       103       217       270
4      700      2996        63       -26       210       210
4      500      5644      -149      -333       221       230
4      400      7288      -285      -448       245       270
4      300      9283      -433     32767       221       430
4      250     10487      -520     32767       222       440
```

Figure 2. Typical NSSL upper-air data entry.

Mandatory pressure levels (NOAA NWS, 1981) were obtained for rawinsonde locations across the United States and northern Mexico. At least one synoptic sounding time prior to and following the tornado event was retrieved to gain the most complete picture possible of large scale atmospheric evolution.

2.3 Infrared Satellite Imagery

Infrared (IR) Satellite Imagery of North American was obtained from archives at the National Environmental Satellite, Data and Information Service for each synoptic sounding time. Each IR image utilized the MB enhancement curve (NOAA NWS, 1986a) and a nominal resolution of 5 nautical miles.

2.4 North American Surface Analyses

Surface weather analyses for North America were obtained from the National Meteorological Center for each sounding time. Surface weather observations were extracted from the analyses and used to construct regional surface weather analyses in Chapter V.

CHAPTER III

METHODOLOGY

3.1 Quasi-geostrophic Theory

Atmospheric processes vary greatly in space and time. At one extreme lie the planetary waves, with space and time dimensions on the order of 10,000 kilometers and weeks; at the opposite end of the spectrum, atmospheric processes are occupied by molecular motions that are limited by the mean free path and fractions of seconds. Between the extremes lies a wide range of atmospheric phenomena, including the so-called "synoptic" or "large-scale" weather. Typically, large-scale atmospheric motions and phenomena have a space scale on the order of thousands of kilometers and a time scale of days (Fujita, 1986). The mid-latitude cyclone is one example of large-scale atmospheric phenomena.

Through scale analysis of the governing dynamical equations, a set of equations describing quasi-geostrophic flow may be derived. These equations represent a fundamental concept in dynamic meteorology for the description of large-scale mid-latitude motions. As the name implies, the equations describe atmospheric motions approximately in geostrophic balance where the Rossby number **Ro** $\approx$ 0.1. A slight imbalance in the flow field is attributable to ageostrophic adjustments arising from the tendency of geostrophic advections of momentum and temperature to disrupt the thermal wind balance. These ageostrophic components are generally an order of magnitude less than the geostrophic flow components, yet they represent the source for vertical velocities in the quasi-geostrophic system (Holton, 1979). An excellent discussion of the disruptive process and resulting ageostrophic circulations is presented by Durran and Snellman (1987).

Assessing Quasi-geostrophic Vertical Velocity

Through manipulation of the quasi-geostrophic thermodynamic and vorticity equations, an expression for vertical velocity, ω, may be found. The expression, known as the quasi-geostrophic omega equation, is defined by (from Holton, 1979):

$$(\nabla^2+\frac{f^2\partial^2}{\sigma\partial p^2})\,\omega=\frac{f_o}{\sigma}\frac{\partial}{\partial p}\,[v_g\cdot\nabla(\frac{1}{f_o}\nabla^2\phi+f)\,]+\frac{1}{\sigma}\nabla^2[v_g\cdot\nabla(\frac{-\partial\phi}{\partial p})\,] \quad (1)$$

A **B** **C**

Where σ is the static stability parameter, f is the coriolis parameter, Φ is the geopotential height, and $\mathbf{V_g}$ is the geostrophic wind. The quasi-geostrophic omega equation (1) is diagnostic with respect to ω since no time derivatives are included. The omega equation also is dependent only upon instantaneous observations of geopotential height, Φ. Traditionally, (1) has been the primary means by which quasi-geostrophic vertical velocities have been computed (Durran and Snellman, 1987). Following Holton (1979), the terms of (1) are interpreted as follows:

Term A is the three-dimensional Laplacian of omega. If omega has a sinusoidal distribution, then it may be assumed that term A is proportional to $-\omega$. Since large-scale midlatitude flow is characterized by a wave-like structure, this assumption provides a general and crude approximation for assessing term A.

Term B is the differential advection of vorticity and is proportional to the rate of change with height of geostrophic advection of absolute vorticity. Strictly interpreted, term B calls for calculation of absolute vorticity advection at multiple levels for the assessment of forcing. However, in practice it is generally assumed that the advection of vorticity near the ground is small compared to the advection aloft (typically 500 mb), and that vorticity advection aloft > 0 implies $\omega < 0$, or rising motion at intermediate levels (e.g. 700 mb). Although this assumption is valid more often than not, there are cases where vorticity advection < 0 at all levels yet rising motion ($\omega < 0$) results. This is the case of strong anticyclonic vorticity advection (AVA) at low levels and relatively weak AVA aloft (Bluestein, 1985).

Term C is the two-dimensional Laplacian of thickness advection. Since thickness is proportional to temperature by the hypsometric equation (Hess, 1979), term C may be considered proportional to negative temperature advection.

This assumption again relies upon a sinusoidal distribution of the thickness field. If this is true, term C greater than zero forces rising motion and term C less than zero forces sinking (Holton, 1979).

Although the static stability parameter σ is considered constant during the derivation of (1), it is variable in the real atmosphere. The magnitude of σ acts to modulate the forcing terms of (1) so that low values of σ yield large values of vertical velocity, and vice versa. The effect is also non-linear since vertical motions act to change static stability.

However, the primary difficulty associated with using (1) to determine vertical velocity arises when attempts are made to compute and evaluate terms B and C. In the real atmosphere the terms often tend to cancel one another thus making even qualitative assessment of omega ambiguous. Trenberth (1978) and Hoskins, **et al.** (1978) have both presented methods for resolution of the omega equation dilemma.

Trenberth's Approximation

The Trenberth approximation (2) offers a quick method for the operational forecaster to qualitatively assess quasi-geostrophic omega (Trenberth, 1978).

$$(\sigma \nabla^2 + f_o \frac{\partial^2}{\partial p^2}) \omega = 2 f_o \frac{\partial v_g}{\partial p} \cdot \nabla (\frac{1}{f_o} \nabla^2 \phi) \quad (2)$$

The approach is similar to that of Sutcliffe (1947) and assumes that quasi-geostrophic vertical velocity is proportional to advection of vorticity by the thermal wind. Since thickness is related to the thermal wind by the thermal wind relation (Holton, 1979), the assessment is made by overlaying fields of thickness and vorticity. Rising motion is inferred where the implied thermal wind blows from high to low vorticity values.

Hoskins's Q-vector

Advances in computer technology have made feasible the computation of forcing terms for the traditional quasi-geostrophic omega equation (1). However, such an exercise may be of little use to the forecaster since the forcing terms are not Galilean invariant. As discussed by Durran and Snellman (1987) and Hoskins, **et al.** (1978), the

advection of thermal vorticity changes as the mean wind speed changes. As a result, forcing calculated for identical weather systems embedded in uniform mean flow differ depending on the speed with which the systems move.

To avoid the problems associated with the traditional omega equation (1), Hoskins, **et al.** (1978) proposed calculating the Q-vector for determining quasi-geostrophic vertical velocity,

$$Q=\left[\frac{\partial v_g}{\partial x}\cdot\nabla\left(\frac{\partial\phi}{\partial p}\right),\frac{\partial v_g}{\partial y}\cdot\nabla\left(\frac{\partial\phi}{\partial p}\right)\right]=\frac{D_g\nabla\theta}{Dt} \qquad (3)$$

Interpreted strictly, Q-vectors are proportional to the component of the horizontal gradient of geostrophic wind that lies parallel to the thickness gradient or, the rate of change of potential temperature gradient following geostrophic flow. An alternative, and perhaps more physically meaningful interpretation, is provided by Hoskins and Pedder (1980). As was previously discussed, ageostrophic circulations associated with disruptions of thermal wind balance are responsible for generation of quasi-geostrophic vertical velocity. The Q-vector, for a layer then, may be considered proportional to the ageostrophic wind below the layer and opposite and proportional to the ageostrophic wind above the layer, as depicted by Figure 3.

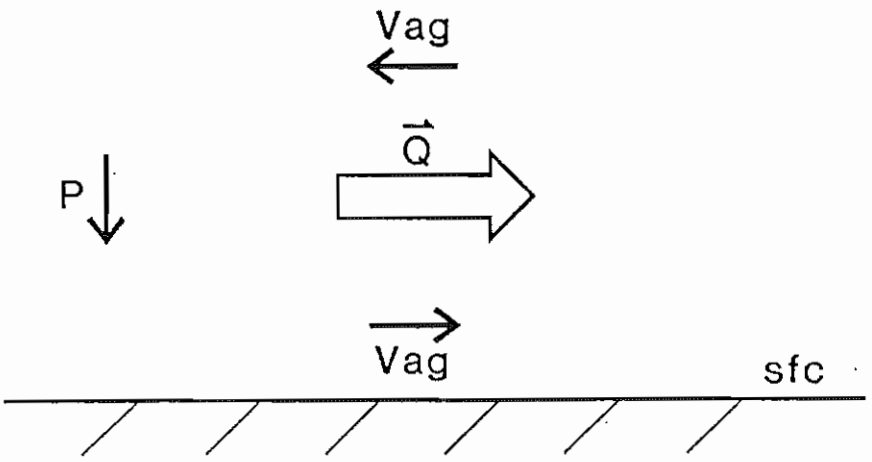

Figure 3. Q-vector and associated ageostrophic circulation (V_{ag}).

The vertical branches of the implied circulation may be determined by equation 4 where:

$$(\sigma\nabla^2+f^2\frac{\partial^2}{\partial p^2})\,\omega=-2\,\nabla\cdot Q+\frac{\partial f}{\partial y}\frac{\partial^2\phi}{\partial x\partial p} \quad (4)$$

A **B**

Term B of (4) typically is one or two orders of magnitude less than term A, and may therefore be assumed negligible (Hoskins and Pedder, 1980). The result leaves omega proportional to minus twice the divergence of the Q-vector, thus

$$(\sigma\nabla^2+f^2\frac{\partial^2}{\partial p^2})\,\omega=-2\,\nabla\cdot Q \quad (5)$$

By evaluating the expression for **Q**, it becomes apparent that Q-vectors point in the direction of the rising branch of the ageostrophic circulation so convergence of **Q** implies rising motion ($\omega < 0$).

It must be stressed that divergence of **Q** is not equal to ω. As with the traditional form of the omega equation (1), vertical velocity in the Q-vector formulation remains modulated by the static stability parameter. Furthermore, the left hand side of (5) must be integrated before ω may be explicitly determined. However, the divergence of **Q** may be used quantitatively to assess forcing for ω since it does not contain opposing terms and is Galilean invariant.

Numerous investigators have utilized Q-vector divergence to assess forcing for omega (Barnes, 1987; Doswell, 1987; Durran and Snellman, 1987). In the case studies examined in Chapter V, Q-vector divergence will be employed to assess forcing for quasi-geostrophic vertical velocity before and during severe weather events in the southern Great Plains.

3.2 Quasi-geostrophy and the Convective Environment

In spite of technological and scientific advances, the forecasting of severe convection remains one of the most formidable tasks facing the operational meteorologist. To meet the challenge, numerous forecast techniques have been developed. Many of these techniques employ synoptic-scale data sets (e.g.twice-daily upper-air soundings) to reach a prognostic decision. Unfortunately, most of the forecast techniques shed little light on the relationship between features on the synoptic-scale and developments on meso and smaller scales, such as severe convection.

Synoptic-scale, or quasi-geostrophic, motions and their interaction with the convective environment is not a new issue to meteorology. Maddox and Doswell (1982), Carlson, **et al.** (1983), Doswell, **et al.** (1985), Doswell (1987), and Rockwood and Maddox (1988) have discussed the roles of synoptic-scale motions as they relate to convective environments and events. However, much of this research, and the associated conceptual models, simply have not been incorporated into the operational forecast environment.

In the sections that follow, quasi-geostrophic synoptic-scale motions will be examined for their role in enhancing the convective environment. It is proposed that these effects have a primary role in modifying stability and wind fields, thereby creating an environment increasingly conducive to convection.

Stability

The thermodynamic structure, or stability, is of prime concern when examining convective environments. Equation 6 relates buoyant energy, B, of a convective parcel to the thermodynamic structure of the environment.

$$B=g\int \frac{\theta_w(z)-\theta(z)}{\theta(z)}dz \quad (6)$$

where $\theta_w(z)$ defines the moist adiabat of the ascending parcel, $\theta(z)$ is the profile of environmental potential temperature, and g is gravity. Furthermore, neglecting pressure perturbation effects, water loading, and mixing, buoyant energy is related to updraft velocity by (Weisman and Klemp, 1986):

$$W_{max}=(2B)^{1/2} \quad (7)$$

Since severe storms are generally associated with large updraft speeds (Doswell, 1985), the importance of buoyant energy is apparent. Inspection of (6) and (7) indicates that buoyant energy is maximized when the difference between $\theta_w(z)$ and $\theta(z)$ is large. In the atmosphere such a difference may arise in environments characterized by steep lapse rates (i.e. low static stability, $\partial\theta/\partial p$ is small) and moist boundary layers. Intuitively then, any processes acting to decrease static stability, or modify moisture profiles, are of importance.

Changes in static stability (i.e. lapse rates) may be examined through Equation 8 (Iribarne and Godson, 1981) which describes the local time-rate change of the static stability parameter, σ, for large-scale quasi-geostrophic flow, in the absence of diabatic heating.

$$\left(\frac{\partial\sigma}{\partial t}\right)_p = -\omega\frac{\partial\sigma}{\partial p} - \sigma\frac{\partial}{\partial p}(\omega) - \left[u\left(\frac{\partial\sigma}{\partial x}\right)_p + v\left(\frac{\partial\sigma}{\partial y}\right)_p\right] \quad (8)$$

A **B** **C**

Vertical Motion Considerations

Although quasi-geostrophic vertical velocities are generally small, on the order of microbars per second (Holton, 1979), they may have substantial effects upon tropospheric lapse rates ($\partial\theta/\partial p$), and hence stability and buoyant energy.

A process for steepening lapse rates may be envisioned by considering an arbitrary "layer" of air. As the layer is lifted pressure decreases and (assuming no condensation) the lapse rate becomes more nearly dry adiabatic ($\partial\theta/\partial p=0$). The opposite is true for sinking air (Hess, 1979). Figure 4 illustrates the concept of "layer lifting" for a layer of air 200 mb thick, lifted 350 mb. Term A of (8) represents static stability changes due to vertical advection of stability, or layer lifting.

Differential lifting of an atmospheric layer so that the layer is "stretched" results in even greater changes to stability. Consider a layer of air 200 mb thick from 700 mb to 500 mb, as shown in Figure 5. If $\omega=0$ at 700 mb and $\omega<0$ at 500 mb (so that a net vertical displacement of 200 mb occurs), the layer will undergo stretching so that the lapse rate steepens and eventually approaches dry adiabatic. Similarly, for a layer undergoing compression and subsidence, the stability would increase. Term B of (8) is simply the change in static stability due to differential lifting, or stretching.

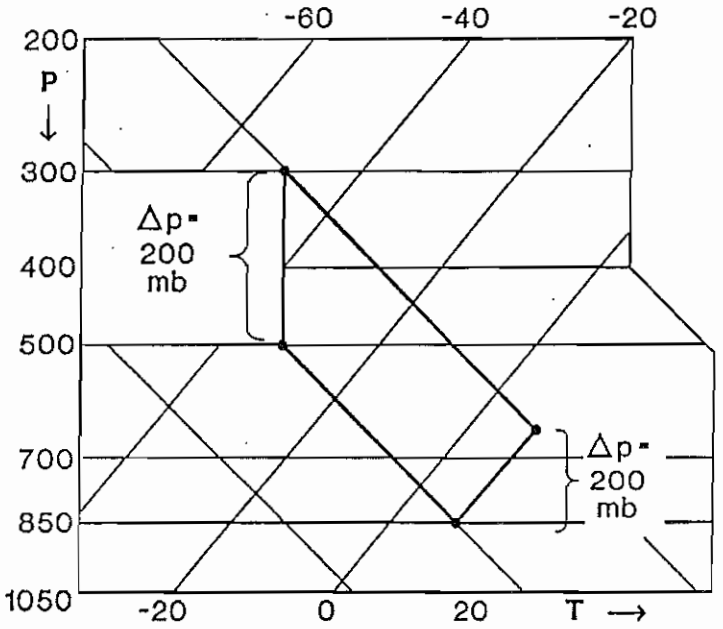

Figure 4. An example of layer lifting.

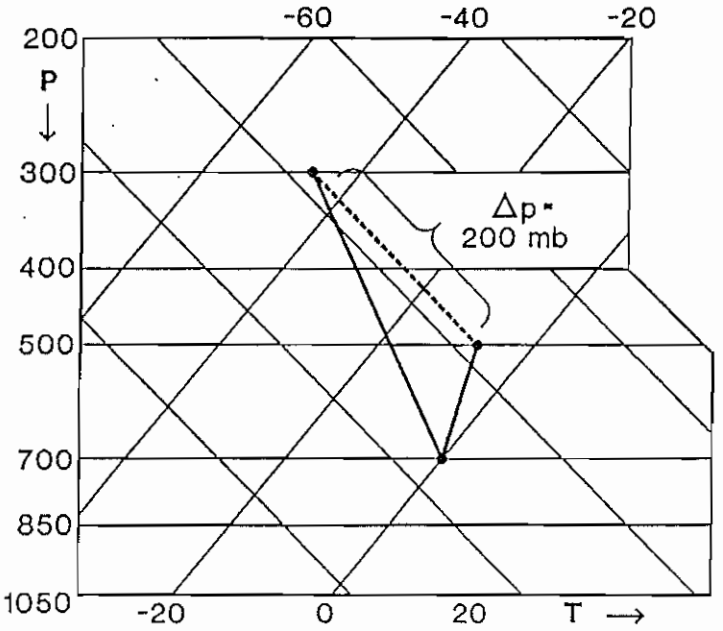

Figure 5. An example of stretching.

Returning to the Q-vector, if it is assumed that the divergence of **Q** is proportional to omega (5), and that vertical motion is the sole mechanism for changes in stability, then a phase relationship (Figure 6) develops between divergence of **Q** and the stability field for parcels moving faster than the quasi-geostrophic disturbance.

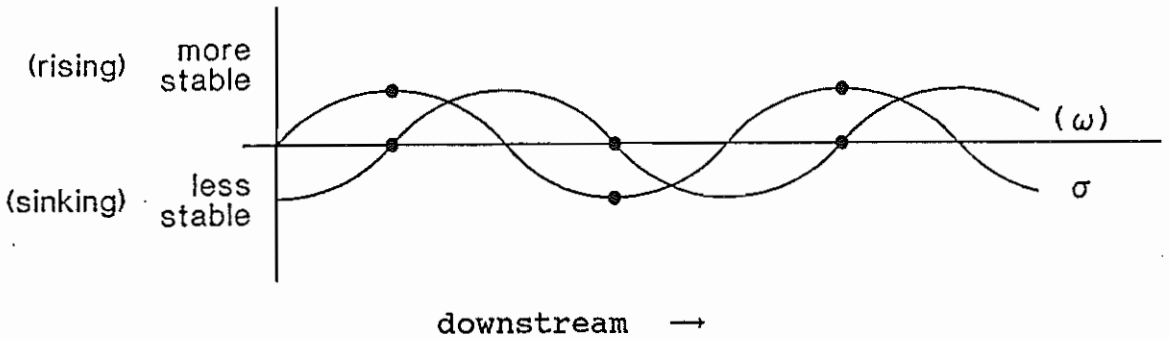

Figure 6. Phase relationship between omega and static stability.

The result is important because it shows that for relative flow through extrema in quasi-geostrophic vertical velocity, maxima and minima in stability are displaced one-quarter wavelength downstream. As an example, consider a parcel moving through a region of subsidence followed by movement through a region of quasi-geostrophic ascent. Initially, the parcel becomes increasingly stable due to subsidence until the midpoint between vertical velocity extrema is reached and omega changes sign. At this point the parcel has stabilized to the maximum extent. As the parcel moves into the region of ascent it begins to lift causing the lapse rate to steepen and stability to decrease. A minimum in stability occurs one-quarter wavelength downstream from the maximum in vertical velocity, again where omega changes sign and the parcel has ascended to the maximum extent.

The phase relationship has potentially important implications in terms of the operational convective forecast. In this case, the steepest lapse rates (and possibly greatest buoyant energy) are in place over the forecast area well before the maximum in quasi-geostrophic vertical velocity arrives.

If the phase speeds of the parcel and quasi-geostrophic vertical velocity extrema are equal, then the stability extrema are coincident with the omega extrema.

Differential Advection

The differential advection of temperature and moisture by the large-scale flow also may act to change the thermodynamic profile of the atmosphere. McNulty (1980), Carlson, **et al.** (1983), and Doswell (1982) have discussed the role of large-scale flow in the convective environment.

Differential temperature advection acting to warm lower layers or cool upper layers of the atmosphere produces a net decrease in stability. In Equation 8, this effect manifests itself in term C which represents the quasi-horizontal advection of stability. Typical values of differential temperature advection taken from severe storm environments imply lapse rate changes on the order of 1 deg C km-1 3 hr-1 are possible (Doswell, 1982).

Differential moisture advection resulting in increasing moisture values at low levels (e.g. below 700 mb), and decreasing values at mid and upper levels (above 700 mb) act to decrease stability and increase buoyancy (Weisman and Klemp, 1986). Newton (1980) demonstrates, for a typical severe storm sounding, that a 1 degree Celsius increase in boundary layer temperature would raise the temperature of a parcel rising moist adiabatically by 0.5 degrees Celsius. In contrast, a 1 degree Celsius increase in dewpoint temperature for the same layer would yield an increase in parcel temperature of 1 degree Celsius. Obviously, both large-scale differential advection of temperature and moisture may have profound effects on the thermodynamic environment.

Carlson, **et al.** (1983) discuss the role of large-scale differential advection in the evolution of the severe storm environment of the southern Great Plains. In their model, a layer of hot, dry air originating from the elevated terrain of Mexico and the southwestern United States is advected eastward, while at lower levels moist air is advected northward from the Gulf of Mexico. The result is a thermodynamic stratification characterized by a moist, potentially unstable boundary layer above which the lapse rate approaches dry adiabatic. For parcels penetrating the capping warm layer (or "lid"), large amounts of potential buoyancy are available (Figure 7).

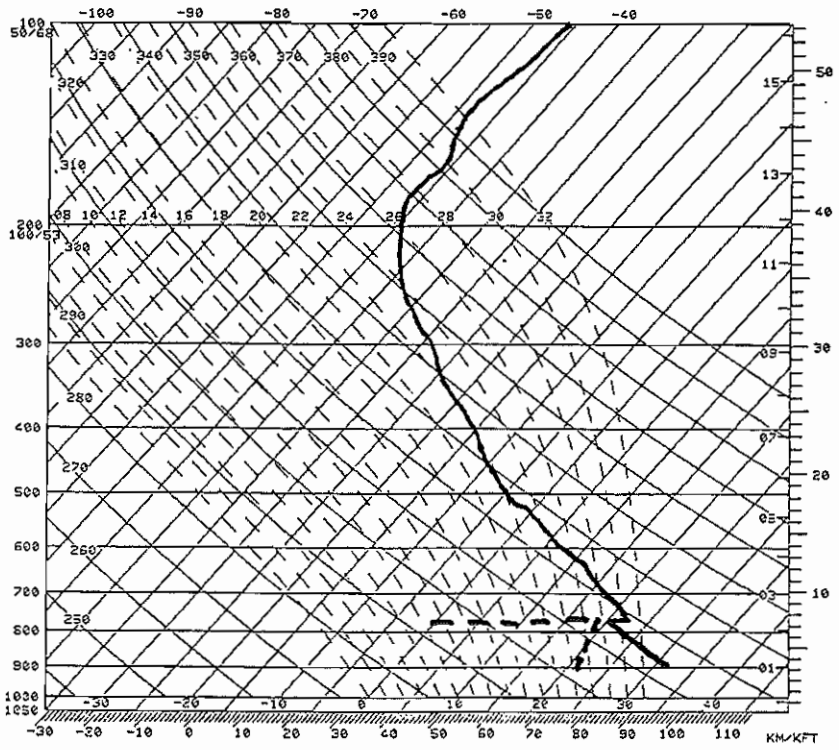

Figure 7. Typical sounding from severe storm environment.

Wind Field Considerations

Previous sections discussed the importance of large-scale differential advection of temperature and moisture in creating an environment suitable for convection. Intuitively then, changes in the large-scale wind field (and hence advection) by quasi-geostrophic processes must be considered.

Uccellini and Johnson (1979) proposed that the ageostrophic circulation associated with a speed maximum in the upper-level jet stream may enhance, or "couple" with, circulations associated with the low-level jet stream. Since the low-level jet plays a key role in moisture transport, such a coupling may accelerate the destabilization of the convective environment. The ageostrophic flow components responsible for the coupling are the horizontal branches of the ageostrophic circulation producing the vertical velocities considered earlier in this chapter (Durran and Snellman, 1987).

Quasi-geostrophic circulations arising from an approaching shortwave trough, or jet streak, also produce pressure falls. In turn, ageostrophic flow associated with the isallobaric wind can contribute toward increased moisture advection and convergence in the lower layers of the atmosphere (Doswell, 1982).

In addition to modifying the thermodynamic profile of the atmosphere, large-scale wind fields and quasi-geostrophic circulations play key roles in the determination of storm type. Klemp and Wilhelmson (1978) have shown through numerical modeling studies that vertical wind shear, in conjunction with buoyancy, determines storm morphology. Results indicate that winds that increase and veer with height are most favorable for the development and maintenance of long-lived organized severe storms (e.g. supercells). These conditions most commonly are found in advance of large-scale midlatitude weather systems where warm advection is occurring and quasi-geostrophic adjustments are acting to veer and strengthen the mean flow.

Summary

Conceptual models have been presented to explain the physical role of large-scale quasi-geostrophic motions in modifying the convective environment. Evidence suggests that these motions exert their primary influence on stability and wind fields.

It must be stressed that diabatic heating and friction have been ignored; and that ageostrophic flow components not described by quasi-geostrophic theory can also be important, and sometimes dominant, in preparing the atmosphere for severe convection. Furthermore, the boundary between large-scale quasi-geostrophic forcing, and forcing from smaller scales (e.g. mesoscale), is sometimes blurred making it difficult to assess sources of relevant forcing. However, several investigators (Doswell, **et al.** 1985; Doswell, 1987; Rockwood and Maddox, 1988) have concluded that in general, the primary role of quasi-geostrophic motions is to create an environment favorable for convection, and the role of mesoscale forcing lies in convective initiation. Analyses of quasi-geostrophic forcing during recent severe weather events in the southern Great Plains will be examined in Chapter V.

CHAPTER IV

Objective Analyses of QG Quantities

Quasi-geostrophic forcing for 25 severe storm events in the southern Great Plains was examined utilizing objectively analyzed quantities from the Upper Air Diagnostics program developed by Foster (1988). In addition to quasi-geostrophic quantities, the Upper Air Diagnostics program provides a large variety of observed and derived meteorological fields from mandatory sounding data (Table 2).

Table 2. UA Diagnostics observed and derived fields.

Data Field	Level Available
Temperature	850, 700, 500, 300, 250, 200 mb
Dewpoint Temperature	850, 700, 500 mb
Mixing Ratio	850, 700, 500 mb
Wind	850, 700, 500, 300, 250, 200 mb
Isotachs	850, 700, 500, 300, 250, 200 mb
Geopotential Height	850, 700, 500, 300, 250, 200 mb
Height Change	850, 700, 500, 300, 250, 200 mb
Temperature Advection	850, 700, 500, 300, 250, 200 mb
Moisture Flux Conv.	850, 700, 500 mb
Moisture Advection	850, 700, 500 mb
Wind Divergence	850, 700, 500, 300, 250, 200 mb
Vorticity	850, 700, 500, 300, 250, 200 mb
Geos. Temp. Advection	700, 500 mb
Laplacian Temp. Adv.	700, 500 mb
Layer-average Q-vector	700, 500 mb
Q-vector Divergence	700, 500 mb
Geostrophic Vorticity	700, 500 mb
Frontogenetical Function	700, 500 mb
850-700 mb Thickness	
700-500 mb Thickness	
700-500 mb Delta Temp.	
850-500 mb Thickness	
850-500 mb Mean Temp.	
700-300 mb Thickness	
700-500 mb Mean Temp.	
Layer-average Stability	
Diff. Thick. Advection	

Analysis Grid

The objective analysis was performed on an 18 X 14 polar stereographic grid having a horizontal resolution of 190.5 km at 60 degrees North. The grid was located so that the analysis included most of the continental United States and northern Mexico, as shown in Figure 8. Since meteorological features of interest generally approached the study area from the west, the grid was centered west of the study area, rather than symmetric about the study region.

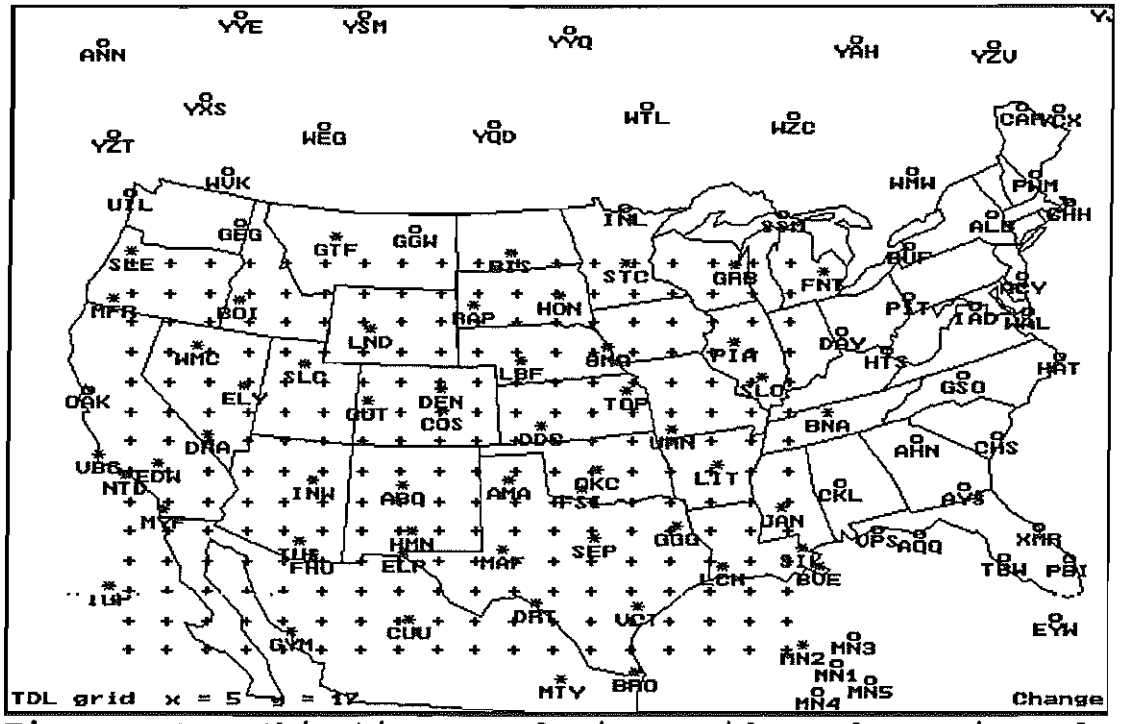

Figure 8. Objective analysis grid and rawinsonde locations. Gridpoints (+), rawinsonde locations considered in analysis (*), rawinsonde locations not considered in analysis (o).

Data Interpolation

Interpolation of height, temperature, moisture, and wind data to the analysis grid was accomplished using a Barnes (1964, 1973) Gaussian weighted two-pass interpolation scheme. The scheme employs weighted averages of observed upper air data to determine values at grid points,

$$G(i,j,) = \frac{\sum w_n f(x,y)}{\sum w_n} \quad (9)$$

where G(i,j) is the interpolated grid point value, and w is the Gaussian weighting function of the form:

$$W = \exp\left(\frac{-r^2}{4k}\right), \quad (10)$$

The weight is determined by r, the distance from the observed datum to the grid point, and k, which determines the shape and "influence radius" of the function. Values for k (Table 3) are similar to those of Barnes (1985) and identical to those of Foster (1988). The value of k varies according to the quantity under analysis and was chosen to reflect (a) the wavelength of the feature to be analyzed, and (b) an analysis comparable to that produced by the National Meteorological Center (Barnes, 1985). If k is chosen to be very large then all observed data will be heavily weighted to determine each grid point value, resulting in loss of detail. Values of k chosen too small may result in a noisy analysis. The values of k chosen for this research allowed substantial energy (approximately 30 percent) near the Nyquist interval of the rawinsonde network (near 800 km) to pass into the analysis. Although this decision produced some noise, it was hoped that more of the atmosphere's amplitude could be retrieved.

Table 3. Weighting (k) and gain factors (g).

k	g	Field
60000 km^2	0.4	Height, Wind
48000 km^2	0.3	Temperature, Dewpoint

During the second interpolation pass, the first pass field is added to residual differences between the observed data, $f(x_n,y_n)$, and the first pass values at data locations, $G_0(x_n,y_n)$. The difference is weighted (w_{ng}) and summed where k values have been multiplied by a gain factor, g, between zero and 1 which acts to diminish the influence radius (Koch, **et.al.**, 1983). The final interpolation value is then the sum of two passes (11).

$$G_1(i,j) = G_0(x_n,y_n) + \frac{\sum w_{ng}[f(x_n,y_n) - G_o(x_n,y_n)]}{\sum w_{ng}} \quad (11)$$

Finite Difference Equations

All derived and quasi-geostrophic quantities were calculated using centered finite difference equations having truncation error on the order of $(\Delta X)^2$ (Hornbeck, 1975). Exceptions were at the lateral boundaries where one-sided differencing techniques were employed.

Q-vector Calculations

Using the centered finite difference form of (3), layer-averaged Q-vectors were calculated for 700 mb and 500 mb. Figure 9 depicts the Q-vector diagnostic model atmosphere. Horizontal variations of the 700 mb and 500 mb geostrophic winds were calculated from reported heights. Horizontal gradients of thickness were derived from the difference between the reported heights at the bottom and top of layers from 850-500 mb and 700-300 mb. Thus, the resulting 700 mb and 500 mb Q-vectors are layer-averaged for 850-500 mb and 700-300 mb, respectively.

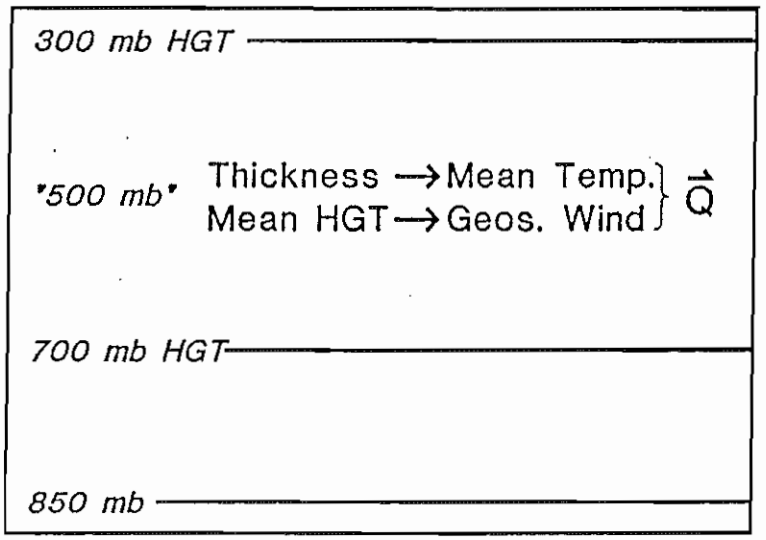

Figure 9. Q-vector model atmosphere.

Stability

"Layer stability" was calculated and represents the difference in mean potential temperature between the 850-500 mb layer and the 700-300 mb layer. Thus, layer stability is simply a vertically averaged measure of static stability, $\partial\theta/\partial p$. In the case of a dry adiabatic lapse rate, layer stability is zero since $\partial\theta/\partial p=0$. Figure 10 graphically shows calculation of layer-averaged stability.

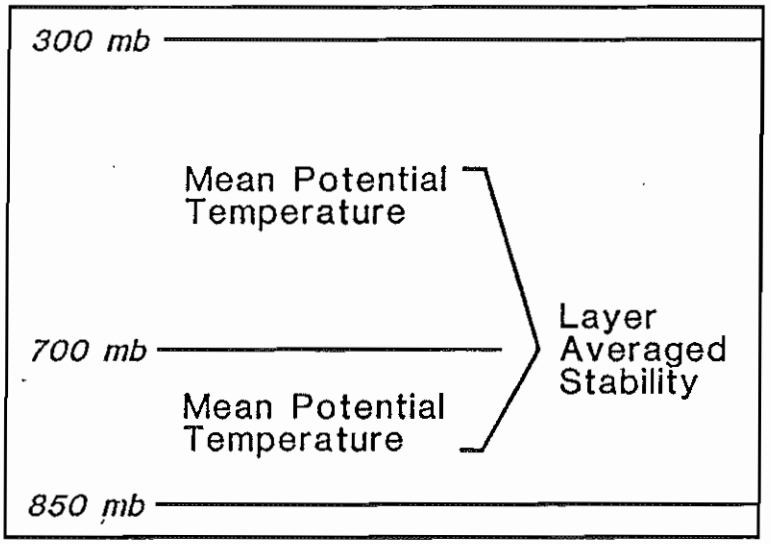

Figure 10. Layer-averaged stability model atmosphere.

To infer changes in static stability, differential thickness advection (DTA) was calculated. Since thickness is proportional to temperature, DTA represents changes in stability due to quasi-horizontal advections of temperature. The calculations were based upon the same layer-averaged model atmosphere (Figure 9) employed for Q-vector calculations. Thus, warm advection at low levels and cold advection aloft (DTA > 0) forces decreasing static stability ($\partial\sigma/\partial t < 0$).

Limitations of the Objective Analysis

Before examining results from the objective analysis, several inherent limitations of the analysis method must be addressed.

Perhaps the most obvious source for error is the rawinsonde observation itself. Slightly inaccurate measurements of temperature and pressure may lead to

substantial errors in calculated heights, which in turn seriously contaminate derivative-based quantities, such as Q-vectors. Barnes (1987) discusses an apparent height anomaly of 20 m at one station, and the resulting impact to Q-vector calculations. In his example, the sign for omega forcing was reversed by the seemingly small error.

Even if the observation is "exact," the NWS observational rawinsonde network is irregularly spaced with an average distance between stations of 400 km. Additional errors arise as these data are interpolated to grid points and finite difference calculations are performed.

Barnes (1986) examined the accuracy of an interpolation scheme, and second-order centered finite difference techniques, nearly identical to those of Foster (1988). Although the results of the Barnes study are too lengthy to discuss in detail, several especially relevant conclusions are:

-- Calculations of derived quantities less than 3 grid points from the lateral boundaries are unreliable.

-- The NWS observational rawinsonde network is marginally adequate for determining third derivatives for height perturbations on a scale the size of the grid domain.

-- The phase of the Q-vector field suffers the least error, while amplitude of the field may be substantially altered.

-- Q-vectors for features near the Nyquist interval of the NWS observational rawinsonde network (2 X 400 km = 800 km, meso-alpha-scale) will reflect no more than 25 percent of the true amplitude.

-- Height fields do not need to be analyzed to the meso-alpha-scale to diagnose forcing on the meso-alpha-scale. This is true since synoptic scale forcing gives rise to ageostrophic adjustments at meso-alpha-scale wavelengths (one-half the wavelength of the height distribution).

-- Vertical velocity fields calculated from conventional rawinsonde data very likely will contain large errors due to 1) previously mentioned errors in derived quantities, and 2) errors introduced through numerical integration.

CHAPTER V

RESULTS

Each of the rawinsonde data sets were objectively analyzed to obtain the quantities listed in Table 2. Of special interest were the layer-averaged calculations of Q-vector divergence, and thus forcing for quasi-geostrophic vertical velocity. The 700 mb layer-averaged Q vector was focused upon since its calculation requires 850 mb height and temperature data, the lowest data level available. It was hoped that the 850 mb data would contain information regarding low-level thermal advection which is considered by some investigators (e.g. Maddox and Doswell, 1982) to be important in some severe convective events.

Results of 700 mb layer-averaged Q-vector divergence calculations are summarized in Table 4 for the sounding time nearest tornadogenesis. The Q-vector convergence values reflect only maximum forcing for rising motion ($\omega<0$) and only forcing observed in the defined Oklahoma-Texas study region, or within 200 km "downstream" or 400 km "upstream" of the study region. Values less than 3 gridpoints from the lateral boundaries were not considered.

Table 4. Tornado events and maximum Q-vector convergence values (10-17 s-3 mb-1) nearest time of tornadogenesis. Values were found within boundaries of geographic study region, or within 200 km downstream or 400 km upstream of the region.

Event	Date	Time (UTC)	Convergence Q
1	13 OCT 81	1200	80
2	14 MAR 82	1200	150
3	16 MAR 82	0000	120
4	19 MAR 82	0000	120
5	03 APR 82	0000	190
6	12 MAY 82	0000	70
7	13 MAY 82	0000	160
8	17 MAY 82	0000	180
9	20 MAY 82	0000	160

Event	Date	Time (UTC)	Convergence Q
10	14 MAY 83	0000	140
11	23 NOV 83	0000	260
12	27 APR 84	0000	580
13	29 APR 84	1200	420
14	02 MAY 84	0000	250
15	01 NOV 84	0000	60
16	13 DEC 84	1200	100
17	22 APR 85	0000	60
18	19 APR 86	1200	110
19	08 MAY 86	0000	100
20	09 MAY 86	0000	130
21	15 MAY 86	0000	170
22	23 MAR 87	0000	350
23	26 MAY 87	0000	60
24	16 NOV 87	0000	120
25	02 APR 88	0000	160

Examination of the results reveals considerable variance within the data set. Forcing extremes are found to differ by an order of magnitude, suggesting that attempts to develop composite values of quasi-geostrophic forcing for severe storm events would be of doubtful value.

Obviously, not all severe weather events occur because of, or during, "strong" quasi-geostrophic forcing. Rather, the results support the hypothesis that quasi-geostrophic motions play their primary role in the creation and maintenance of environments favorable for convection, and mesoscale forcing acts to initiate the convective event (Doswell, 1987).

In an effort to identify the effects of quasi-geostrophic motions in convective environments, four specific events will be examined in detail. The events have been chosen to reflect an "illustrative event," maximum observed omega forcing, minimum observed omega forcing, and the occurrence of an outbreak of violent tornadoes. Additional analyses of 700 mb layer-averaged Q-vector divergence, corresponding to Table 4, are shown in the Appendix.

4.1 An Illustrative Event -- March 22, 1987

On March 22, 1987 severe thunderstorms erupted over portions of western Texas and northwest Oklahoma, producing eight tornadoes and hail up to 7 cm in diameter. The strongest tornado, an F3 lasting 40 minutes, struck Lipscomb county, Texas at 2345 UTC (Figure 11).

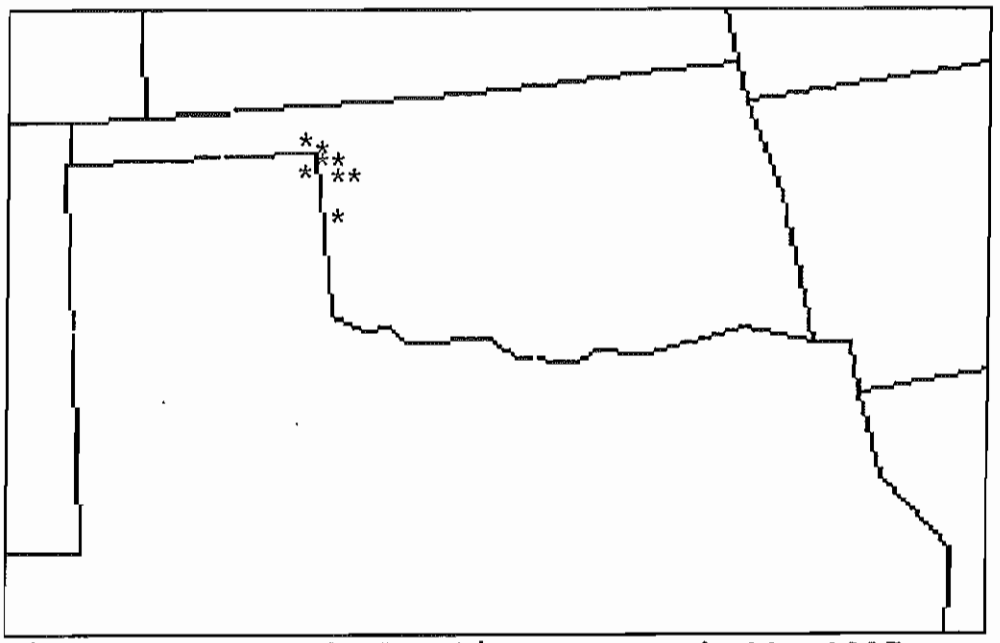

Figure 11. Tornado locations on March 22, 1987.

At 1200 UTC, approximately 12 hours prior to tornadogenesis, soundings revealed a deep longwave trough over the western United States. Near the base of the longwave, a shortwave trough was evident over Arizona (Figure 12).

The 1200 UTC surface weather analysis (Figure 13) indicated a weak low pressure center over southeast Colorado, with a dryline extending southward along the Texas-New Mexico border. Temperatures were near 10 degrees Celsius across western Texas and western Oklahoma. Dewpoint temperatures were near 8 degrees Celsius, with higher values upstream across southcentral Texas.

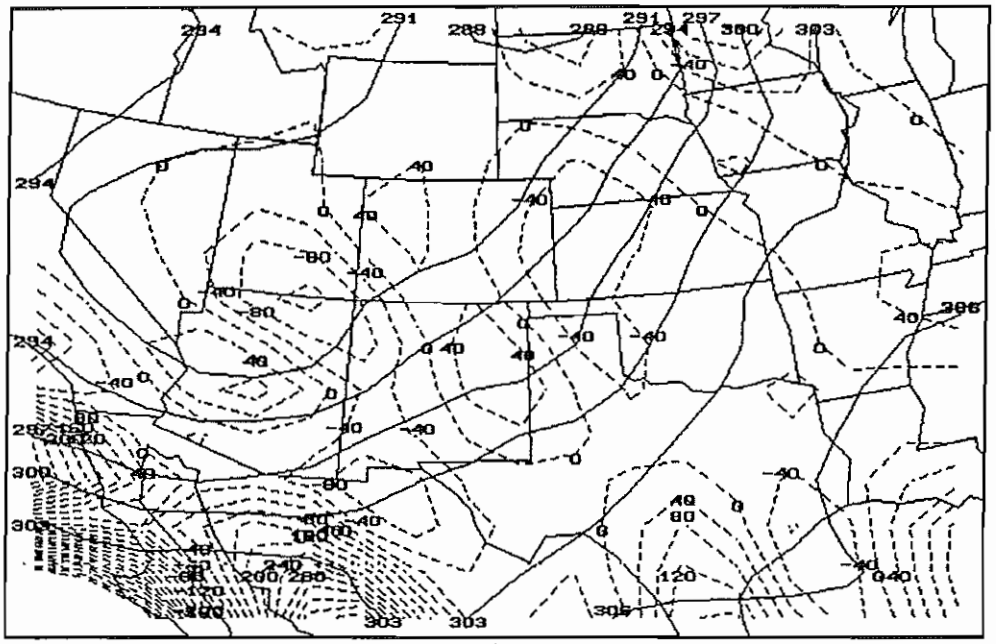

Figure 12. 700 mb Height (dm) and Q-vector Divergence (10-17 s-3 mb-1) 22 March 1987 1200 UTC.

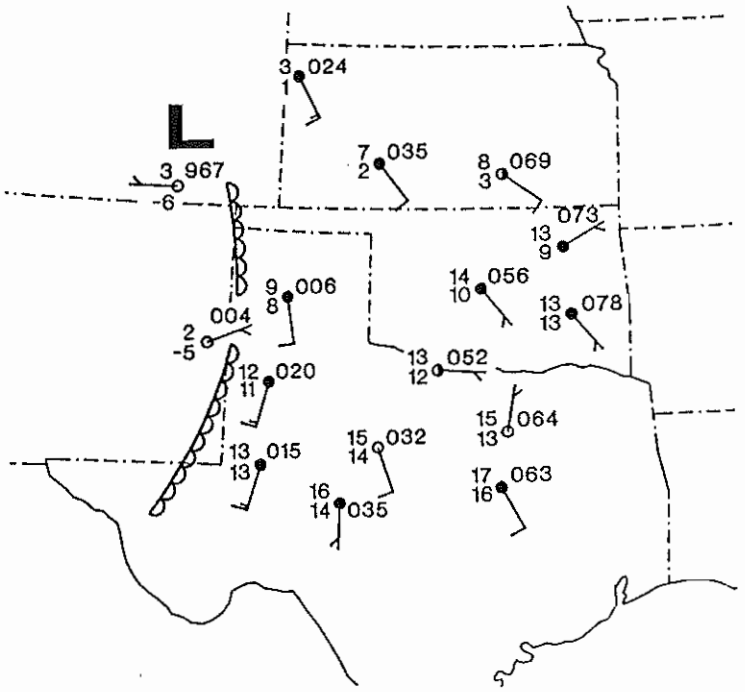

Figure 13. Surface weather analysis 22 March 1987 1200 UTC. Temperatures and dewpoints in degrees Celsius, wind speed in knots, pressure in tenths of millibars.

Differential thickness advection (DTA) at 1200 UTC (Figure 14), revealed a maximum in the advection field over western Kansas and western Texas. Recall that DTA values greater than zero force decreasing static stability with time ($\partial\sigma/\partial t<0$). Thus, the large scale flow was acting to effect a net decrease in static stability across the region through the horizontal advective term of (8). The 24 unit maximum of DTA may be interpreted as steepening lapse rates by approximately 1.4 K per 100 mb in 12 hours.

The analysis of 700 mb layer-averaged Q-vector divergence (Figure 12) implied weak quasi-geostrophic vertical motion across the region and therefore slight contribution from the vertical velocity term of (8). Layer-averaged stability for 1200 UTC (Figure 15) suggested relatively low values of static stability already in place across western Texas and Oklahoma.

Differential advection of moisture also was occurring over the study region as evidenced by the analyses of 850 mb and 500 mb moisture advection, Figures 16 and 17, respectively. As a result, moisture at the 850 mb level was increasing with time, while at 500 mb the air was drying.

Thus, through differential advections of temperature (thickness, DTA) and moisture by the large-scale flow, buoyant energy was increasing across the study region, producing an environment increasingly favorable for deep moist convection.

As boundary layer heating occurred during the afternoon, the surface dryline mixed eastward into eastern sections of the Texas Panhandle. By 2240 UTC, the first reports of severe weather (large hail) were received from the eastern Texas panhandle.

To assess the role of large-scale quasi-geostrophic motions near this time, the upper air soundings for 0000 UTC March 23, 1987 were objectively analyzed.

Positive values of DTA and 850 mb moisture advection persisted (Figure 18 and 19), indicating the large-scale flow was continuing to decrease static stability and increase buoyant energy.

The 23/0000 UTC analyses of 700 mb layer-averaged stability (Figure 20) revealed a pronounced minimum in the static stability field across western Texas. When compared to the 850 mb dewpoint field (Figure 21), it is observed that the stability minimum was located upstream and overlapped the low-level (850 mb) moist axis, a result similar to that documented by Doswell, **et. al.**,(1985).

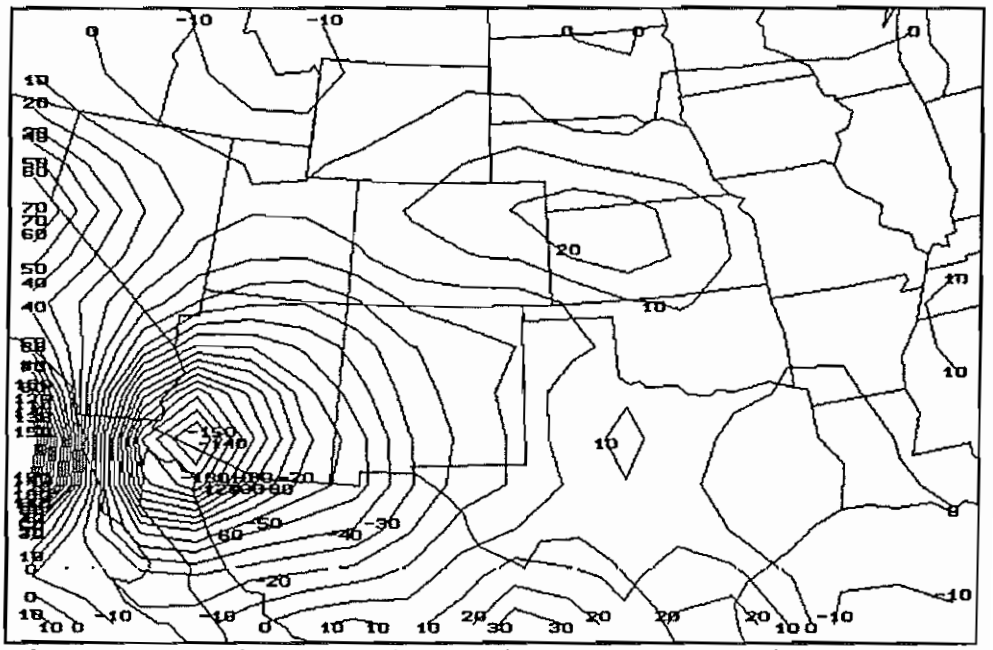

Figure 14. Differential Thickness Advection (10-2 K hr-1 dp-1) 22 March 1987 1200 UTC.

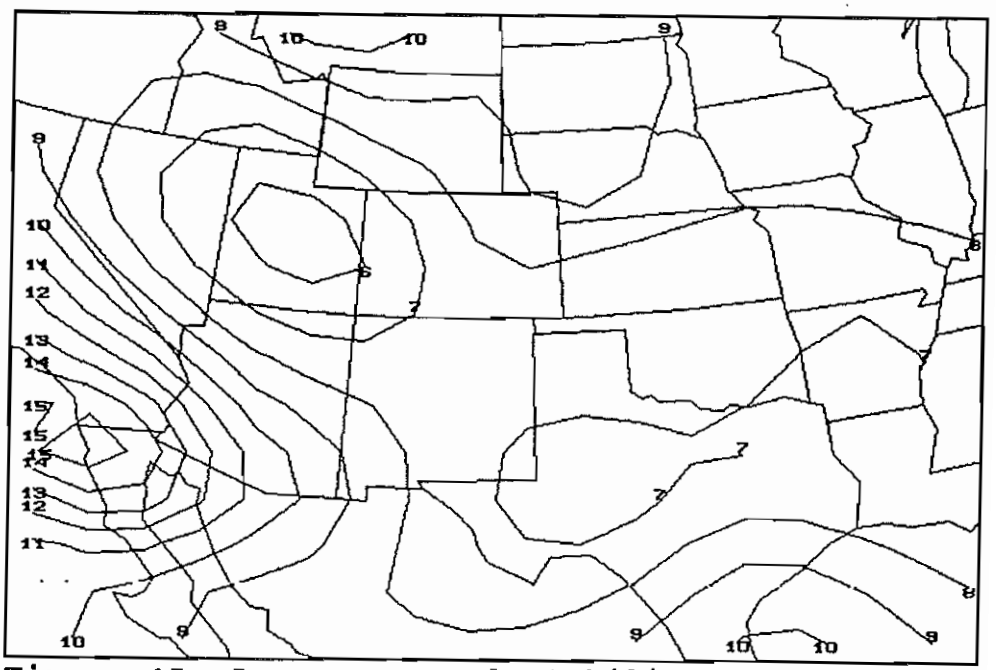

Figure 15. Layer-averaged Stability (K) 22 March 1987 1200 UTC.

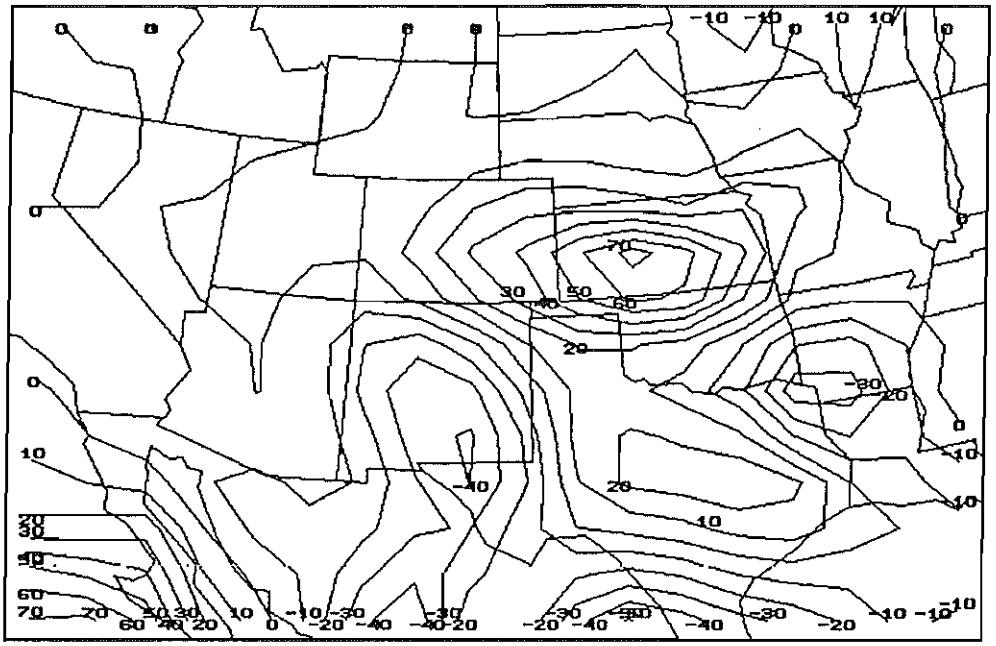

Figure 16. 850 mb Moisture Advection (g kg-1 hr-1 x 10) 22 March 1987 1200 UTC.

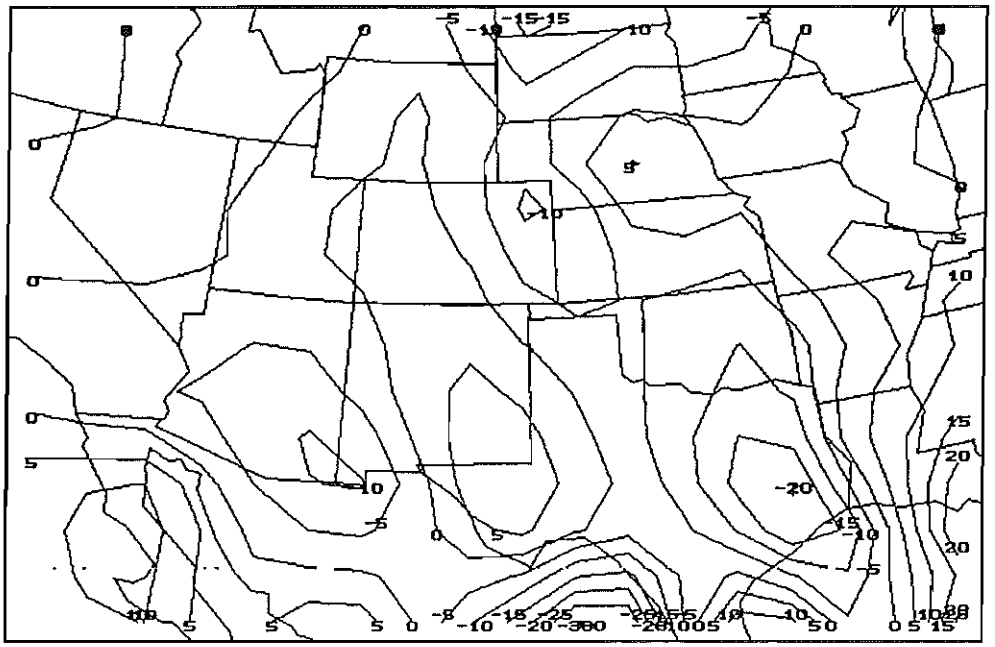

Figure 17. 500 mb Moisture Advection (g kg-1 hr-1 x 10) 22 March 1987 1200 UTC.

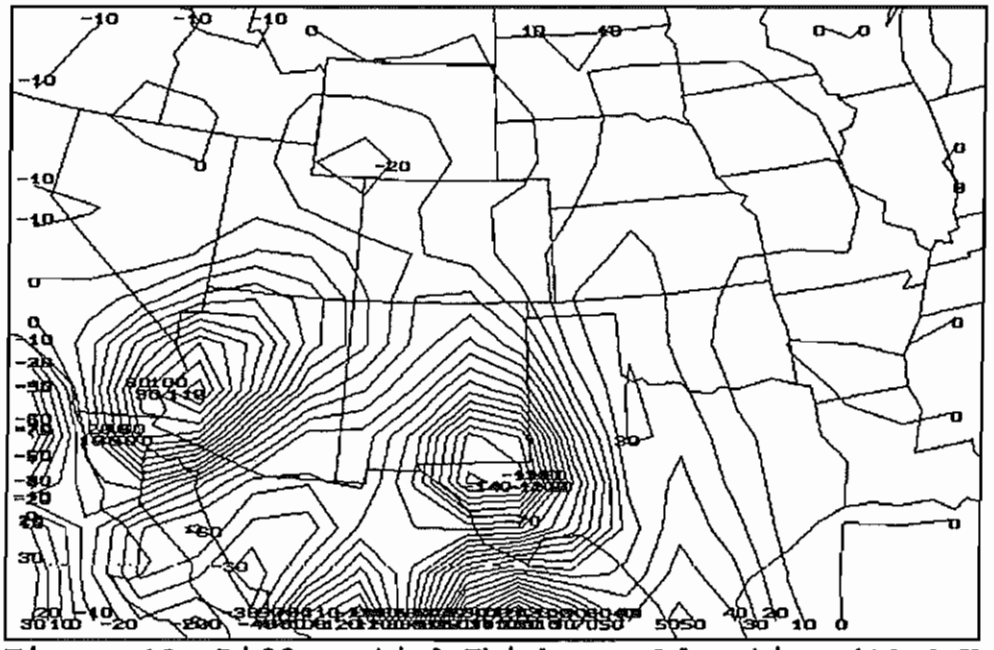

Figure 18. Differential Thickness Advection (10-2 K hr-1 dp-1) 23 March 1987 0000 UTC.

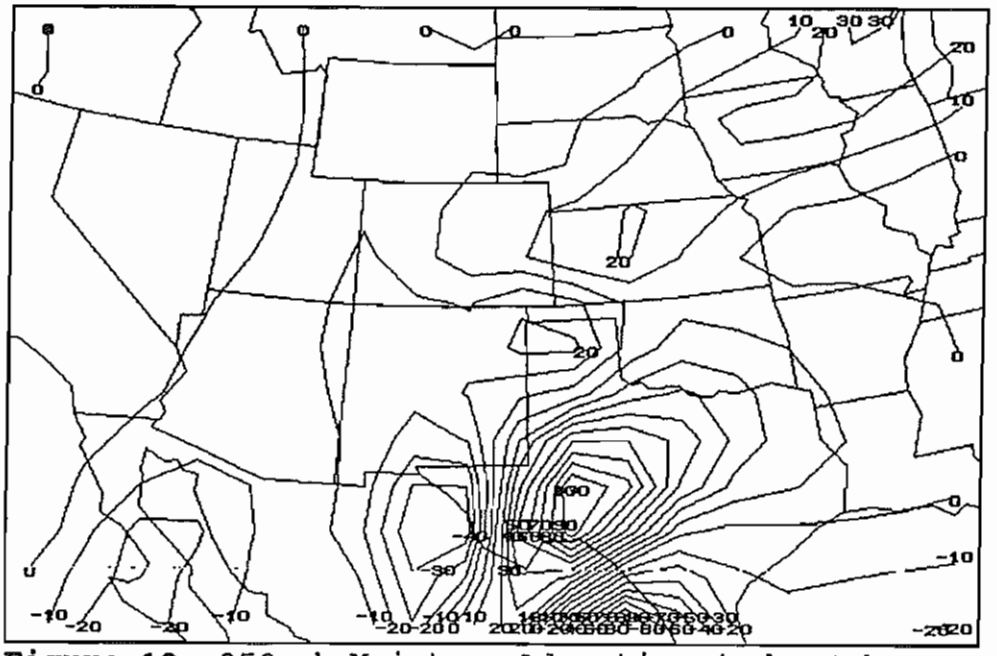

Figure 19. 850 mb Moisture Advection (g kg-1 hr-1 x 10) 23 March 1987 0000 UTC.

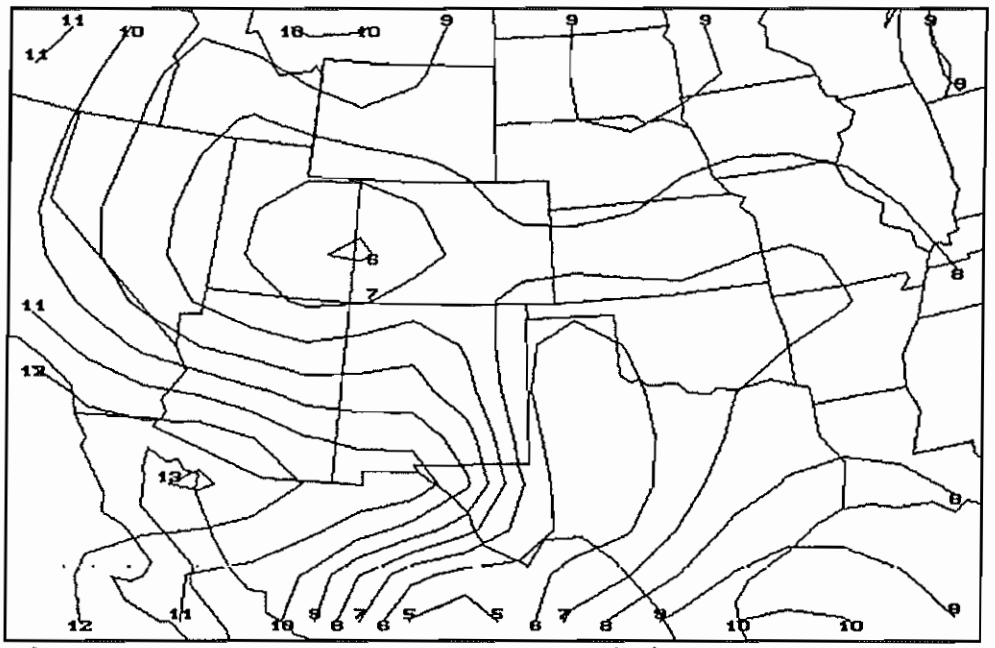

Figure 20. Layer-averaged Stability (K) 23 March 1987 0000 UTC.

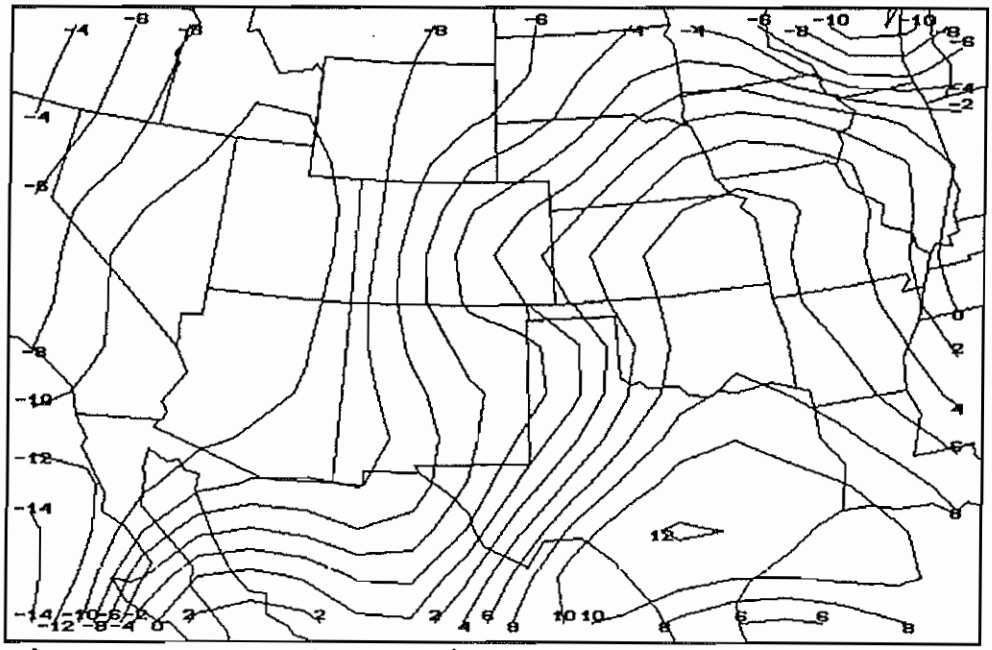

Figure 21. 850 mb Dewpoint Temperature (C) 23 March 1987 0000 UTC.

Examination of 700 mb layer-averaged Q-vector divergence also yielded interesting results. Figure 22 shows observed 700 mb height and layer-averaged Q-vector divergence. Of particular interest is the approaching short wave trough over the western tip of Texas, and apparently weak omega forcing across the eastern Texas Panhandle into northwest Oklahoma, where severe storms were underway. The apparent lack of quasi-geostrophic vertical velocity further suggests mesoscale effects associated with the dryline were responsible for convective initiation. Figure 23 is the enhanced infrared satellite image valid at 23/0000 UTC showing the severe storms over northwest Oklahoma; other storms were located near the dryline and stationary front across Kansas and Nebraska. Also of interest is the comma cloud associated with the shortwave trough moving through western New Mexico.

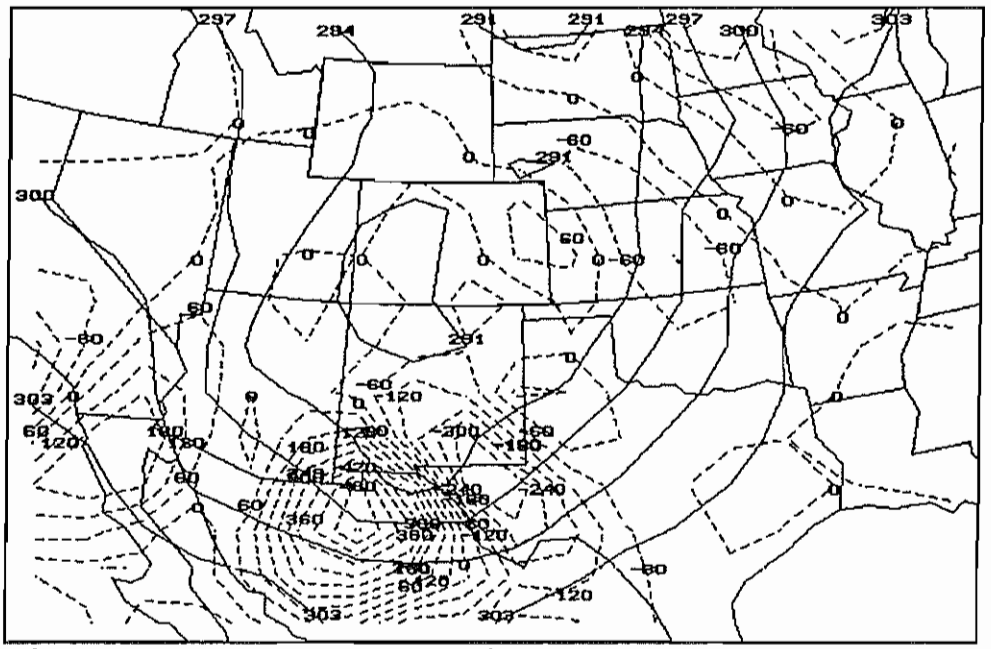

Figure 22. 700 mb Height (dm) and Q-vector Divergence (10-17 s-3 mb-1) 23 March 1987 0000 UTC.

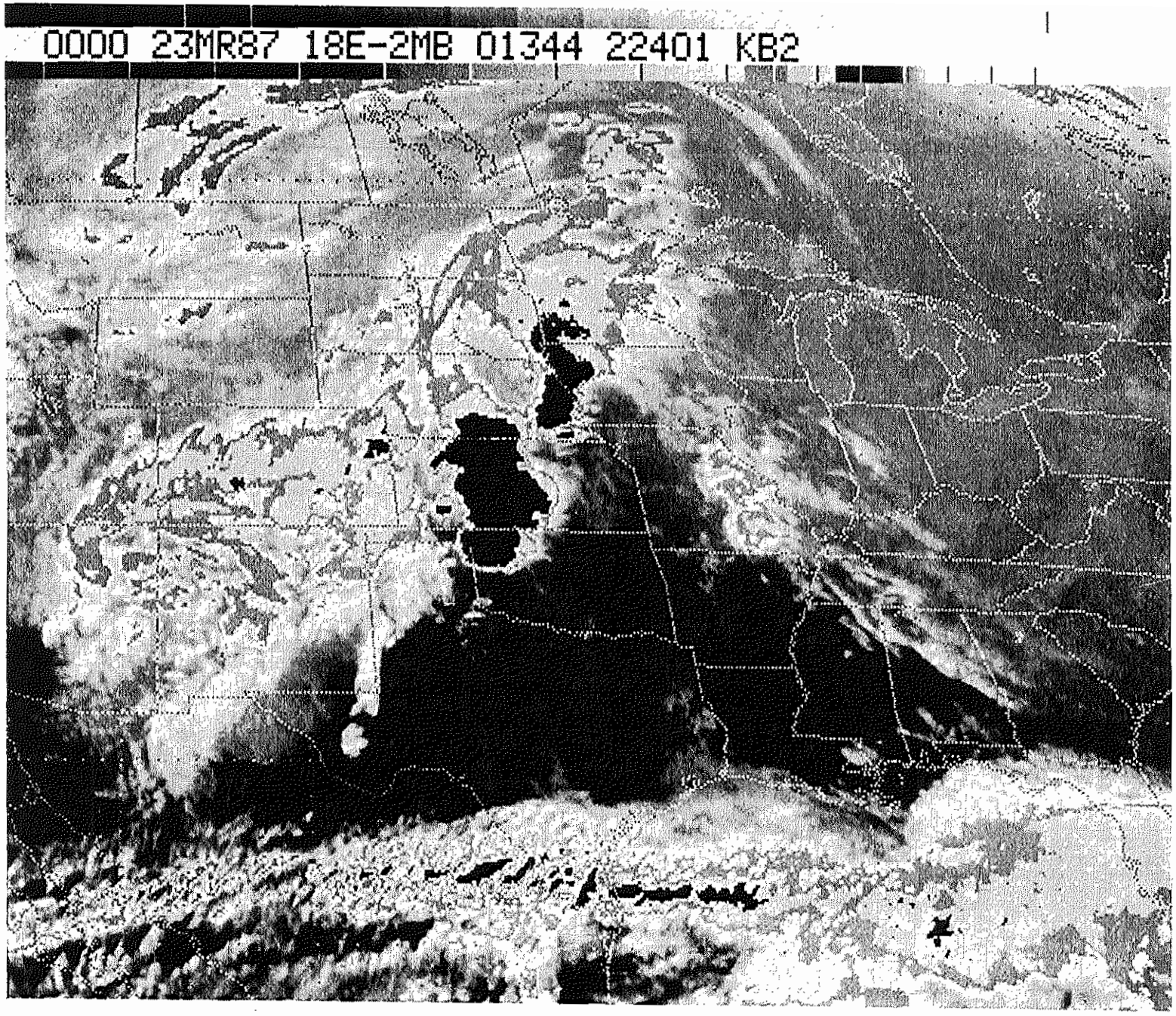

Figure 23. Enhanced infrared satellite image 23 March 1987 0000 UTC.

Comparison of Figures 20 and 22 indicates that the region of lowest static stability was located over western Texas, immediately downstream from a strong maximum in Q-vector convergence thus suggesting that omega was acting to decrease static stability through "stretching," or the vertical velocity term of (8). The result was a thermodynamic structure favorable for convection. Another weak maximum of Q-vector convergence may be noted just west of the area of strongest convection indicating the presence of a weak short wave trough, or perhaps noise in the analysis.

As the evening progressed, additional severe storms developed southward into southwest Texas ahead of the surface cold front which entered west Texas after 23/0000 UTC.

Summary

In summary, evidence has been presented to suggest large-scale differential advections of temperature and moisture were important in the production and maintenance of an environment suitable for deep moist convection.

Furthermore, the convection was observed to occur in an area characterized by weak forcing for quasi-geostrophic omega, suggesting mesoscale vertical motions associated with the surface dryline were responsible for convective initiation.

The case of March 22, 1987 also illustrates the relationship of quasi-geostrophic omega, as implied by Q-vector divergence, and modification of static stability through the vertical velocity term of (8). The observation that the lowest static stabilities, and hence steepest lapse rates, were immediately downstream from the implied omega rise center suggests they were, at least in part, dynamic in origin and associated with the quasi-geostrophic vertical motion field. Here the primary effect of the approaching shortwave trough was to increase buoyant energy in the severe storm region, and to do so before the associated maximum of rising vertical velocities arrived.

4.2 The Case of Maximum Observed Forcing -- April 26-27, 1984

During the evening of April 26 and early morning hours of April 27, 1984 severe thunderstorms produced eleven tornadoes across central and eastern Oklahoma (Figure 24). The first tornado touched down in southwest Logan county at 26/2353 UTC and the final tornado lifted shortly after 27/0830 UTC in Latimer county. Between 27/0400 and 27/0430 UTC an F4

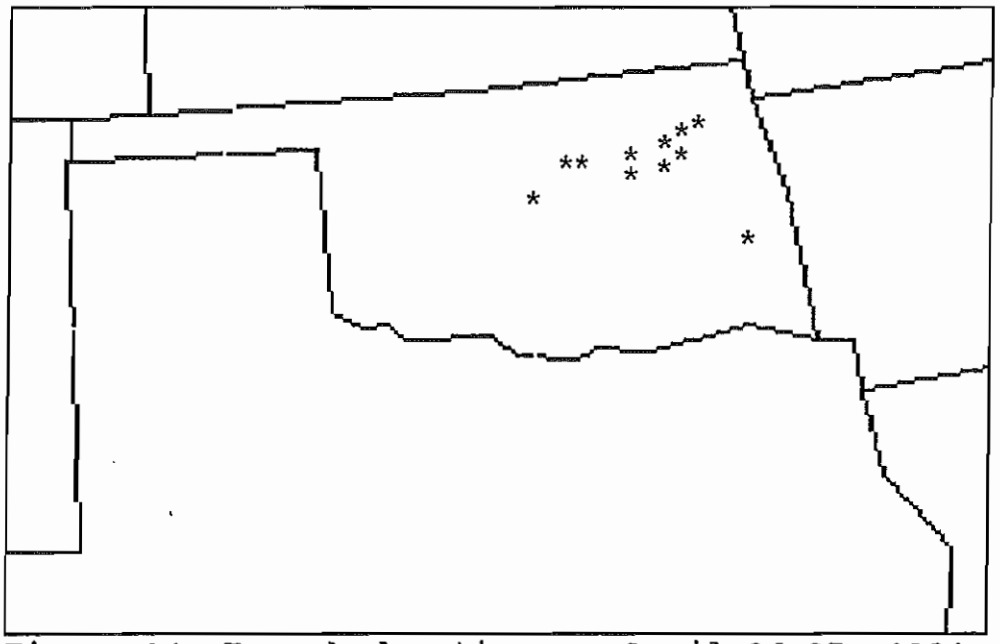

Figure 24. Tornado locations on April 26-27, 1984.

tornado struck portions of Creek and Pawnee counties, causing three fatalities. Eight fatalities occurred shortly before 27/0600 UTC when an F3 tornado destroyed sections of Morris, Oklahoma. Large hail, up to 11 cm in diameter, accompanied a few of the storms.

Upper-air data valid 26/1200 UTC indicated a sharp longwave trough centered over the Rocky mountains. Embedded within the longwave were several shortwave troughs, propagating from southwest to northeast. Figure 25 depicts the observed 700 mb height field and analysis of 700 mb layer-averaged Q-vector divergence. One shortwave was evident over the Texas panhandle, while another appeared to be approaching southwest Texas from northern Mexico. Actual height values and Q-vector calculations associated with the second wave are questionable due to the relative sparseness of Mexican data and the proximity of the wave to the boundary of the analysis grid.

At 850 mb, the moist axis extended from Louisiana to Iowa (Figure 26). Figure 27 depicts the analysis of moisture advection. Although moisture advection calculations suggest

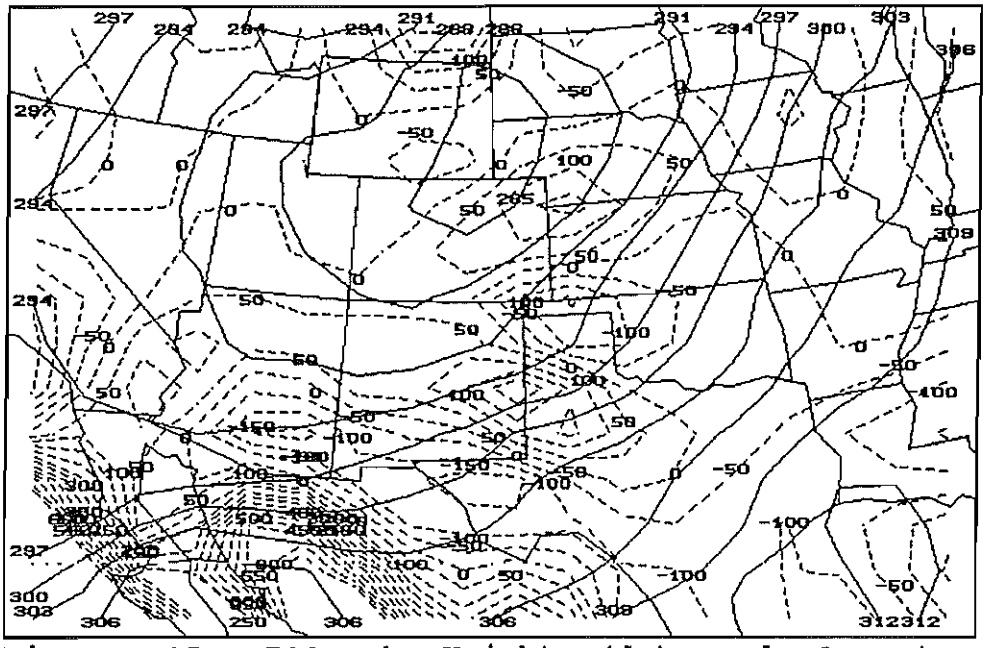

Figure 25. 700 mb Height (dm) and Q-vector Divergence (10-17 s-3 mb-1) 26 April 1984 1200 UTC.

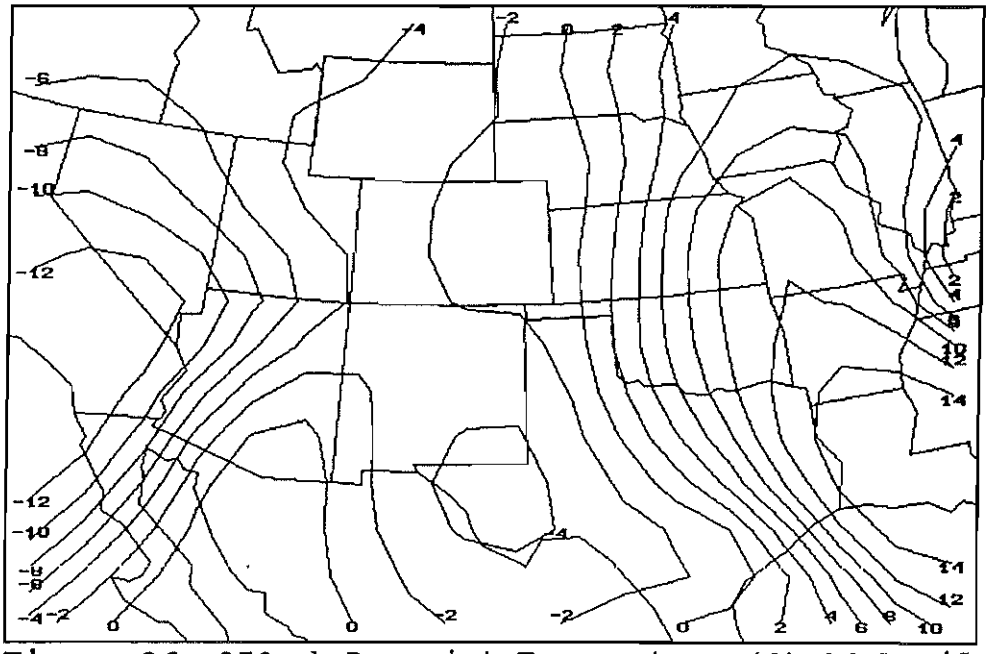

Figure 26. 850 mb Dewpoint Temperature (C) 26 April 1984 1200 UTC.

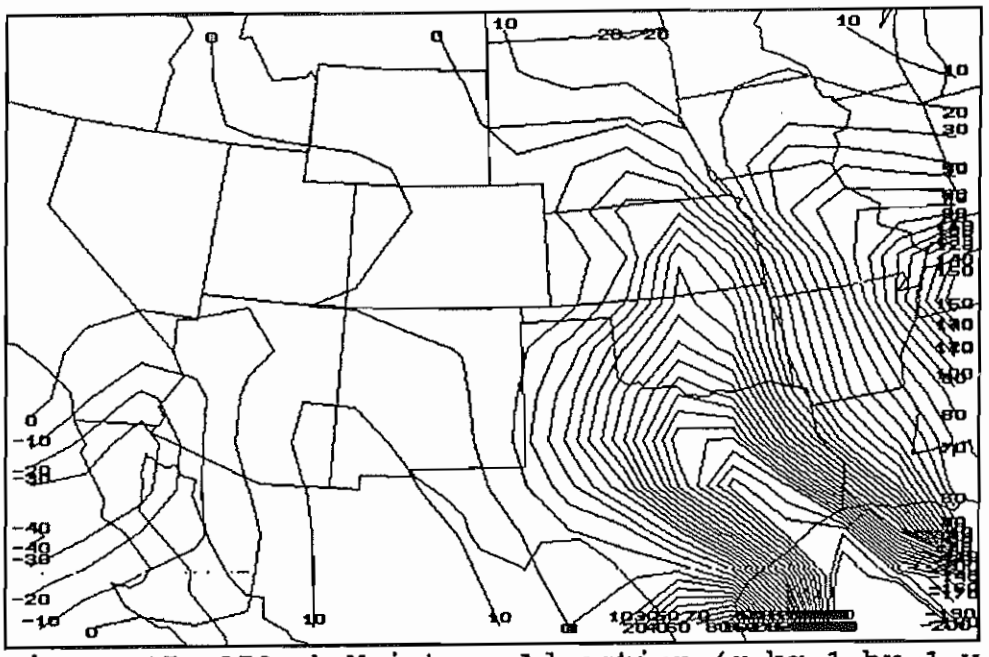

Figure 27. 850 mb Moisture Advection (g kg-1 hr-1 x 10) 26 April 1984 1200 UTC.

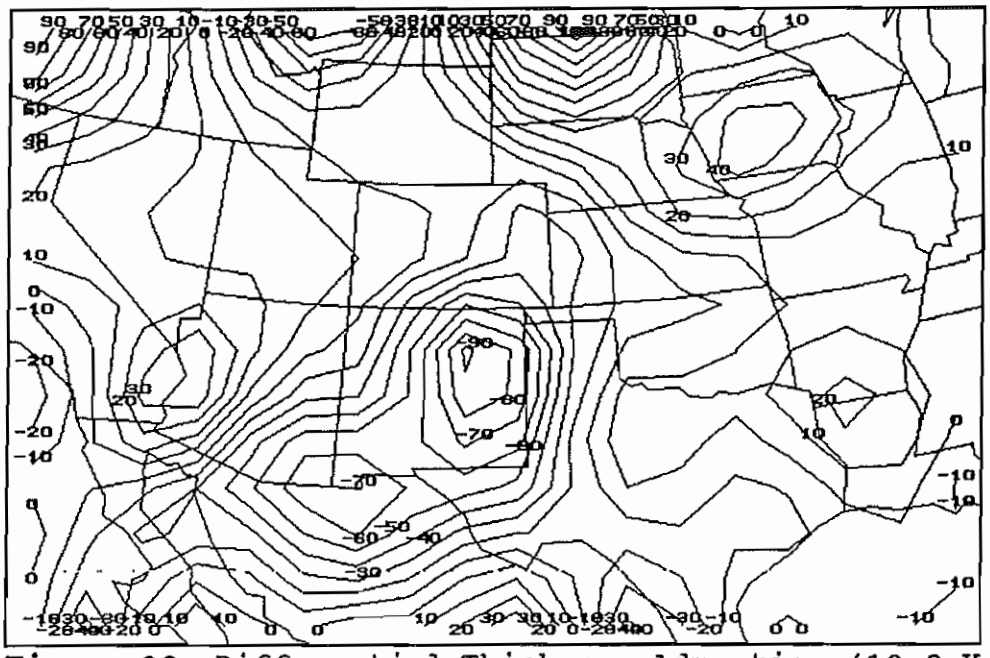

Figure 28. Differential Thickness Advection (10-2 K hr-1 dp-1) 26 April 1984 1200 UTC.

decreasing values of moisture over Oklahoma, and hence buoyant energy, calculations of DTA (Figure 28) indicate values greater than zero throughout most of the study region, implying decreasing static stability (increasing buoyant energy). The large negative values of moisture advection are attributable to a strong 850 mb wind field which contained a westerly component, parallel to the gradient of moisture.

Examination of the 1200 UTC surface analysis (Figure 29) revealed a stationary front lying from central Kansas southwestward into southeast New Mexico. A dryline intersected the front in the eastern Texas Panhandle then extended southward into Rio Grande Valley. In contrast to the negative values of moisture advection observed at 850 mb, the surface analysis indicated higher values of dewpoint temperature advecting into central and eastern Oklahoma.

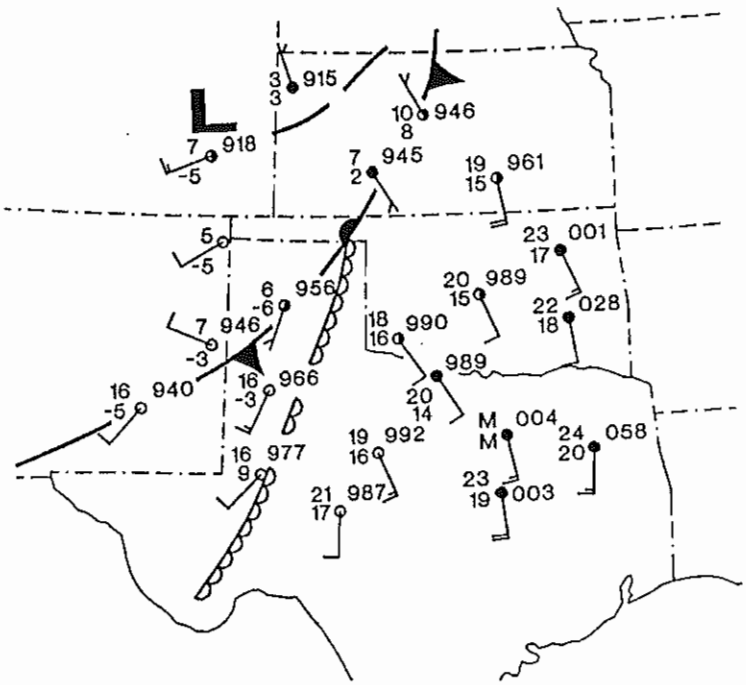

Figure 29. Surface weather analysis 26 April 1984 1200 UTC. Temperatures and dewpoints in degrees Celsius, wind speed in knots, pressure in tenths of millibars.

The combination of higher dewpoint temperatures advecting northward below 850 mb, and moderately strong DTA, provides evidence that the large-scale flow field was acting to increase buoyant energy and enhance the convective environment across Oklahoma.

Layer-averaged stability (Figure 30) at 1200 UTC indicated low values of static stability throughout the study region of Oklahoma and Texas. Comparison with the 700 mb layer-averaged Q-vector divergence field revealed little apparent correlation between static stability and implied omega vertical velocity extrema. This result occurs because omega becomes less effective in modifying static stability as $\partial\theta/\partial p$ approaches zero.

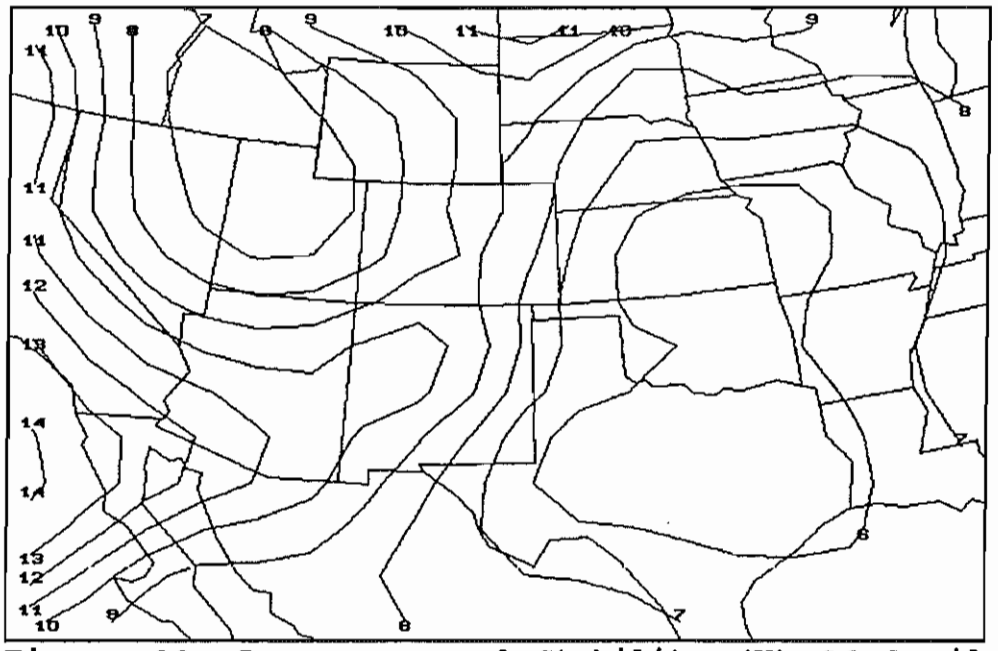

Figure 30. Layer-averaged Stability (K) 26 April 1984 1200 UTC.

By 2100 UTC the surface dryline had progressed into western Oklahoma where thunderstorms were initiated, presumably in the region of boundary layer convergence near the dryline. Additional severe thunderstorms developed around 26/2300 UTC in northwest Oklahoma near an advancing cold front (stationary at 1200 UTC). Detailed discussions of specific storm events during the evening of April 26 and morning of April 27, 1984 may be found in Burgess and Curran (1985) and Woodall and Bluestein (1988).

An analysis of upper-air data from 0000 UTC April 27, 1984 identified a strong negatively tilted shortwave trough in the 700 mb height field over west Texas (Figure 31). Overlaid values of 700 mb layer-averaged Q-vector divergence are the **maximum observed** in the study region for the entire 25 event data set. Convergent values near 580 10-17 s-3 mb-1 were analyzed over the Oklahoma Panhandle, implying strong quasi-geostrophic ascent. Comparison of the Q-vector divergence pattern with analyzed 300 mb divergence of the observed wind (Figure 32) further supported the presence of a strong ageostrophic vertical motion couplet over western Texas and New Mexico.

The analysis of layer-averaged stability (Figure 33) showed a minimum in static stability from eastern Kansas across Oklahoma into southwest Texas. A well defined maximum was observed from the Texas Panhandle into central New Mexico. The minimum (<4 K) over southwest Texas was well correlated with an analyzed maximum in DTA at 0000 UTC (Figure 34) in the same region, indicating quasi-horizontal advections were dominating stability changes there.

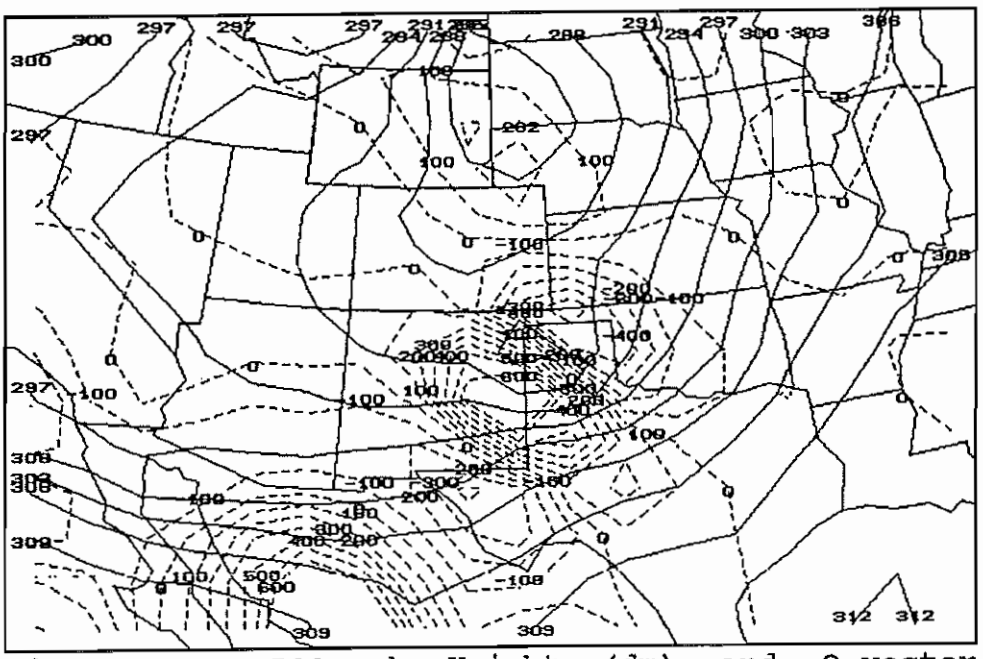

Figure 31. 700 mb Height (dm) and Q-vector Divergence (10-17 s-3 mb-1) 27 April 1984 0000 UTC.

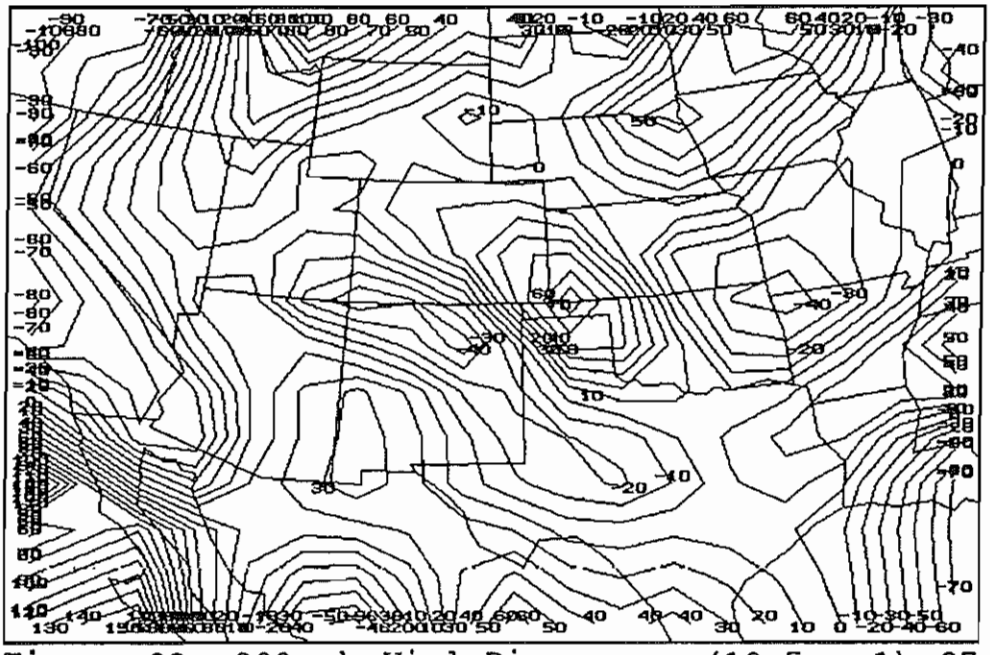

Figure 32. 300 mb Wind Divergence (10-5 s-1) 27 April 1984 0000 UTC.

Changes also were noted in the large-scale wind fields between 1200 UTC and 0000 UTC. Winds aloft across the region were observed to increase 10 to 20 knots during the 12 hours, thus increasing the vertical wind shear and enhancing the potential for supercell thunderstorms.

Summary

Evidence was presented which suggests that synoptic-scale motions were acting to create an environment increasingly favorable for convection through differential advections of temperature and moisture, and through changes in static stability associated with vertical motion. However, convection was observed to **initiate** near two mesoscale boundaries; the dryline, and later a cold front.

Values of Q-vector divergence analyzed at 27/0000 UTC were the maximum observed for the entire data set. Remarkable qualitative agreement was found between the pattern of Q-vector forcing and the pattern of divergence calculated from the observed 300 mb wind. This result provides further evidence of the relationship between Q-vectors and ageostrophic circulations.

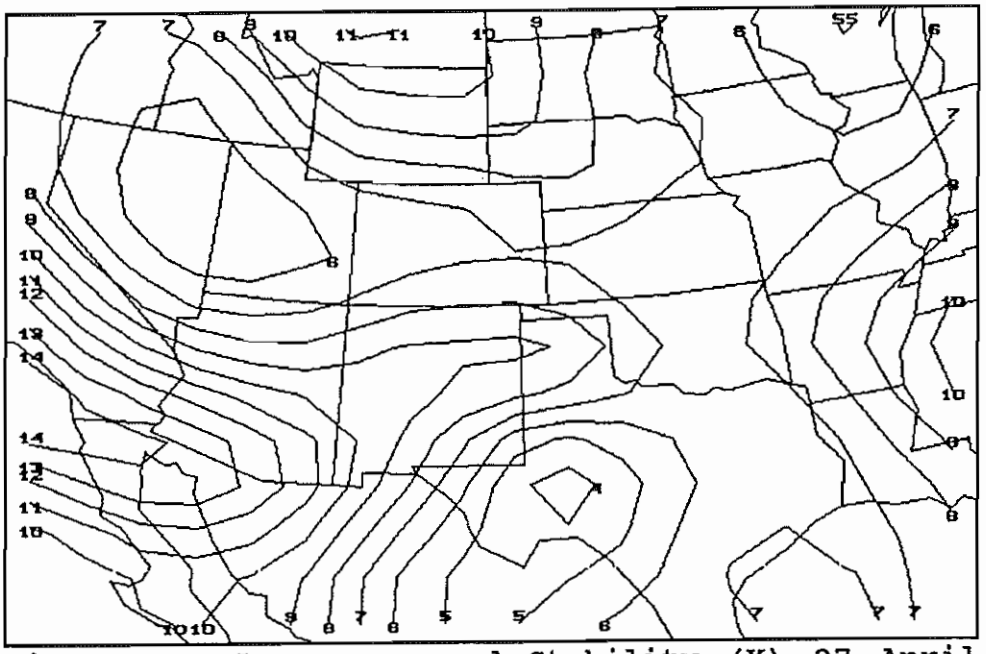

Figure 33. Layer-averaged Stability (K) 27 April 1984 0000 UTC.

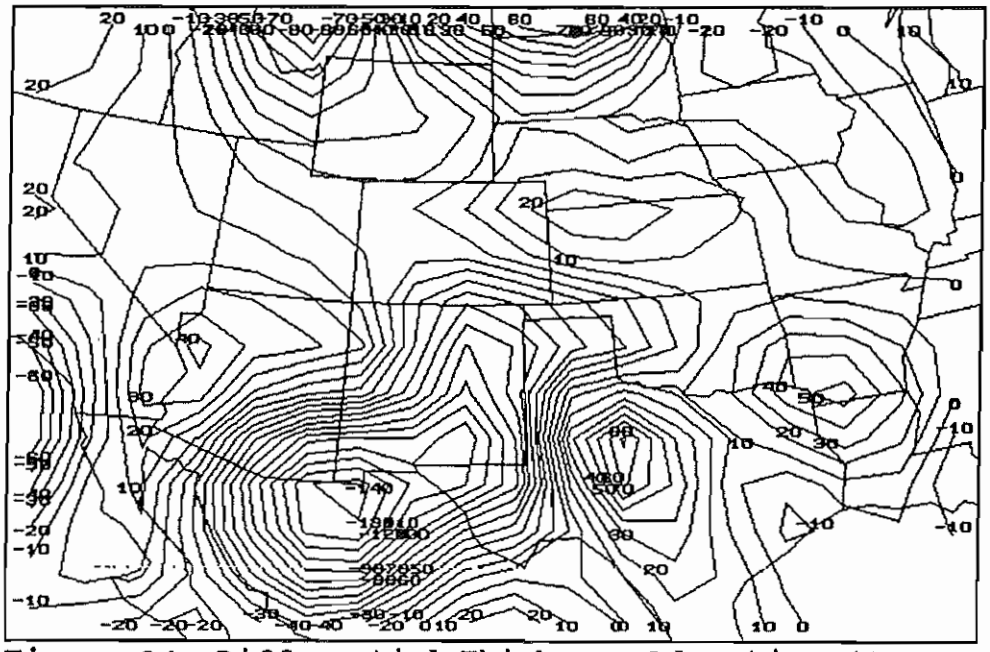

Figure 34. Differential Thickness Advection (10-2 K hr-1 dp-1) 27 April 1984 0000 UTC.

4.3 A Case of Minimum Observed Forcing -- October 31, 1984

On the evening of October 31, 1984, four tornadoes touched down in Oklahoma, three in the northwest, and one in the southeast (Figure 35). The strongest tornado, an F3, occurred in Woodward and Major counties of northwest Oklahoma between 31/2356 UTC and 01/0035 UTC.

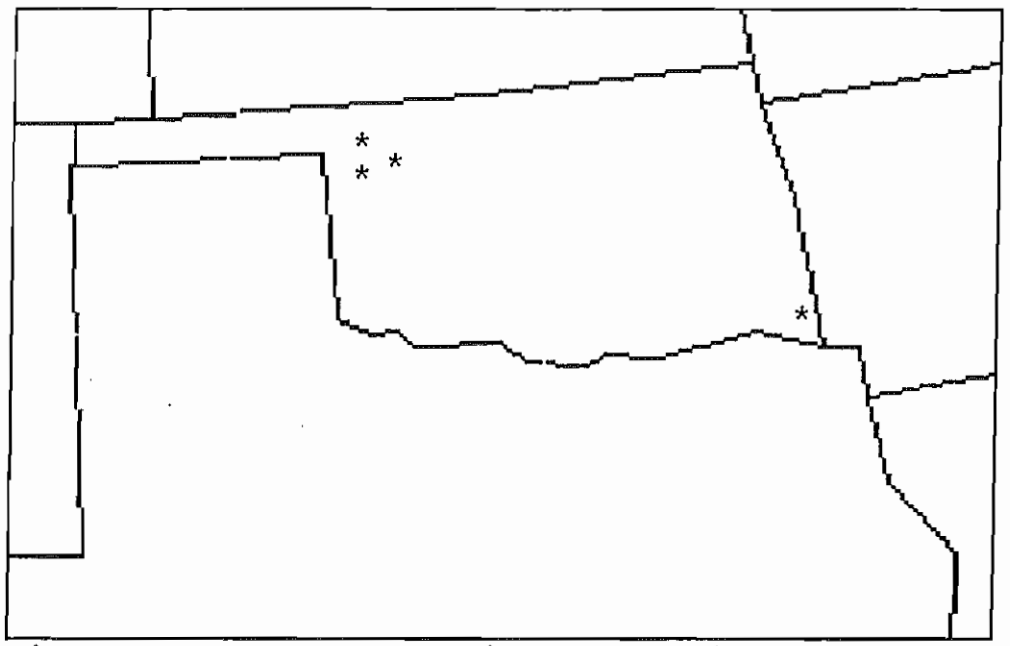

Figure 35. Tornado locations on October 31, 1984.

On the morning of October 31, 1984 a potentially unstable airmass already was present across Oklahoma. Upper air data valid at 1200 UTC indicated 850 mb dewpoint temperatures (Figure 36) up to 12 degrees Celsius, with layer-averaged stability (Figure 37) near 10 K.

A longwave trough was evident over the western United States with an embedded shortwave present from Colorado into Northwest Texas. Figure 38 provides the height analysis for 700 mb valid at 1200 UTC overlaid with the 700 mb layer-averaged Q-vector divergence field. Maxima and minima for omega forcing ($\omega<0$) were located over the Oklahoma panhandle and from Colorado into New Mexico, respectively.

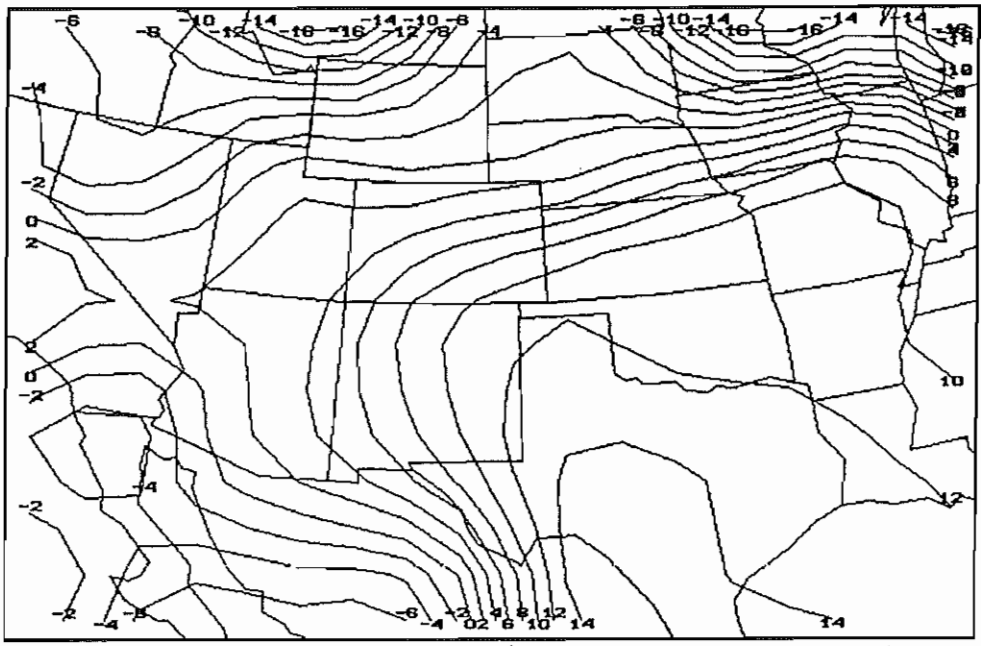

Figure 36. 850 mb Dewpoint Temperature (C) 31 October 1984 1200 UTC.

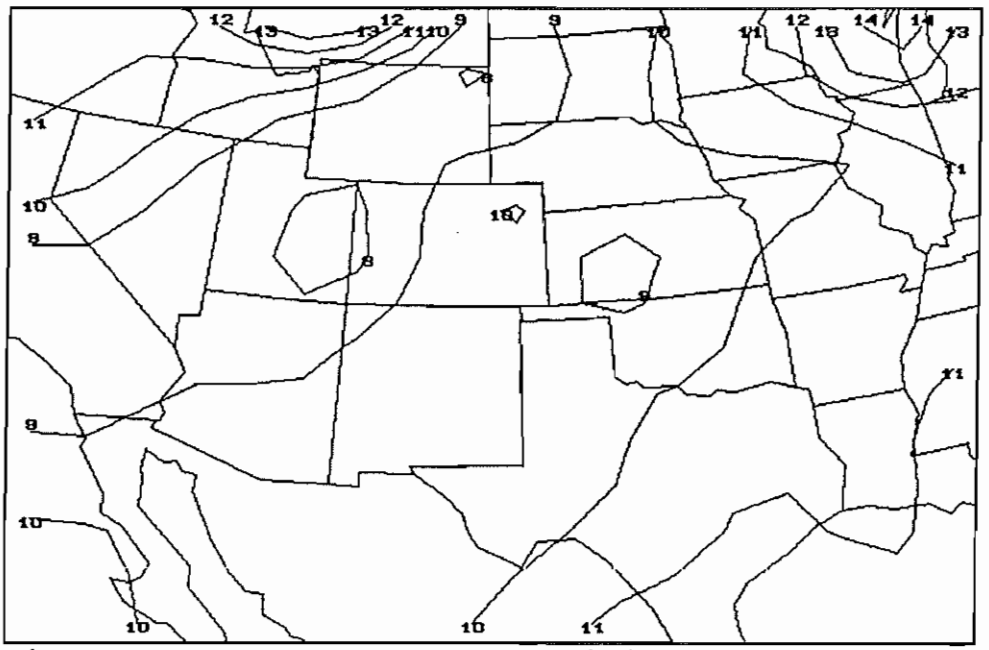

Figure 37. Layer-averaged Stability (K) 31 October 1984 1200 UTC.

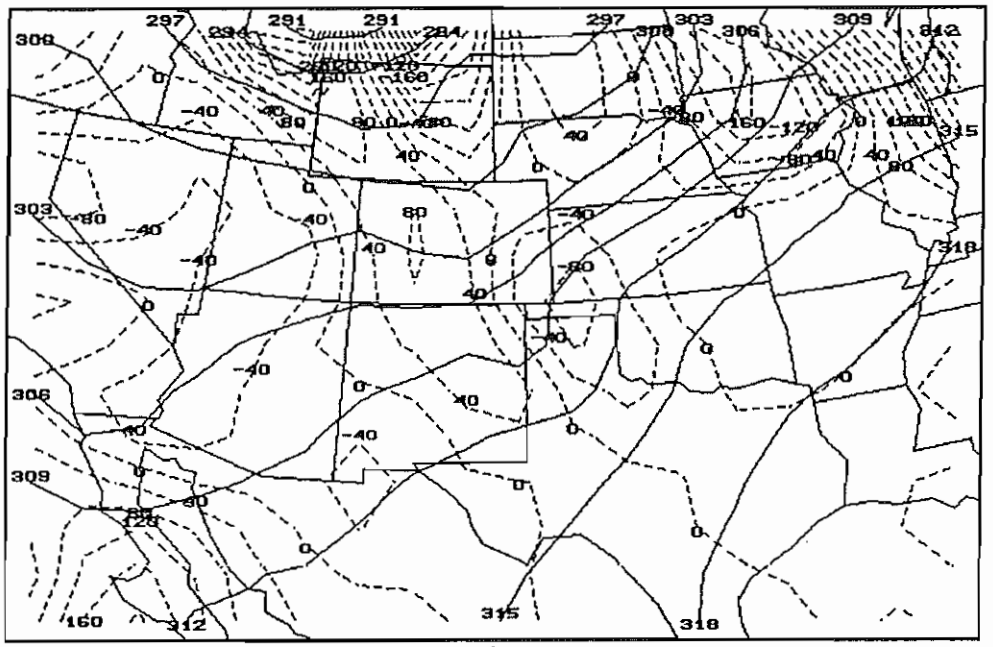

Figure 38. 700 mb Height (dm) and Q-vector Divergence (10-17 s-3 mb-1) 31 October 1984 1200 UTC.

Further inspection of the upper air data revealed several factors acting to enhance the atmospheric thermodynamic structure in favor of deep moist convection.

Comparison of the 700 mb layer-averaged Q-vector divergence and layer-averaged stability suggests that the vertical motion field was acting to decrease static stability over southwest Kansas and northwest Oklahoma. The presence of a minimum in layer-averaged stability (< 9K) over southwest Kansas, immediately downstream from the implied omega rise center supports this contention.

Furthermore, analyses of DTA (Figure 39) and advections of 850 mb and 500 mb moisture (Figures 40 and 41, respectively) indicate that quasi-horizontal advections also were acting to decrease static stability and increase buoyant energy.

By 01/0000 UTC, convection was underway in the vicinity of a weak trough of low pressure extending from northwest Oklahoma into eastern Kansas (Figure 42). Additional convection was present over southeast Oklahoma. The latter area of convection did not have a readily apparent association with any feature in the 01/0000 UTC surface data.

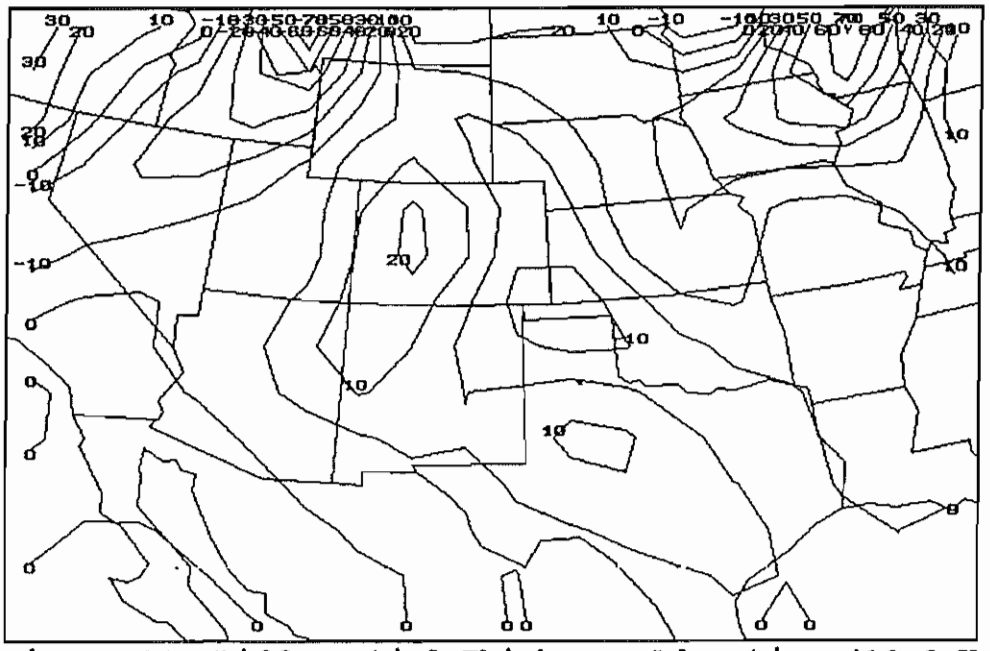

Figure 39. Differential Thickness Advection (10-2 K hr-1 dp-1) 31 October 1984 1200 UTC.

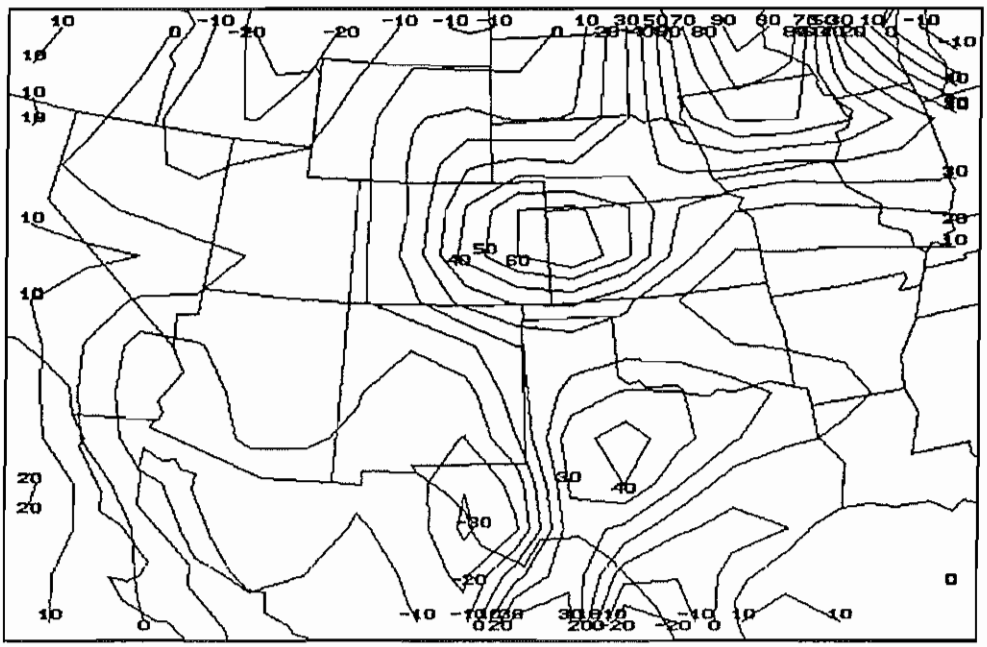

Figure 40. 850 mb Moisture Advection (g kg-1 hr-1 x 10) 31 October 1984 1200 UTC.

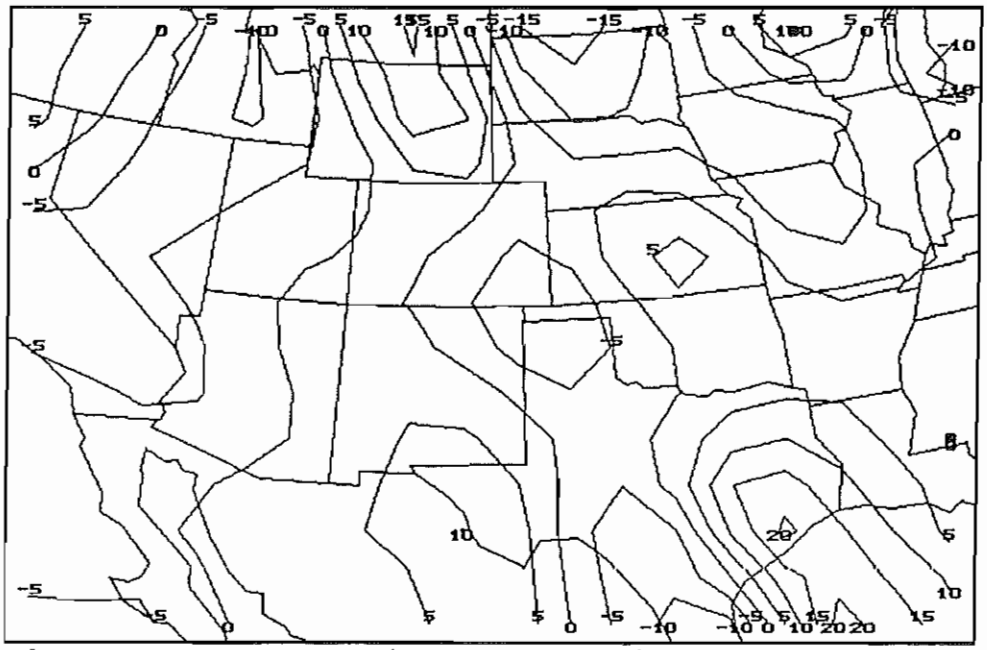

Figure 41. 500 mb Moisture Advection (g kg-1 hr-1 x 10) 31 October 1984 1200 UTC.

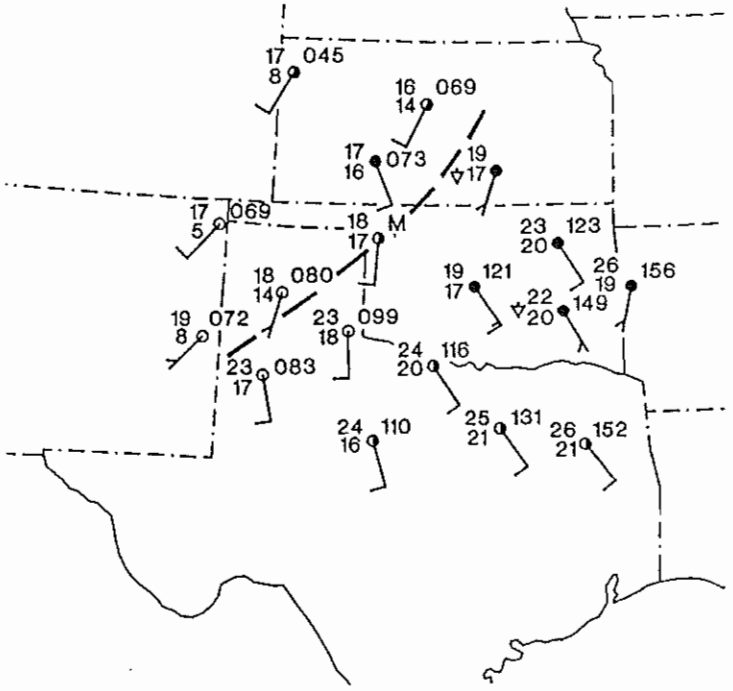

Figure 42. Surface weather analysis 01 November 1984 0000 UTC. Temperatures and dewpoints in degrees Celsius, wind speed in knots, pressure in tenths of millibars.

Upper-air data valid at 01/0000 UTC and within one hour of F3 tornadogenesis in northwest Oklahoma indicated that previously noted mechanisms were effective in enhancing the convective environment.

The analysis of 850 mb dewpoint temperatures (Figure 43) indicated increases near two degrees Celsius across Oklahoma during the preceding 12 hours. A similar increase was observed in 850 mb temperature (Figure 44), though changes in layer-averaged stability (Figure 45) were negligible as low-level warming was offset by warming aloft.

Near the time of F3 tornadogenesis, an analysis of 700 mb layer-averaged Q-vector divergence (Figure 46) provided the **minimum forcing** values for rising motion that was observed in the entire 25 event data set (similar values also were noted on April 25, 1985 and May 26, 1987). Note that the maximum forcing for $\omega < 0$ has shifted into northern Kansas leaving values near -30 10-17 s-3 mb -1 over the northwest portion of Oklahoma. Also note the minimum in layer-averaged stability over southern Nebraska suggesting the vertical motion contribution to $\partial\sigma/\partial t$ has shifted northward, as well.

Even weaker forcing for omega was present over southeast Oklahoma where a cluster of thunderstorms produced flash flooding and an isolated weak (F1) tornado.

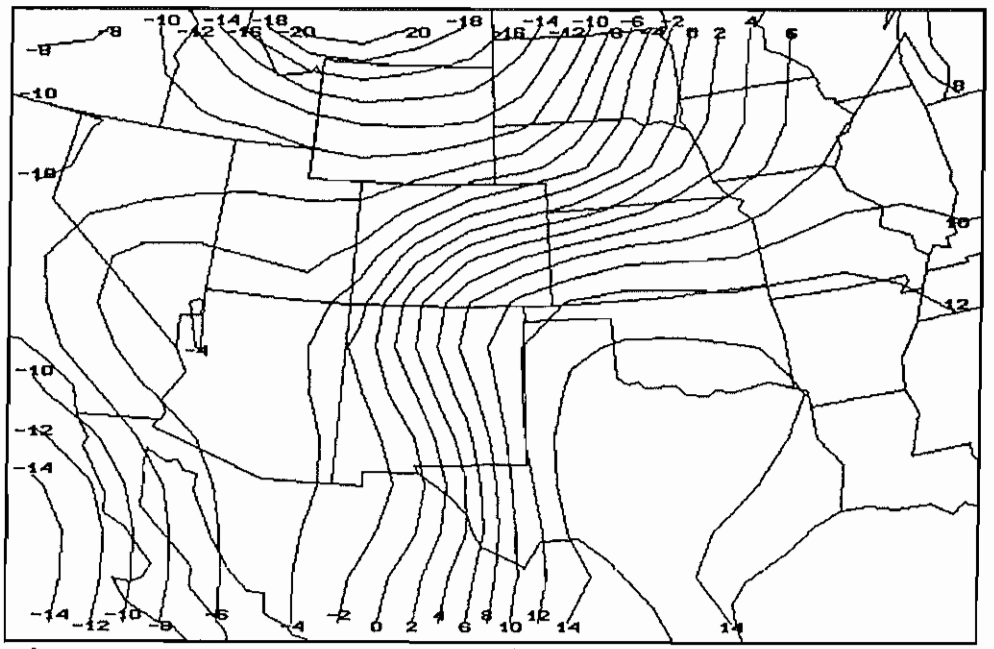

Figure 43. 850 mb Dewpoint Temperature (C) 01 November 1984 0000 UTC.

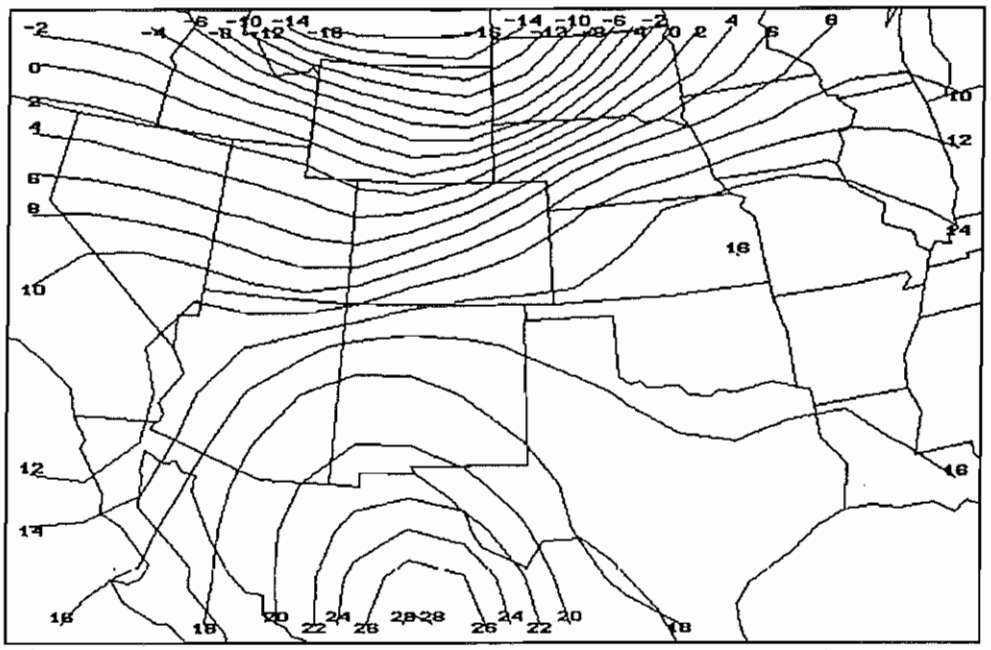

Figure 44. 850 mb Temperature (C) 01 November 1984 0000 UTC.

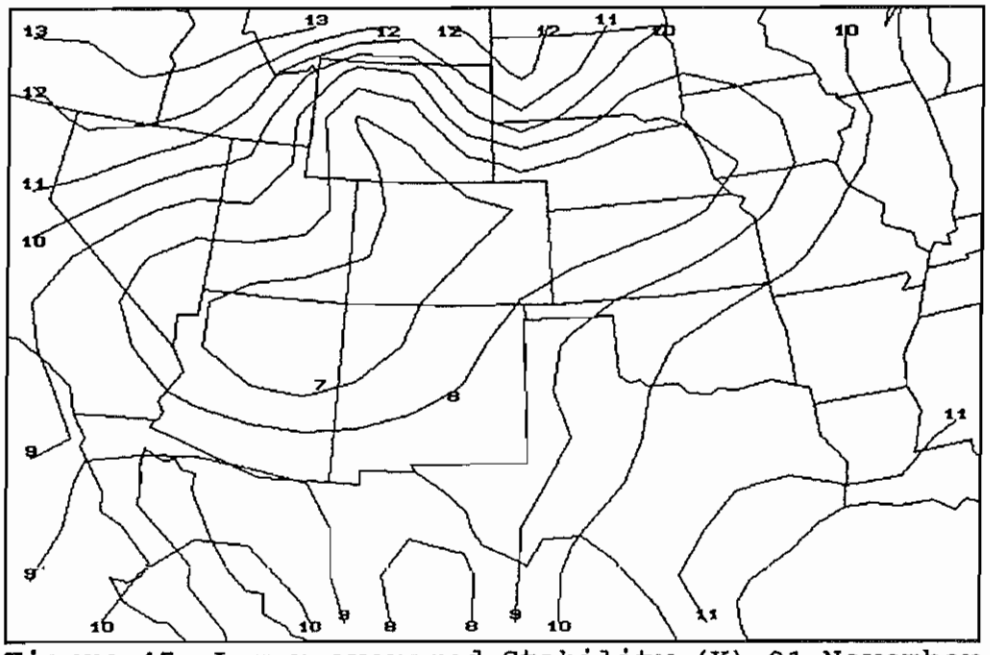

Figure 45. Layer-averaged Stability (K) 01 November 1984 0000 UTC.

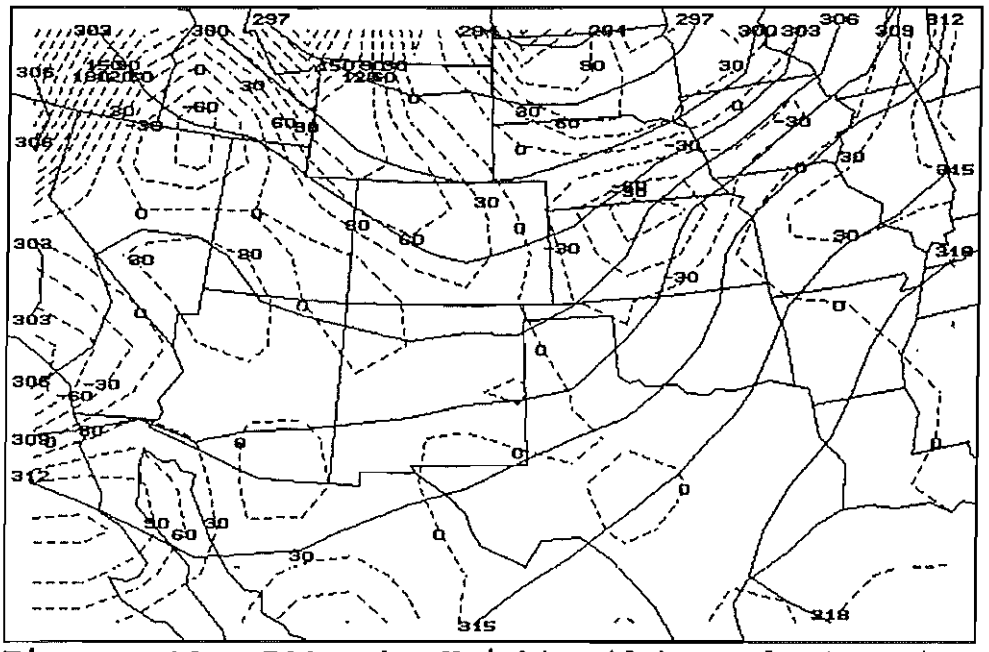

Figure 46. 700 mb Height (dm) and Q-vector Divergence (10-17 s-3 mb-1) 01 November 1984 0000 UTC.

Summary

Available data suggests large-scale quasi-geostrophic motions were important in the enhancement and maintenance of an environment favorable for deep moist convection. Furthermore, the location of the convection in northwest Oklahoma, relative to the surface low pressure trough, suggests mesoscale convergence near the trough was the primary mechanism working to initiate and focus convection. In southeast Oklahoma, the mesoscale influence responsible for convective initiation was unclear.

5.4 The Strongest Tornado Event -- April 2, 1982

The most devastating outbreak of tornadoes to strike the study area during the 1980s occurred across eastern Oklahoma and eastern Texas on April 2, 1982. A total of 16 tornado touchdowns were recorded (Figure 47), seven of which were rated F3, or higher. The most powerful tornado, an F5, began at 2150 UTC and tracked 53 miles across Choctaw and McCurtain counties of southeastern Oklahoma. Although no fatalities

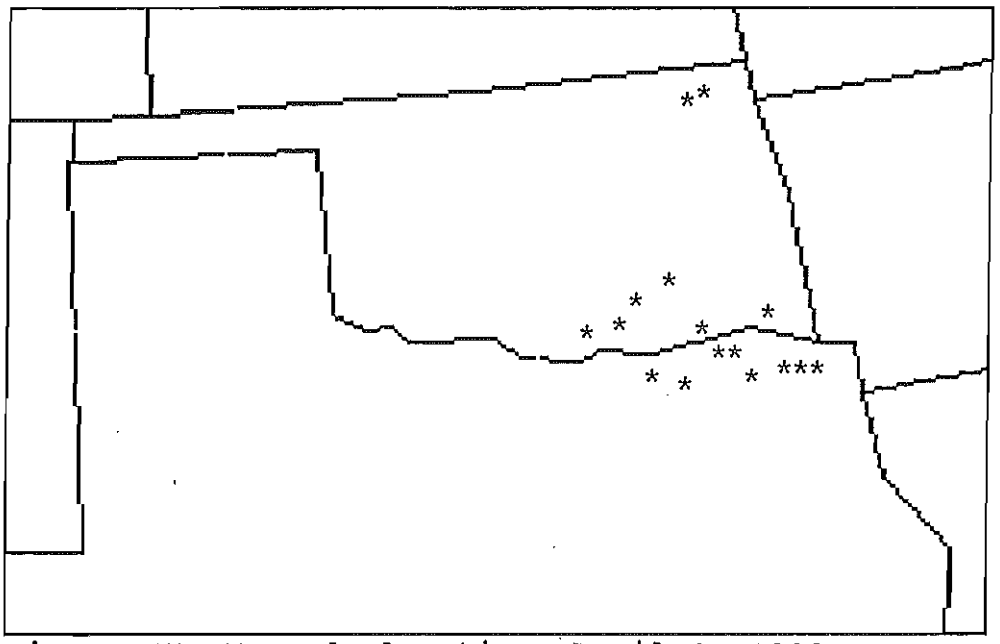

Figure 47. Tornado locations April 2, 1982.

occurred with this tornado, another tornado (F4), swept through Paris, Texas between 2100 UTC and 2130 UTC, killing eight persons.

Infrared satellite imagery from 1130 UTC (Figure 48) showed cold-topped convection already underway across portions of northeast Texas. These storms produced large hail and were the first of two groups of severe storms to affect Oklahoma and Texas that day. Also evident in the satellite imagery was a low-level thermal gradient across extreme western Oklahoma and west Texas,indicating cooler morning air west of the surface dryline.

Figure 49 depicts surface weather features at 1200 UTC, including the dryline, a maritime polar front moving through New Mexico, a continental polar front moving southward through Wyoming, and low pressure centers in South Dakota and northeast Colorado. Low-level moisture, reflected by dewpoint temperatures greater than 15 degrees Celsius, extended as far northward as northern Kansas.

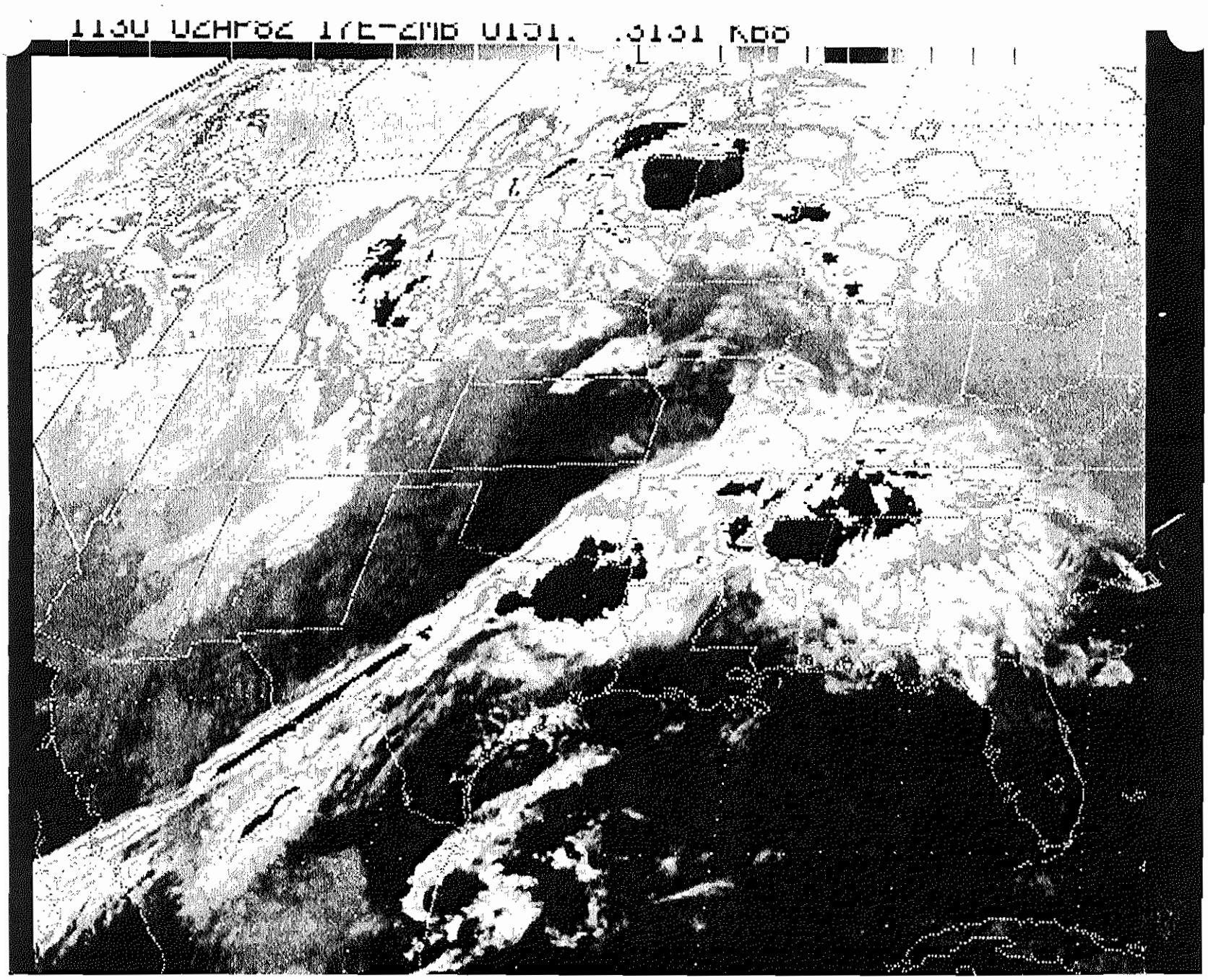

Figure 48. Enhanced infrared satellite image 02 april 1982 1130 UTC.

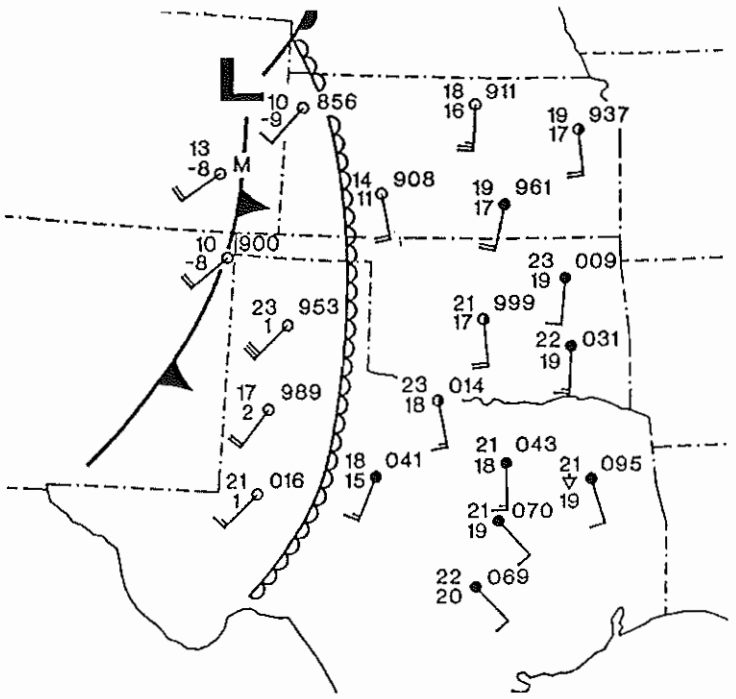

Figure 49. Surface weather analysis 02 April 1982 1200 UTC. Temperatures and dewpoints in degrees Celsius, wind speed in knots, pressure in tenths of millibars.

Upper-air data at 1200 UTC indicated a deep longwave trough over the Rocky Mountains (Figure 50). A well defined moist axis at 850 mb was located from southern Texas across eastern Oklahoma (Figure 51). Layer-averaged stability (Figure 52) showed a pronounced minimum in static stability from Texas into the Dakotas, while a maximum was located over Arizona.

The 1200 UTC analysis of DTA (Figure 53) indicated positive values across eastern sections of the study region, while negative values were found throughout the southern Rockies and high plains. Comparison with Figure 52 suggests that quasi-horizontal advection of temperature was acting to decrease static stability with time in the outbreak region. Note that the maxima and minima in the advection field were located immediately downstream from the corresponding minima and maxima in layer-averaged stability. This displacement may be used to infer the direction of propagation for the stability maxima and minima.

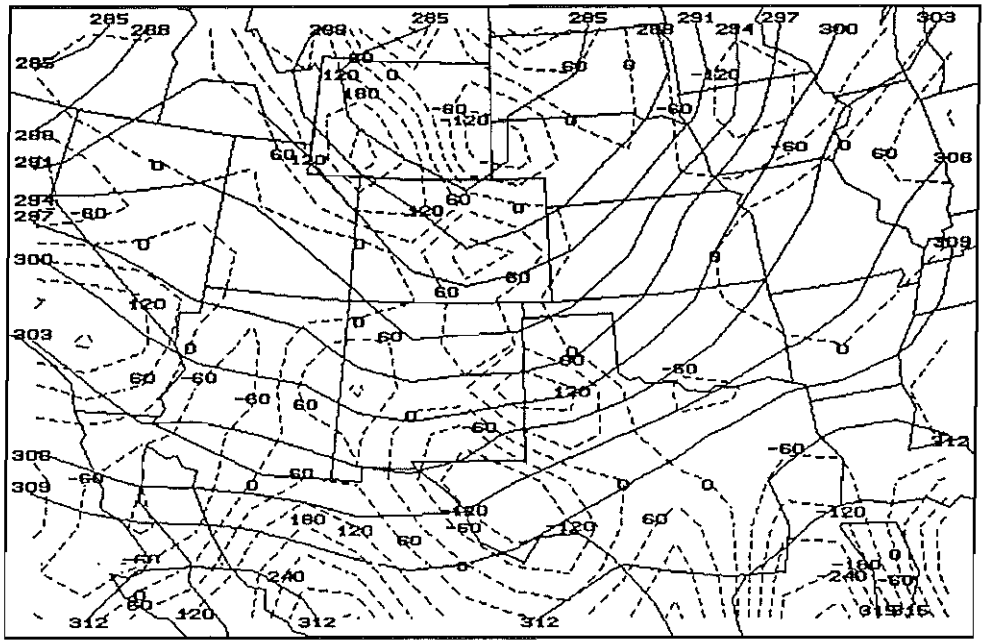

Figure 50. 700 mb Height (dm) and Q-vector Divergence (10-17 s-3 mb-1) 02 April 1982 1200 UTC.

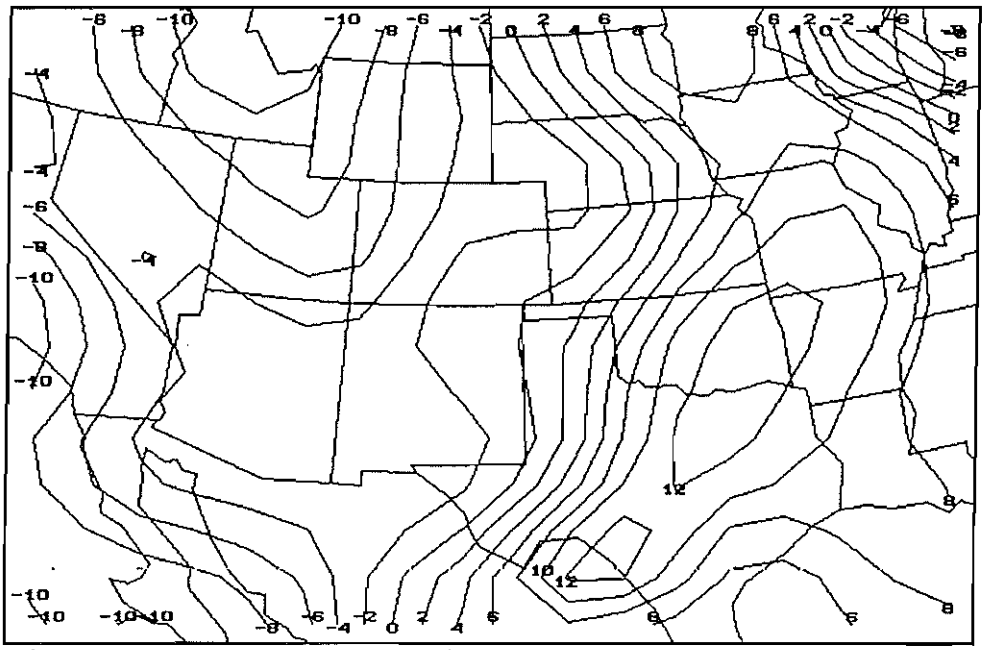

Figure 51. 850 mb Dewpoint Temperature (C) 02 April 1982 1200 UTC.

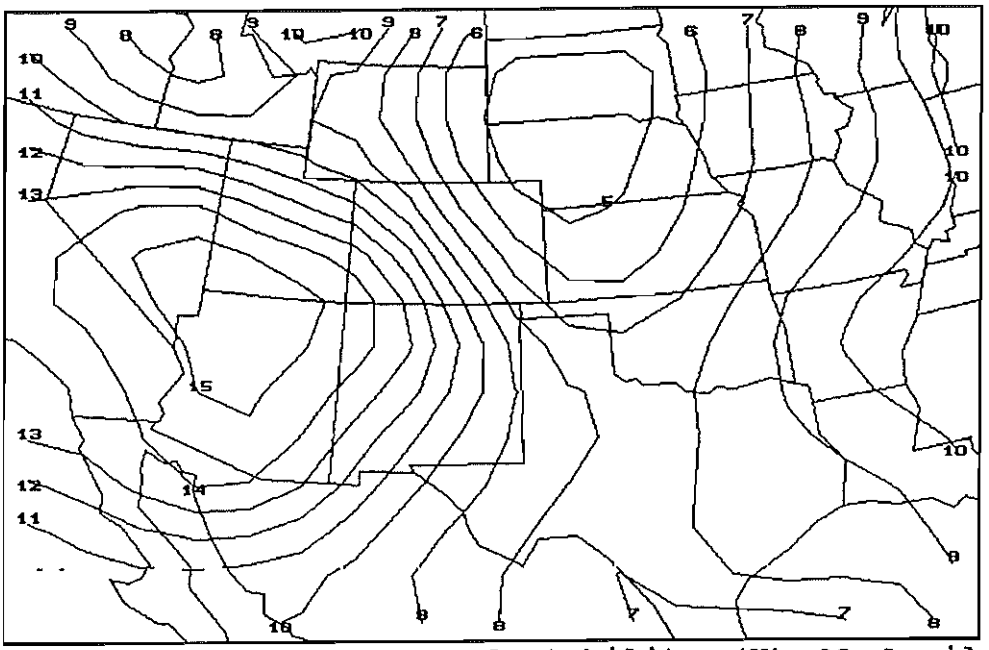

Figure 52. Layer-averaged Stability (K) 02 April 1982 1200 UTC.

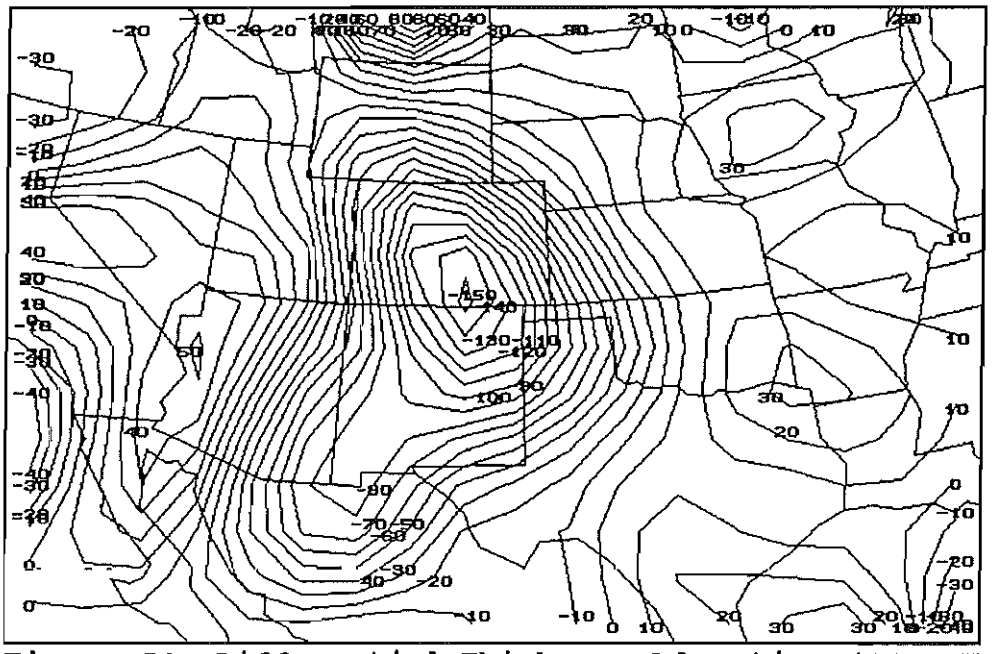

Figure 53. Differential Thickness Advection (10-2 K hr-1 dp-1) 02 April 1982 1200 UTC.

The analysis of 700 mb layer-averaged Q-vector divergence (Figure 50) indicated a region of forcing for rising motion from central New Mexico into southwest Texas, reflecting the presence of a shortwave trough. Weak convergence of Q also was analyzed near the convection across northeast Texas.

As the morning progressed, the northeast Texas convection moved into southeast Oklahoma and produced large hail before weakening and moving eastward.

The second round of severe convection developed shortly after 1800 UTC as the maritime polar front overtook the dryline in central Oklahoma and Texas. Details of the convective evolution may be found in Moller and Boots (1983).

By 03/0000 UTC, the surface weather analysis (Figure 54) indicated the maritime polar front from western Missouri into southern Texas. A strong surface low was over southern Minnesota with a continental polar front extending from eastern Kansas pushing into northwest Texas.

Satellite imagery (Figure 55) indicated the region of strongest convection from Arkansas into northeast Texas. Although the tornado outbreak across eastern Oklahoma and eastern Texas was nearly over by 03/0000 UTC, several interesting details emerged from the upper-air data.

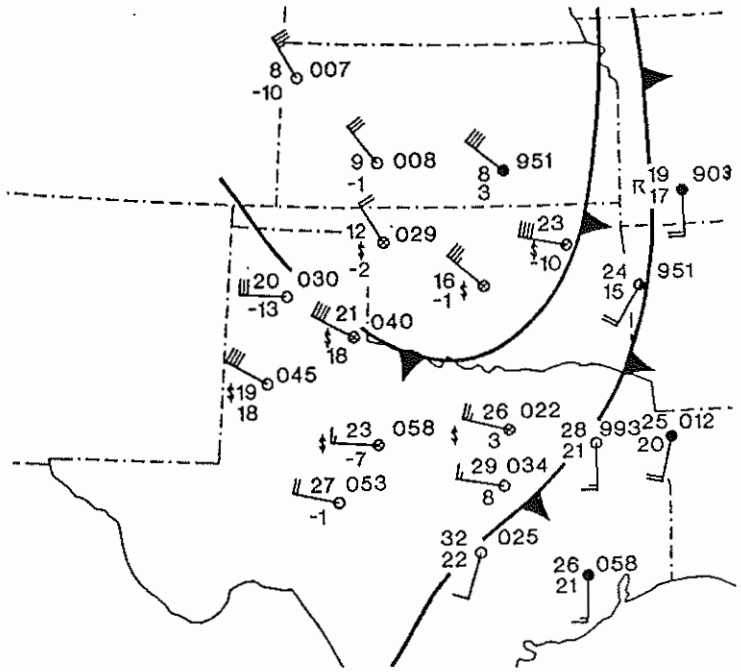

Figure 54. Surface weather analysis 03 April 1982 0000 UTC. Temperatures and dewpoints in degrees Celsius, wind speed in knots, pressure in tenths of millibars.

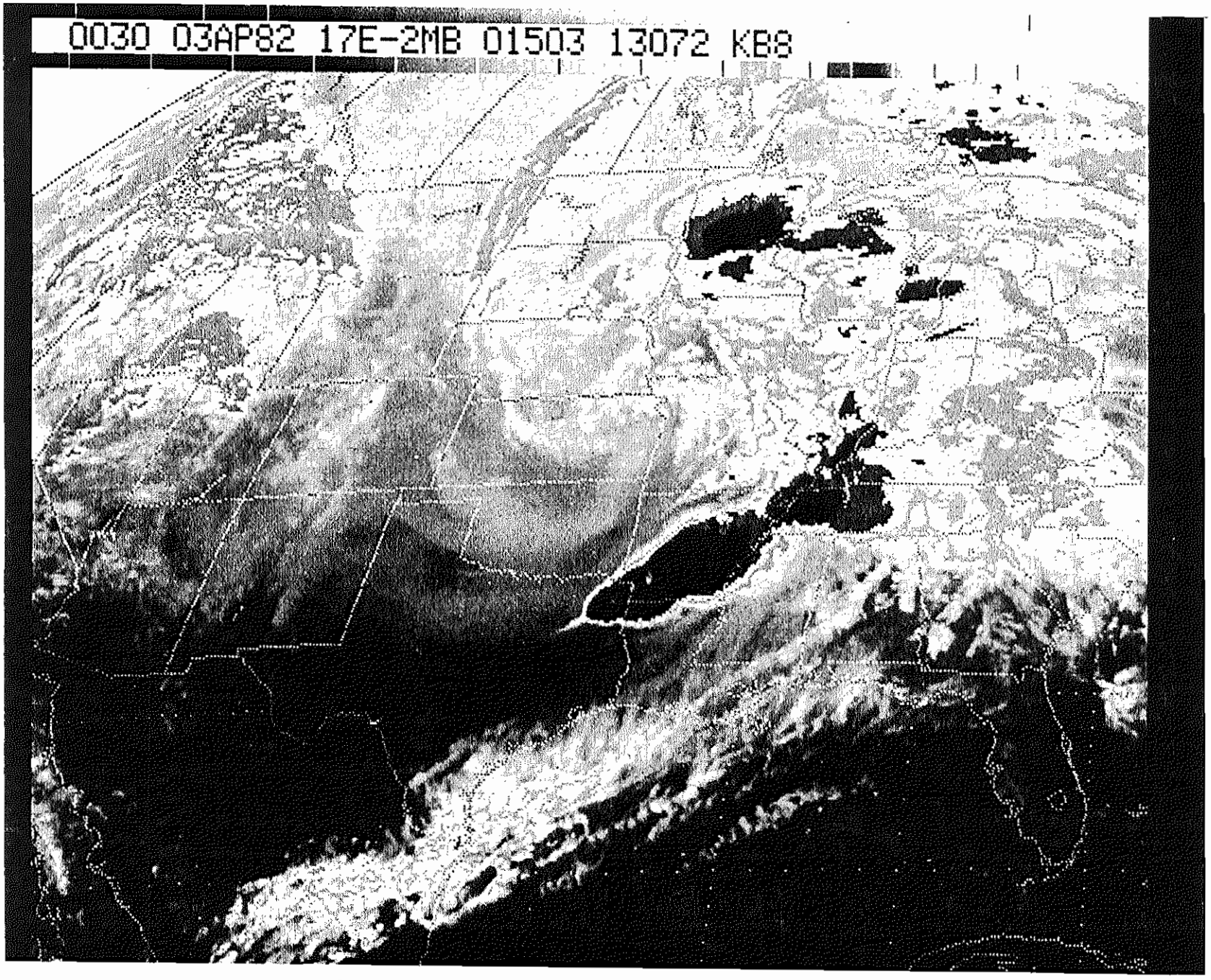

Figure 55. Enhanced infrared satellite image 03 April 1982 0030 UTC.

The analysis of 700 mb height and layer-averaged Q-vector divergence (Figure 56) showed that the strong shortwave trough over the Rocky Mountains at 02/1200 UTC, had moved eastward to extend from northeast Kansas across eastern Oklahoma into northeast Texas. The strongest forcing for rising motion also shifted rapidly eastward and was approaching the Mississippi Valley by 03/0000 UTC.

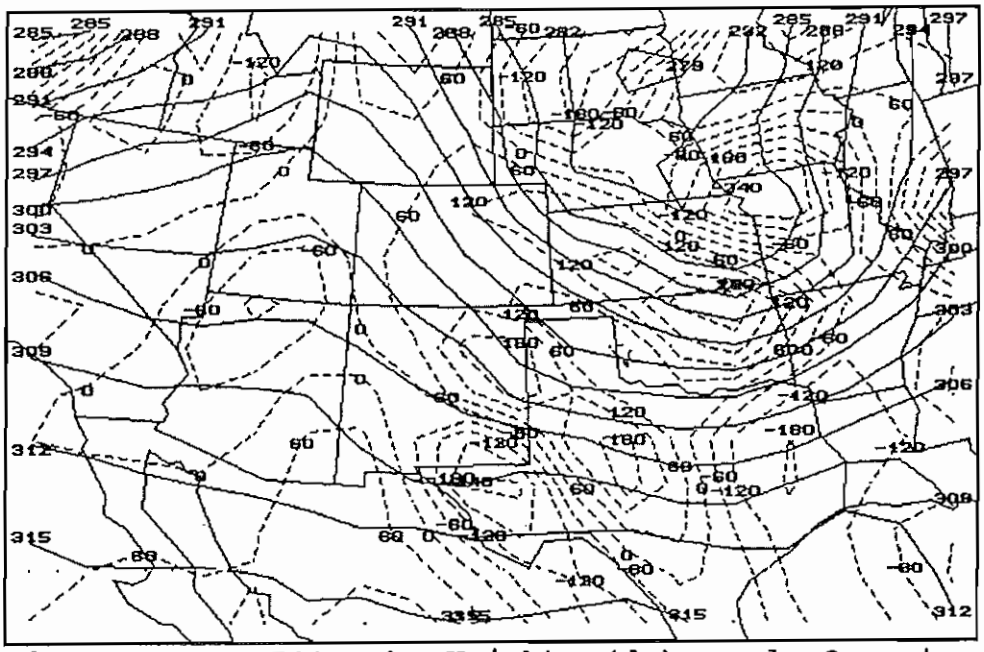

Figure 56. 700 mb Height (dm) and Q-vector Divergence (10-17 s-3 mb-1) 03 April 1982 0000 UTC.

DTA at 03/0000 UTC (Figure 57) showed positive values over the Mississippi Valley, with strongly negative values from Missouri across eastern Oklahoma into Texas suggesting rapid stabilization was occurring.

The combined effects of vertical motion, as implied from the divergence of Q, and quasi-horizontal advections of temperature on static stability are readily apparent in Figure 58. Of particular note was the replacement of the stability minimum over the central Great Plains 12 hours earlier, by a well defined maximum.

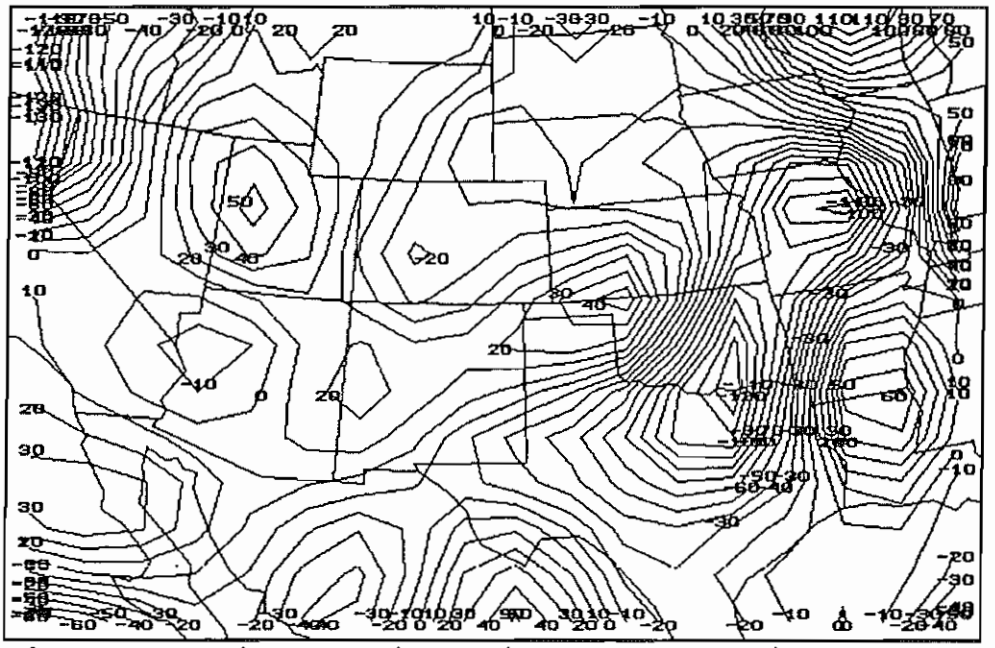

Figure 57. Differential Thickness Advection (10-2 K hr-1 dp-1) 03 April 1982 0000 UTC.

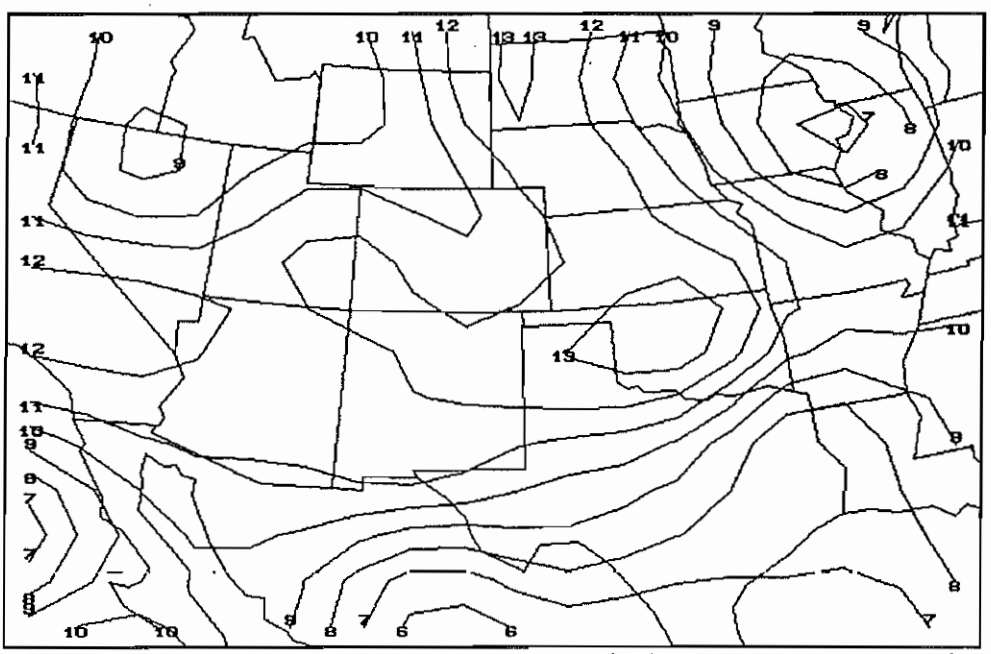

Figure 58. Layer-averaged Stability (K) 03 April 1982 0000 UTC.

Wind fields across the region were very strong, with a 300 mb speed maximum of in excess of 120 knots observed at Amarillo (Figure 59). It is interesting to note that the most severe convection occurred in the right-front quadrant of the speed maximum, a region generally considered unfavorable for severe convection (Beebe and Bates, 1955). However, Maddox and Doswell (1982) found similar results in some instances.

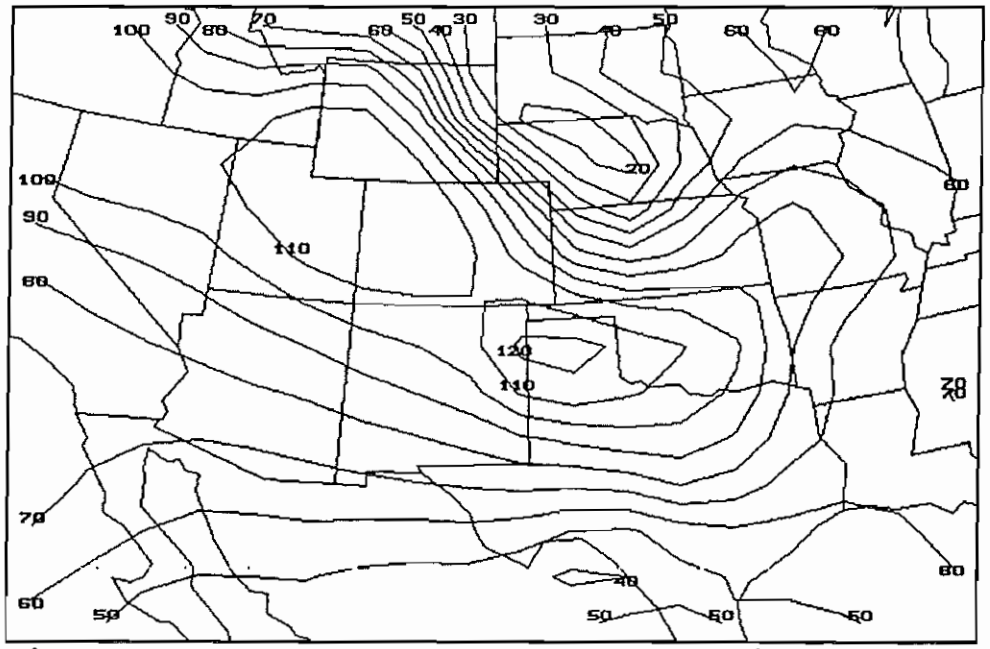

Figure 59. 300 mb Isotachs (kts) 03 April 1982 0000 UTC.

Moore, **et. al.**(1990) have shown that for a cyclonically curved jet maximum, as was observed in this case, the classic four-cell vertical motion pattern is modified so that subsidence associated with the right front exit region is diminished.

Summary

In summary, April 2, 1982 was a day characterized by strong wind fields, low static stability, and substantial amounts of low-level moisture. The result was an atmosphere rich in vertical wind shear and buoyant energy, an environment favorable for supercell thunderstorms and strong tornadoes. Although the exact role of the shortwave trough was unclear, it remained a distinct (and strong) feature from 02/1200 UTC to 03/0000 UTC. It is likely that the vertical motion field associated with the shortwave trough acted to decrease static stability during the day. However, it should be noted that the convection developed near the dryline suggesting mesoscale boundary layer convergence was the primary mechanism responsible for convective initiation (though the QG omega field may have assisted by eroding any capping inversion).

CHAPTER VI

CONCLUSIONS

This research employed objectively analyzed upper-air data to examine the large-scale convective environments associated with 25 severe weather events in Oklahoma and Texas. More specifically, attempts were made to: 1) demonstrate how the analyses may be used to quantitatively assess factors important to convection (e.g. static stability and moisture), 2) identify the large-scale quasi-geostrophic mechanisms present and their role in altering the convective environment, 3) examine the range of forcing for quasi-geostrophic omega observed for significant severe storm events over the southern Great Plains.

Results indicate the analysis routines were successful in providing quantitative information to identify large-scale mechanisms acting to alter moisture and static stability in the convective environment. More specifically, differential quasi-horizontal advections of temperature and moisture were found to be important in the creation and maintenance of atmospheric thermodynamic structures favorable for convection. These findings are consistent with those of Newton (1980) and Doswell (1982).

Examination of the results also suggests that quasi-geostrophic omega was important in the modification of static stability across the southern Great Plains. To what degree changes in static stability were due to horizontal versus vertical motions remains unclear. In a few cases (such as March 22, 1987) the hypothesized one-quarter wavelength phase relationship between static stability and omega was discernible. However, in the majority of the 25 cases the phase relationship was not evident or very weak, and was perhaps masked by the effects of quasi-horizontal advections. The interdependence of σ and ω further complicated the assessment.

In the 25 events selected for study, the results indicated that convection was generally initiated along a source of mesoscale boundary layer convergence, such as a cold front or dryline. Furthermore, initiation took place in regions of low static stability downstream from maxima in Q-vector convergence and forcing for $\omega<0$. Thus, convection was typically oriented parallel to mesoscale forcing patterns, not patterns of quasi-geostrophic omega forcing. These results imply that mesoscale processes were responsible for convective initiation in most instances, while large-scale quasi-geostrophic motions acted to alter or maintain a thermodynamic and wind profile favorable for convection. Doswell (**et.al.**, 1985, 1987) previously proposed a similar scale interaction hypothesis to explain the role of quasi-geostrophic motions in the convective environment.

However, this is not to say that quasi-geostrophic motions play no role in the initiation process. Since convective development was observed downstream from maxima of quasi-geostrophic omega it is possible that the vertical motion may act, in some situations, to erode capping inversions or to increase boundary layer convergence through horizontal contributions of the ageostrophic circulation.

Through examination of layer-averaged stability analyses, it was found that the change in static stability typically was negative over the convective region during the 12 hours preceding the tornado event. This observation suggests that mechanisms acting to force $\partial\sigma/\partial t<0$ (DTA>0 and $\omega<0$) have predictive value.

With these points in mind, the emphasis for the operational meteorologist focuses on how quasi-geostrophic features are acting to create an environment capable of sustaining convection, rather than initiation of convection by the quasi-geostrophic vertical motion field.

Finally, the results were used to develop a climatology for quasi-geostrophic omega forcing during severe weather events in the southern Great Plains. The range of observed forcing varied by an order of magnitude for comparable tornado events ($\geq$ F3). The large range of forcing emphasizes the importance of mesoscale, and smaller, motions in the formation of severe storms. Unfortunately, the large variance suggests the development of composite values as a forecast tool would not be meaningful.

6.1 Recommendations

In order to create a data set of manageable size, this research focused only upon those days in Oklahoma and Texas where tornadoes ≥ F3 were documented. Questions regarding variations in quasi-geostrophic forcing for non-tornadic severe storm days, non-severe thunderstorm days, non-convective days, and from one geographic region to the next (e.g. midwest), remain unanswered.

Temporal variations in forcing also remain largely unaddressed. These variations likely occur not only hour-to-hour, but seasonally, as well.

Although this research primarily focused upon quasi-geostrophic effects upon stability, there is evidence to suggest that ageostrophic components to the wind field arising from quasi-geostrophy may play an important role in the convective environment (Doswell, 1982). Since the Q-vector is proportional to these ageostrophic components, study of its relation to changes in the vertical wind profile (e.g. shear and helicity) may prove useful in the forecasting of convective storm type. The role of ageostrophic advections of moisture also may be examined.

As new observing systems are implemented in the operational meteorological community, additional information regarding upper air winds, temperature, and moisture will become available. By meshing this new information with the present rawinsonde network, analyses of quasi-geostrophic quantities likely will improve.

In addition to diagnostic uses, the Foster Upper Air Diagnostic package also would seem to offer promise in the assessment of numerical model forecast results. By integrating numerical model results into the UA Diagnostic package, the forecaster would be free to change contour intervals and examine quantities not commonly available (e.g. temperature advection), thus providing insight into the physical mechanisms at work.

BIBLIOGRAPHY

Barnes, S.L., 1964: A technique for maximizing details in numerical weather map analysis. J. Appl. Meteor., 3, 396-409.

------, 1973: Mesoscale objective map analysis using weighted time-series observations. NOAA Technical Memorandum ERL NSSL-62. National Severe Storms Laboratory, Norman, Oklahoma.

------, 1985: Omega Diagnostics as a supplement to LFM/MOS guidance in weakly forced convective situations. Mon. Wea. Rev., 113, 2122-2141.

------, 1986: The Limited-Area Fine-Mesh model and quasi-geostrophic theory: a disturbing case study. Weather and Forecasting, 1, 89-96.

------, 1987: Analysis of quasi-geostrophic forcing during the AIMCS project. NOAA Technical Memorandum ERL ESG-27. Environmental Research Laboratories, Environmental Sciences Group, Boulder, Colorado.

Beebe, R.G., and F.C. Bates, 1955: A mechanism for assisting the release of convective instability. Mon. Wea. Rev., 83, 1-10.

Bothwell, P.B., 1988: Forecasting convection with the AFOS data analysis programs (ADAP-Version 2.0). NOAA Technical Memorandum NWS SR-122, Scientific Services Division, Fort Worth, Texas.

Bluestein, H.B., 1985: Synoptic meteorology (class notes).

Burgess, D.W., and E.B. Curran, 1985: The relationship of the storm type to environment in Oklahoma on 26 April 1984. Preprints, 14th Conf. on Severe Local Storms. Indianapolis, Amer. Meteor. Soc., Boston, 208-211.

Byers, H.R., and R.R. Braham, Jr., 1949: The Thunderstorm. U.S. Govt. Printing Office, Washington, D.C., 287 pp.

Carlson, T.N., S.G. Benjamin, G.S. Forbes, and Y.-F. Li, 1983: Elevated mixed layers in the regional severe storm environment: conceptual model and case studies. Mon. Wea. Rev., 111, 1453-1473.

Charba, J.P., 1977: Operational system for predicting severe local storms two to six hours in advance. NOAA Technical Memorandum NWS TDL-65, National Oceanic and Atmospheric Administration, U.S. Dept. of Commerce, 24 pp.

Colquhoun, J.R., 1987: A decision tree method of forecasting thunderstorms, severe thunderstorms, and tornadoes. Weather and Forecasting, 2, 337-345.

Department of Commerce. STORM DATA. National Climatic Data Center, Asheville, NC, October 1981-June, 1988.

Doswell, C.A.,III, 1982: The Operational Meteorology of Convective Weather, Volume I: Operational Mesoanalysis. NOAA Technical Memorandum NWS NSSFC-5, Kansas City, Missouri.

------, 1985: The Operational Meteorology of Convective Weather, Volume II: Storm Scale Analysis. NOAA Technical Memorandum ERL ESG-15. Environmental Sciences Group, Boulder, Colorado.

------, F. Caracena, and M. Magnano, 1985: Temporal Evolution of 700-500 mb lapse rate as a forecasting tool -- a case study., Preprints, 14th Conf. Severe Local Storms. Indianapolis, Indiana, Amer. Meteor. Soc., 398-401.

------, 1987: The distinction between large-scale and mesoscale contribution to severe convection: A case study example. Weather and Forecasting, 2, 3-16.

Durran, D.R., and L.W. Snellman, 1987: The diagnosis of synoptic-scale vertical motion in an operational environment. Weather and Forecasting, 2, 17-31.

Fawbush, E.J., and R.C. Miller, 1954: The types of airmasses in which American tornadoes form. Bull. Amer. Meteor. Soc., 35, 154-165.

Foster, M.P., 1988: Upper-Air Analyses and Quasi-geostrophic Diagnostics for Personal Computers. Scientific Services Division, Southern Region, Fort Worth, Texas.

Fujita, T.H., 1981: Tornadoes and downbursts in the context of generalized planetary scales. J. Atmos. Sci., 38, 1511-1534.

------, 1986: Mesoscale Classifications: Their History and Their Application to Forecasting. Mesoscale Meteorology and Forecasting., P.S. Ray, Ed., American Meteorological Society.

Hess, S.L., 1959: Introduction to Theoretical Meteorology. Holt, Rhinehart and Winston, 362 pp.

Holton, J.R., 1979: An Introduction to Dynamic Meteorology. Academic Press, 391 pp.

Hornbeck, R.W., 1975: Numerical Methods. Prentice-Hall, Inc. 310 pp.

Hoskins, B.J., I. Draghici, and H.C. Davies, 1978: A new look at the ω-equation. Quart. J. Roy. Meteor. Soc., 104, 31-38.

--------, B.J., and M.S. Pedder, 1980: The diagnosis of middle latitude synoptic development. Quart. J. Roy. Meteor. Soc.,106, 707-719.

Iribarne, J.V., and W.L. Godson, 1981: Atmospheric Thermodynamics. D. Reidel Publishing Company, 259 pp.

Klemp, J.B., and R.R. Wilhelmson, 1978: The simulation of three-dimensional convective storm dynamics. J. Atmos. Sci., 35, 1070-1096.

Koch, S.E., M. DesJardins, and P.J. Kocin, 1983: An interactive Barnes objective map analysis scheme for use with satellite and conventional data. J. Climate Appl. Meteor., 22, 1487-1503.

Maddox, R.A., and C.A. Doswell, III, 1982: An examination of jetstream configurations, 500 mb vorticity advection and low-level thermal advection patterns during extended periods of intense convection. Mon. Wea. Rev., 110, 184-197.

McNulty, R.P., 1980: Differential advection of wet-bulb potential temperature and convective development. Preprints, 8th Conf. Weather Forecasting and Analysis. Denver, Colorado, Amer. Meteor. Soc., 286-291.

Miller, R.C., 1972: Notes on Analysis and Severe-Storm Forecasting Procedures of the Air Force Global Weather Central. Air Weather Service Tech. Rep. 200 (Rev.), Air Weather Service, Scott Air Force Base, IL., 190 pp.

Moller, A.R., and D. Boots, 1983: The role of community preparedness and the national weather service's watch/warning systems in the Paris, Texas tornado. Preprints, 13th Conf. on Severe Local Storms. Tulsa, Oklahoma, Amer. Meteor. Soc., J12- J15.

Moore, J.T., G.E. VanKnowe, and R.C. Molinaro, 1990: A comparison of vertical motion approximations under varying jet streak curvatures. Preprints, 16th Conf. on Severe Local Storms. Kananaskis Park, Alta., Canada, Amer. Meteor. Soc., 137-140.

Newton, C.W., 1980: Overview on Convective Storms., Proceedings of CIMMS Symposium (Y.K. Sasaki, N. Monji, and S. Bloom, Eds.), Norman, OK, 3-107.

NOAA NWS, 1981: Rawinsonde Observations, Federal Meteorological Handbook No. 3, U.S. Dept. of Commerce and U.S. Dept. of Defense, Washington, D.C.

NOAA NWS, 1986a: Satellite Imagery Interpretation for Forecasters., Weather Service Forecasting Handbook No. 6, National Weather Service Headquarters, Office of Meteorology.

NOAA NWS, 1986b: Operations Manual, C-40., National Weather Service Headquarters, 49 pp.

NOAA NWS, 1989: Strategic plan for the modernization and associated restructuring of the National Weather Service.

NOAA NWS, 1990: AWARE: Warning Coordination and Hazard Awareness Report, July 1990, 22pp.

Rockwood, A.A., and R.A. Maddox, 1988: Mesoscale and synoptic scale interactions leading to intense convection: the case of 7 June 1982. Weather and Forecasting, 3, 51-68.

Sutcliffe, R.C., 1947: A contribution to the problem of development. Quart. J. Roy. Meteor. Soc., 73, 370-383.

Trenberth, K.E., 1978: On the interpretation of the diagnostic quasi-geostrophic omega equation. Mon. Wea. Rev., 106, 131-137.

Uccellini, L.W., and D.R. Johnson, 1979: The coupling of upper and lower jet streaks and implications for the development of severe convective storms. Mon. Wea. Rev., 107, 682-703.

Weisman, M. L., and J. B. Klemp, 1986: Characteristics of Isolated Convective Storms. Mesoscale Meteorology and Forecasting., P.S. Ray, Ed., American Meteorological Society.

Woodall, G.R. and H.B. Bluestein, 1988: Detailed observations of a splitting, "low-precipitation" (LP) severe storm and its evolution into a supercell. Preprints, 15th Conf. on Severe Local Storms. Baltimore, Amer. Meteor. Soc., Boston, 280-283.

APPENDIX

ANALYSES OF 700 MB HEIGHT AND Q-VECTOR DIVERGENCE

Analyses of 700 mb height and layer-averaged Q-vector divergence for the sounding time nearest genesis of F3 or greater intensity tornado. Analyses correspond to events listed in Table 4.

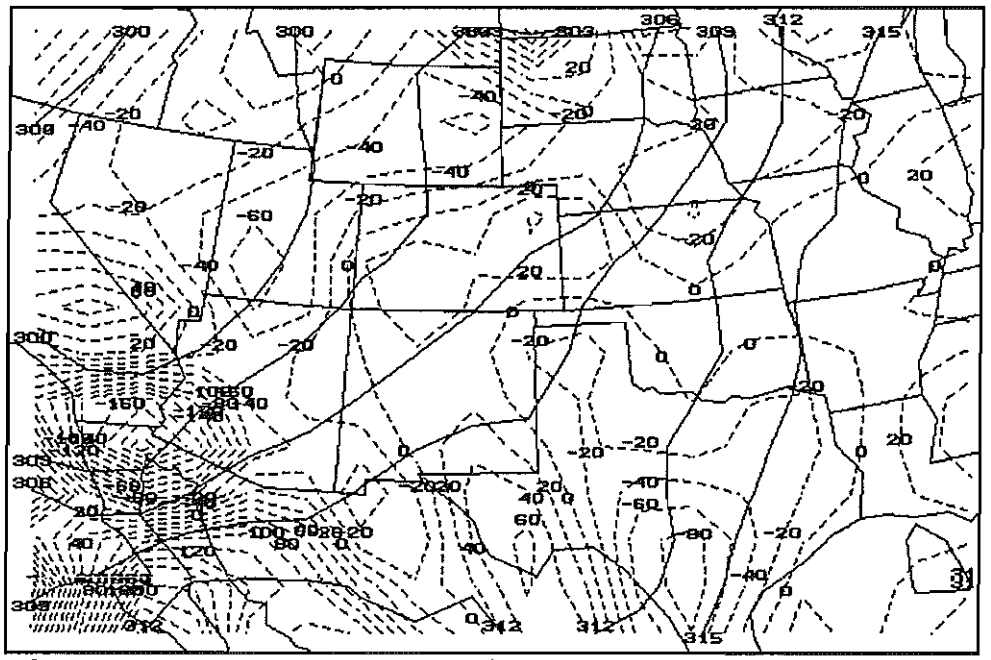

Figure 60. 700 mb Height (dm) and Q-vector Divergence (10-17 s-3 mb-1) 13 October 1981 1200 UTC.

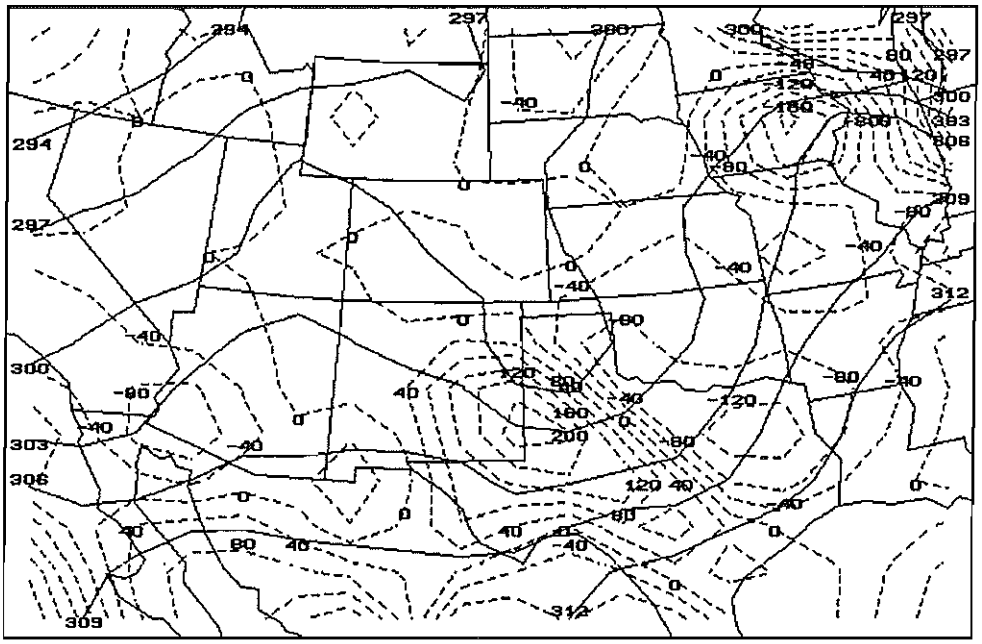

Figure 61. 700 mb Height (dm) and Q-vector Divergence (10-17 s-3 mb-1) 14 March 1982 1200 UTC.

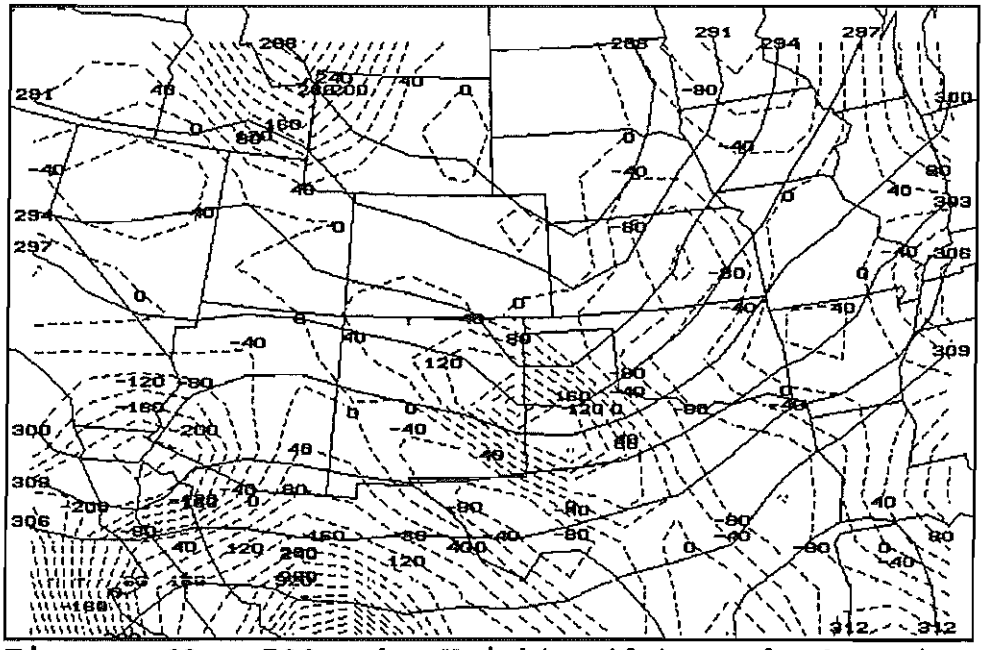

Figure 62. 700 mb Height (dm) and Q-vector Divergence (10-17 s-3 mb-1) 16 March 1982 0000 UTC.

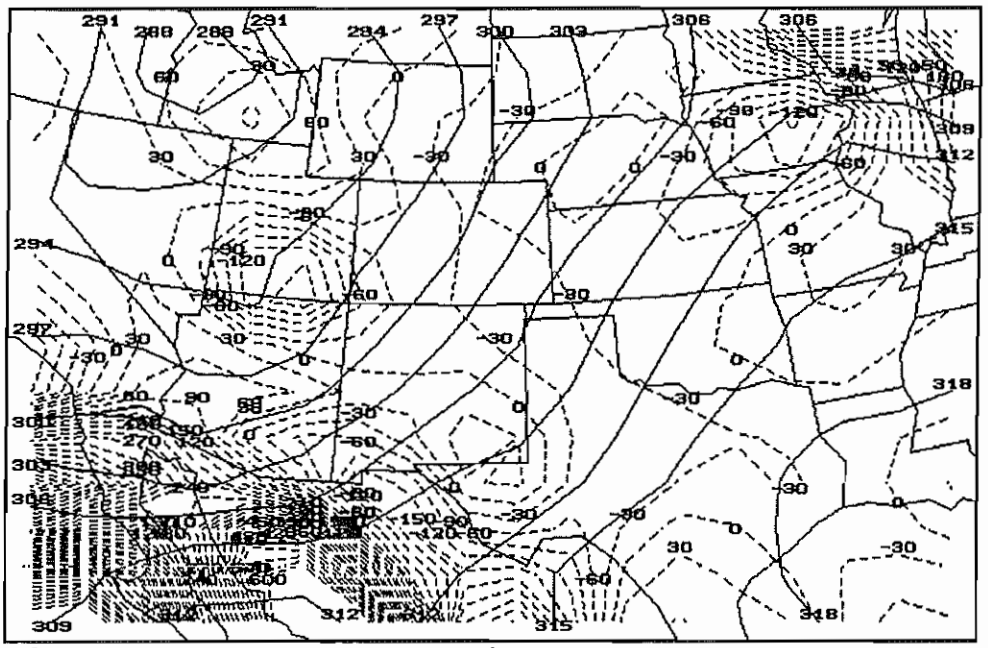

Figure 63. 700 mb Height (dm) and Q-vector Divergence (10-17 s-3 mb-1) 19 March 1982 0000 UTC.

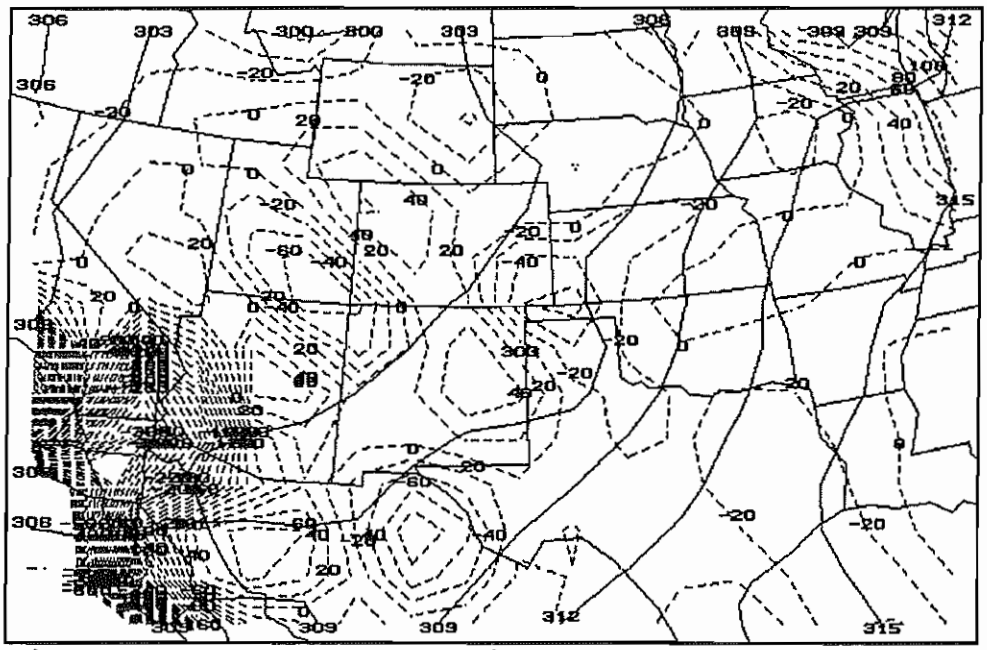

Figure 64. 700 mb Height (dm) and Q-vector Divergence (10-17 s-3 mb-1) 12 May 1982 0000 UTC.

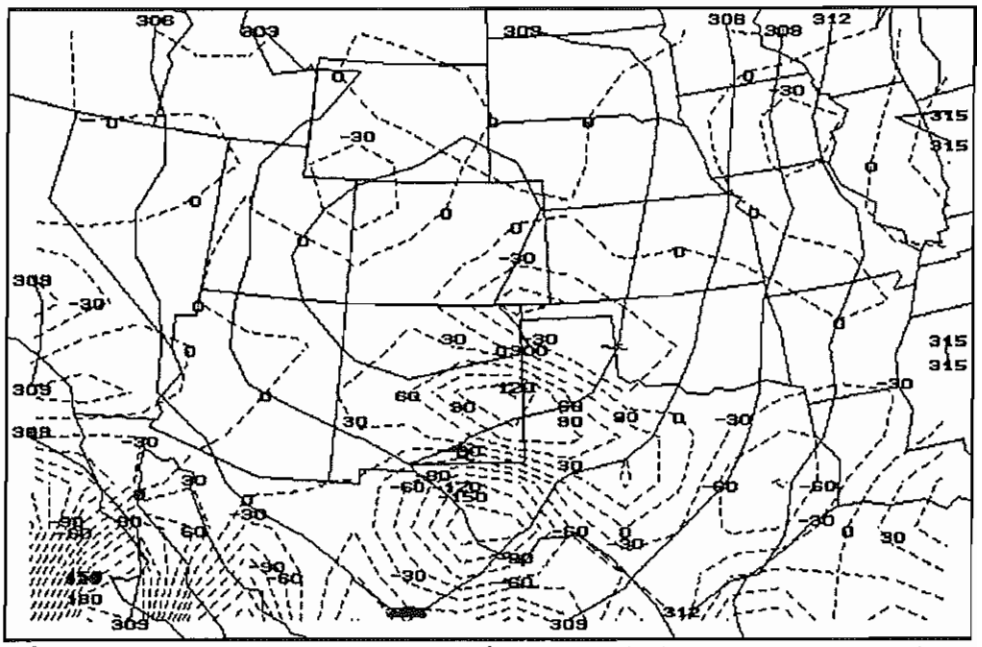

Figure 65. 700 mb Height (dm) and Q-vector Divergence (10-17 s-3 mb-1) 13 May 1982 0000 UTC.

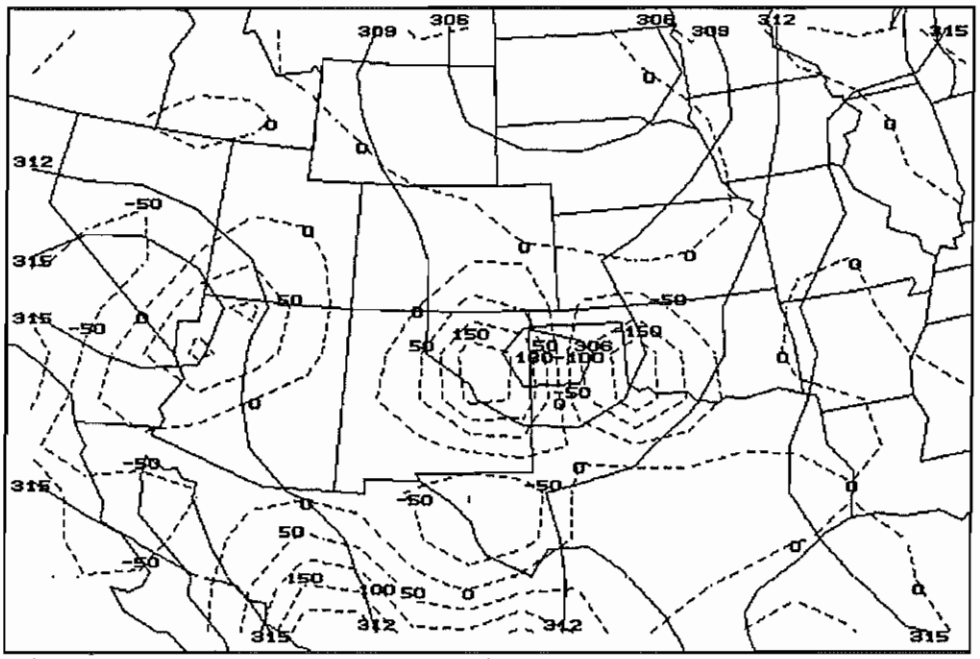

Figure 66. 700 mb Height (dm) and Q-vector Divergence (10-17 s-3 mb-1) 17 May 1982 0000 UTC.

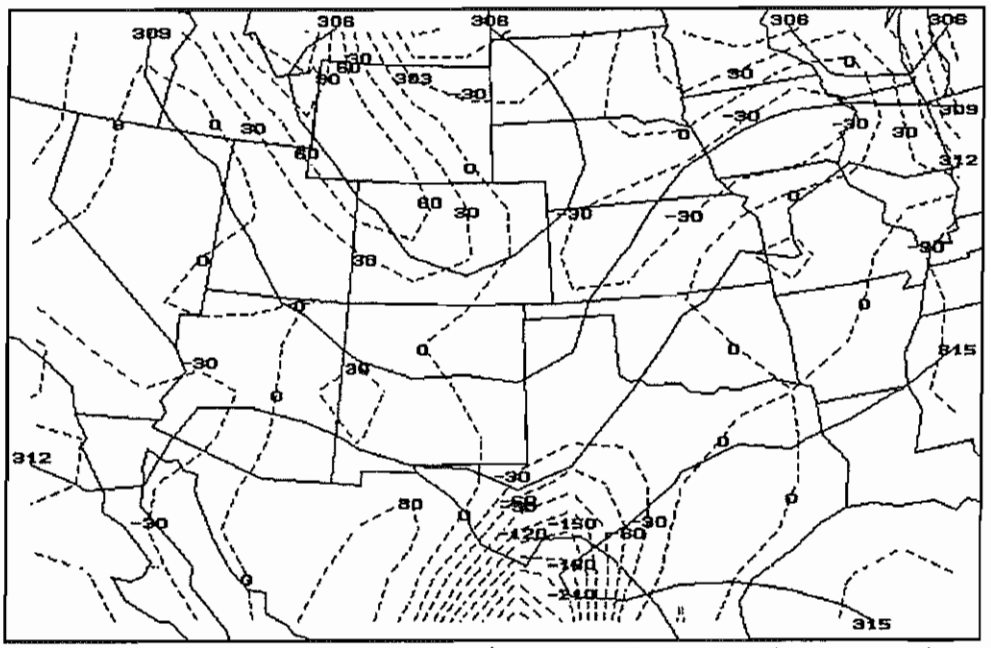

Figure 67. 700 mb Height (dm) and Q-vector Divergence (10-17 s-3 mb-1) 20 May 1982 0000 UTC.

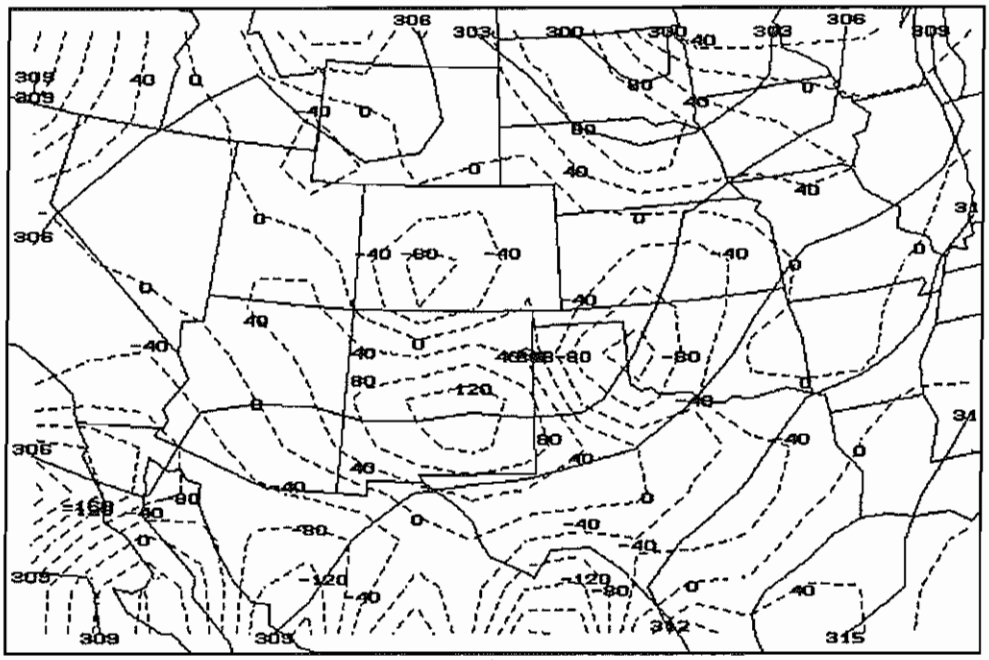

Figure 68. 700 mb Height (dm) and Q-vector Divergence (10-17 s-3 mb-1) 14 May 1983 0000 UTC.

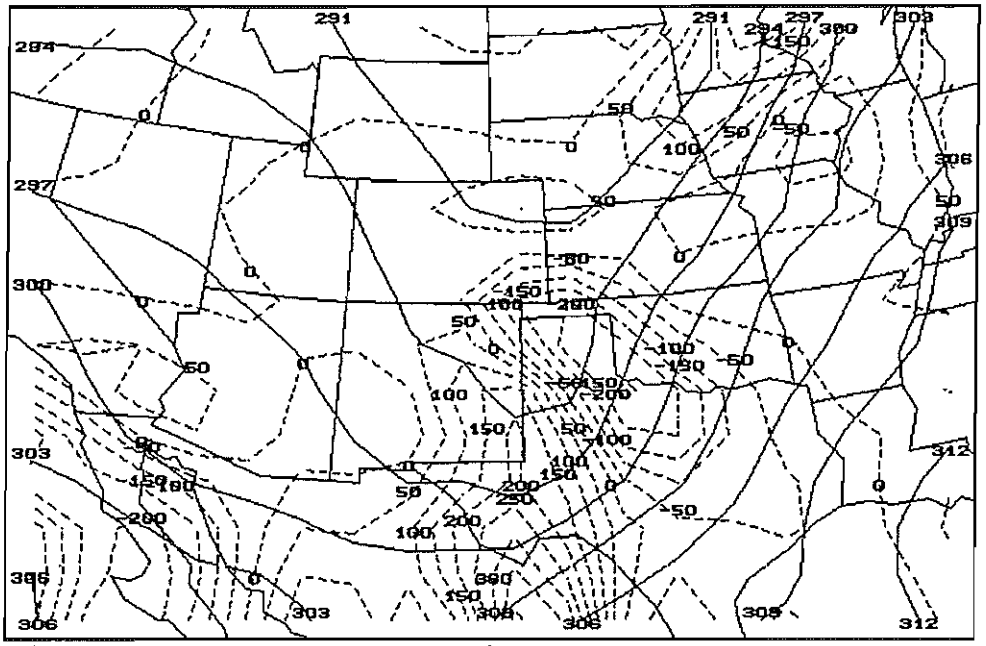

Figure 69. 700 mb Height (dm) and Q-vector Divergence (10-17 s-3 mb-1) 23 November 1983 0000 UTC.

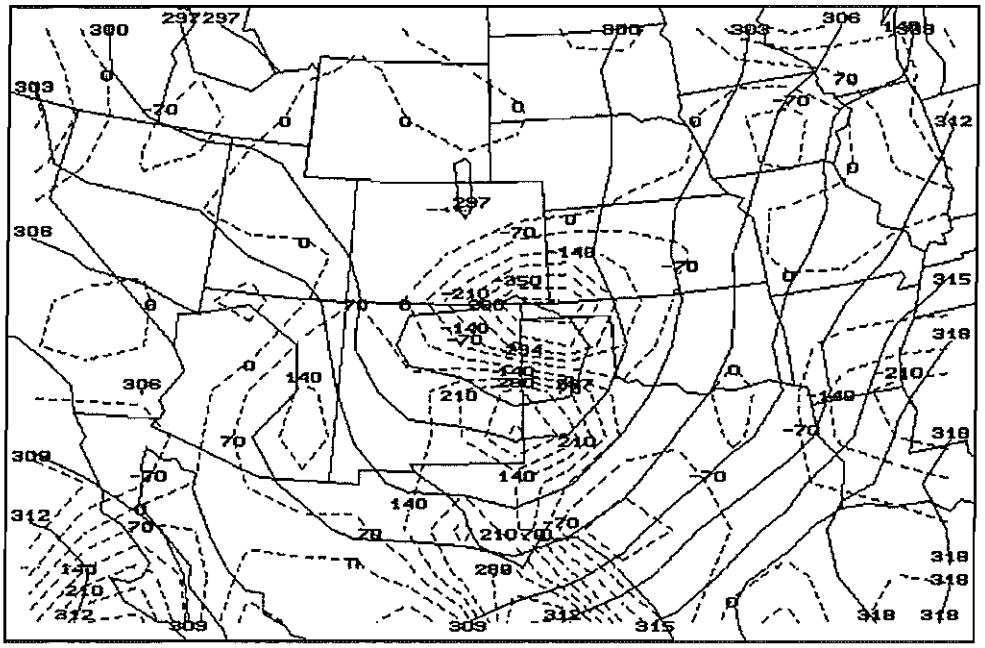

Figure 70. 700 mb Height (dm) and Q-vector Divergence (10-17 s-3 mb-1) 29 April 1984 1200 UTC.

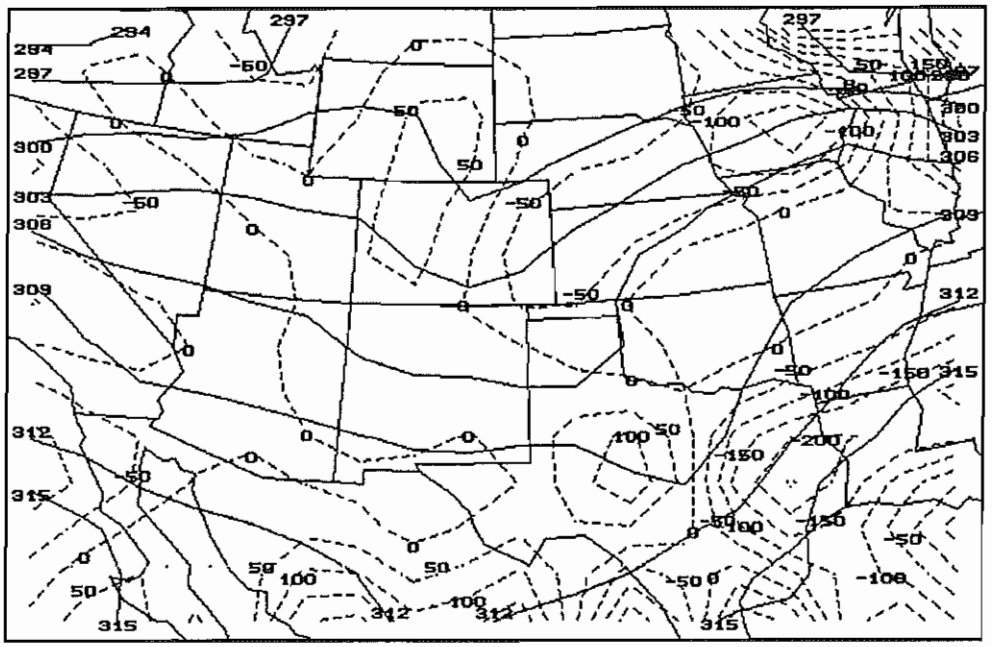

Figure 71. 700 mb Height (dm) and Q-vector Divergence (10-17 s-3 mb-1) 02 May 1984 0000 UTC.

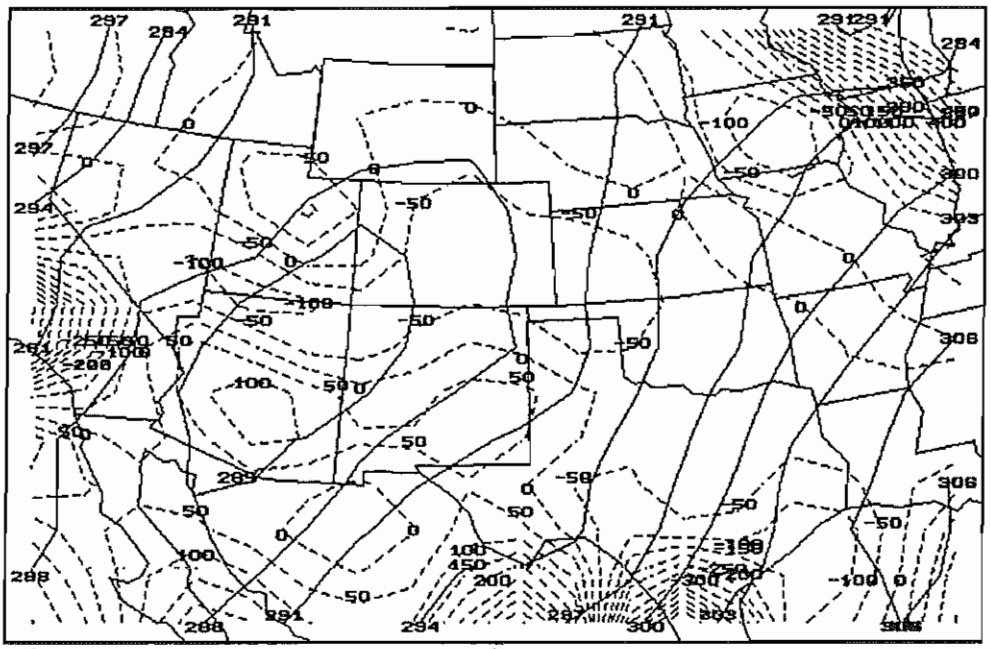

Figure 72. 700 mb Height (dm) and Q-vector Divergence (10-17 s-3 mb-1) 13 December 1984 1200 UTC.

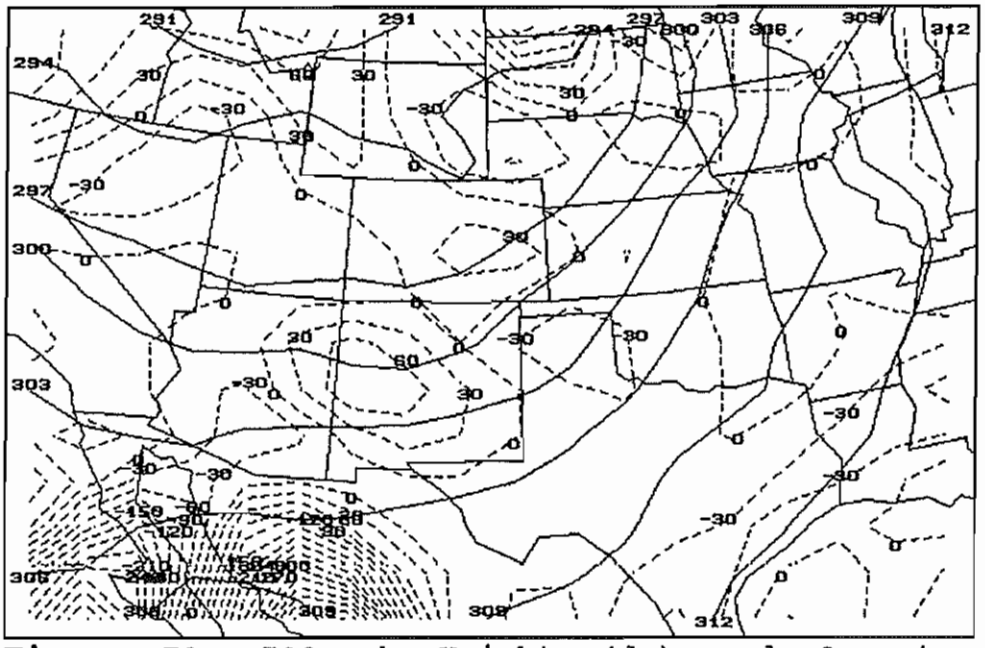

Figure 73. 700 mb Height (dm) and Q-vector Divergence (10-17 s-3 mb-1) 22 April 1985 0000 UTC.

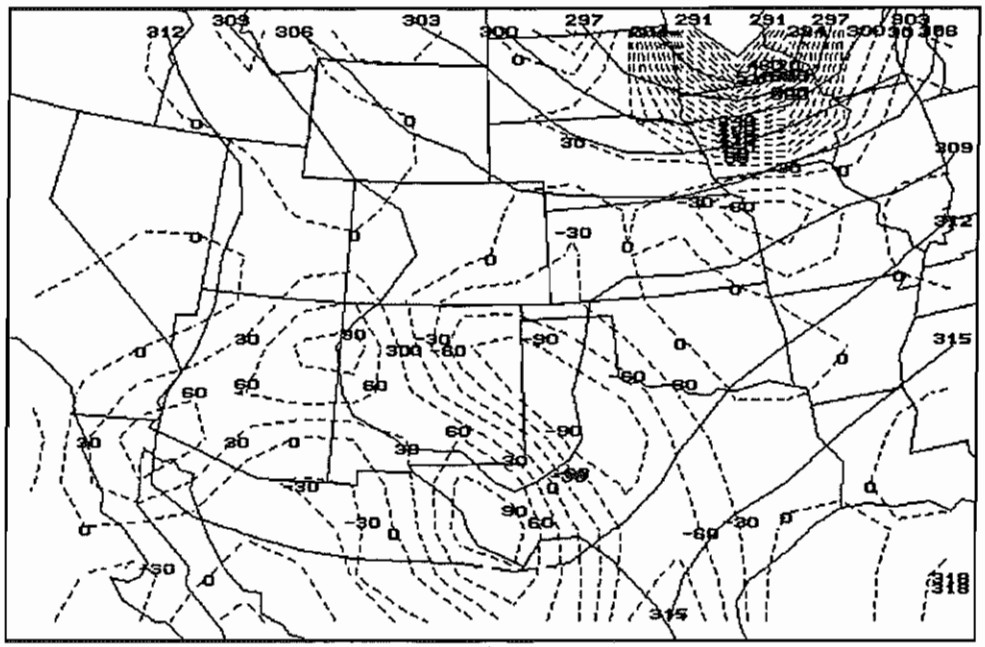

Figure 74. 700 mb Height (dm) and Q-vector Divergence (10-17 s-3 mb-1) 19 April 1986 1200 UTC.

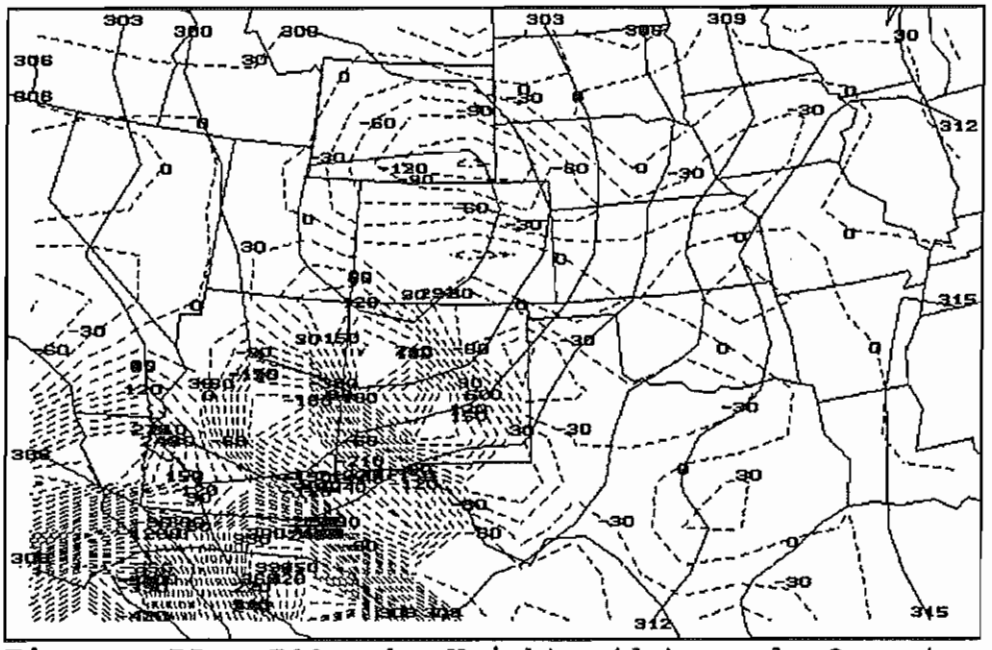

Figure 75. 700 mb Height (dm) and Q-vector Divergence (10-17 s-3 mb-1) 08 May 1986 0000 UTC.

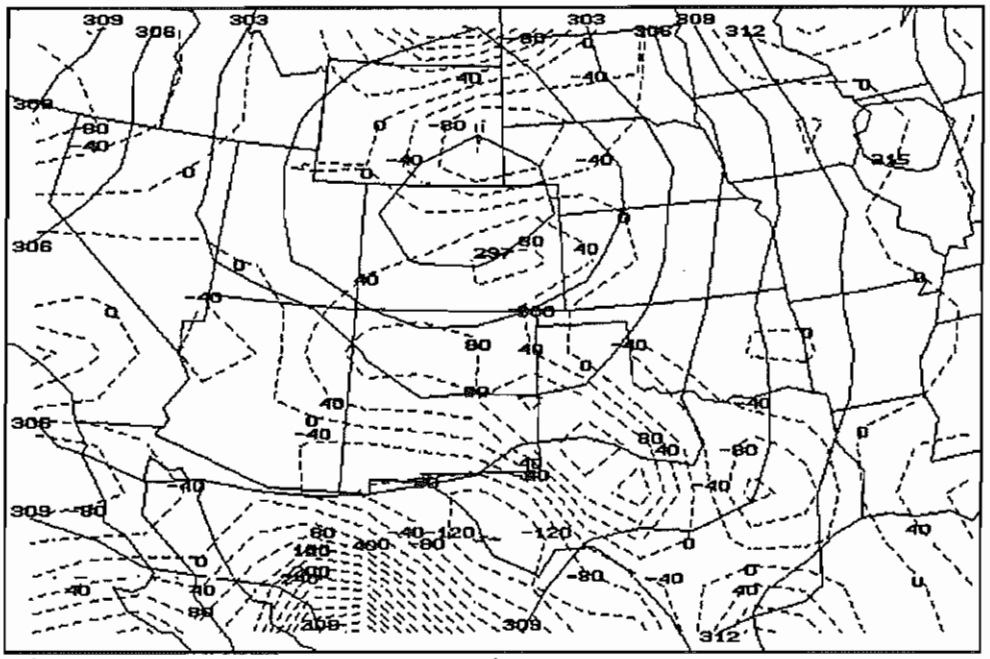

Figure 76. 700 mb Height (dm) and Q-vector Divergence (10-17 s-3 mb-1) 09 May 1986 0000 UTC.

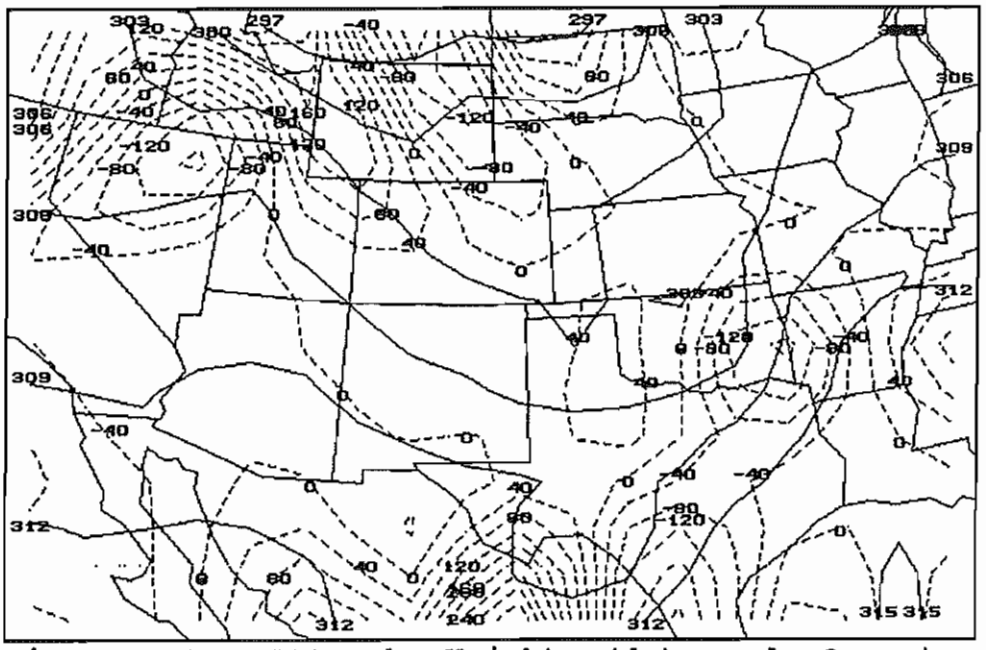

Figure 77. 700 mb Height (dm) and Q-vector Divergence (10-17 s-3 mb-1) 15 May 1986 0000 UTC.

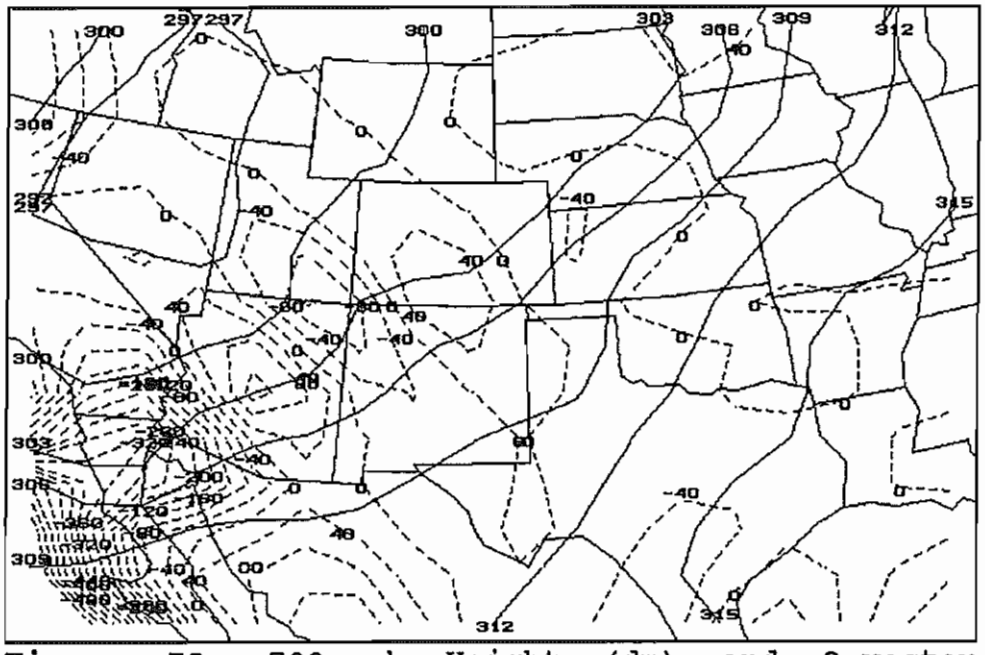

Figure 78. 700 mb Height (dm) and Q-vector Divergence (10-17 s-3 mb-1) 26 May 1987 0000 UTC.

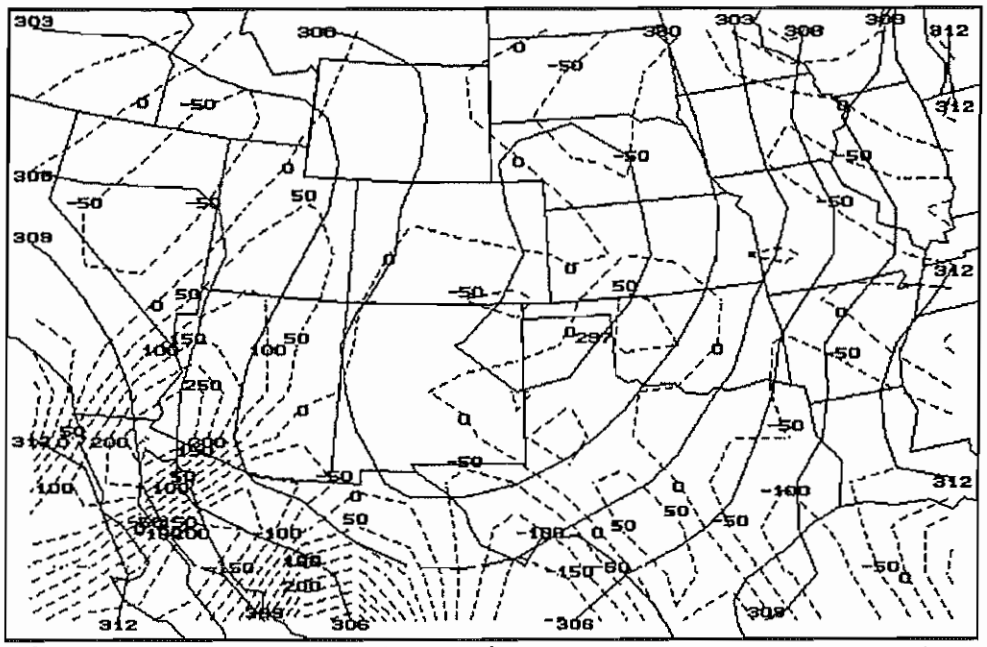

Figure 79. 700 mb Height (dm) and Q-vector Divergence (10-17 s-3 mb-1) 16 November 1987 0000 UTC.

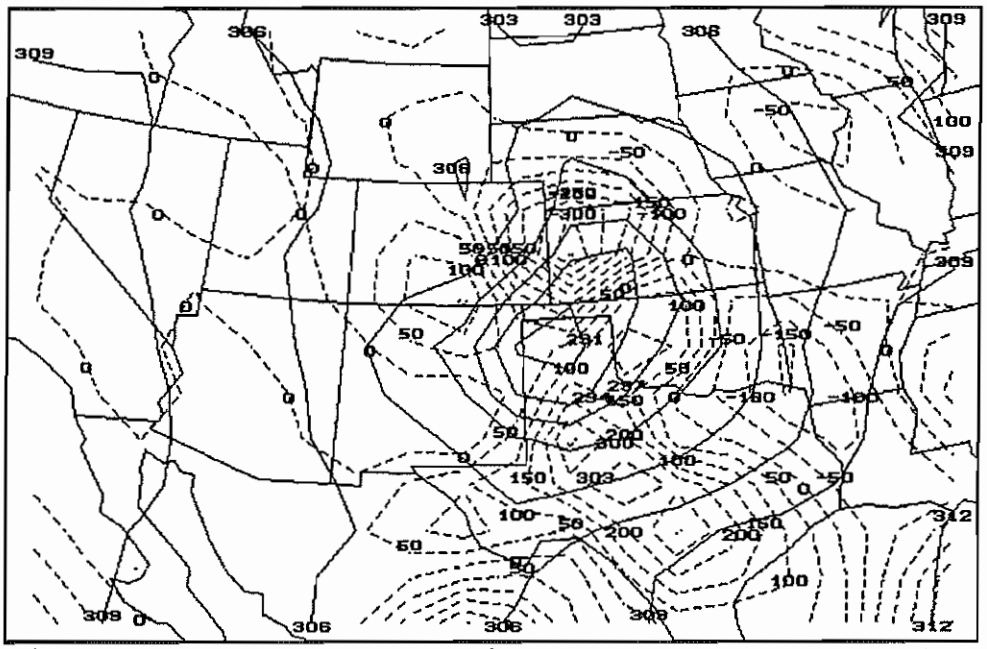

Figure 80. 700 mb Height (dm) and Q-vector Divergence (10-17 s-3 mb-1) 02 April 1988 0000 UTC.